DESIGN AND PREPARATION OF PLANT OIL-BASED POLYMERS AND THEIR APPLICATIONS

by

BYUNG-JUN KOLLBE AHN

B.S., Konkuk University, Korea, 2000
M.S., Konkuk University, Korea, 2003

AN ABSTRACT OF A DISSERTATION

submitted in partial fulfillment of the requirements for the degree

DOCTOR OF PHILOSOPHY

Department of Grain Science and Industry
College of Agriculture

KANSAS STATE UNIVERSITY
Manhattan, Kansas

2011

Abstract

Renewable materials are desirable for many applications due to the finite fossil resources and environmental issues. Plant oil is one of the most promising renewable feedstocks. Plant oils and functionalized oleo-chemicals including functionalized soybean oils have become attractive sustainable chemicals for industrial applications. Especially, epoxidized oleo-chemicals such as epoxidized soybean oil (ESO) are one of the most well-known readily available inexpensive functionalized plant oils. In this study, novel polymers and nanocomposites for sustainable materials applications were designed and prepared via ring-opening of epoxide in plant oils, and their chemical and physical properties were characterized.

The novel transparent elastomers derived from functionalized plant oils have a great potential as flexible electronic and biological applications with their inherent low toxicity. Especially, their rheological properties showed a potential for pressure sensitive adhesives (PSAs). The dominant thermal stability and transparency were obtained via green processing: one pot, single step, fast reactions in moderate conditions, or solvent-free UV curing conditions. These oleo-based elastomers presented excellent end-use properties for PSAs application comparable to commercial PSA tapes. Based on the principal chemical studies, the roles of the each component have been identified: polymer derived from the ring-opening of epoxides as an elastomer, and dihydroxylated triglycerides as a tackifier. Their interaction was also elucidated with an element label analysis. The mechanical and rheological properties of the oleo-polymer as PSAs were able to be improved with a rosin ester tackifier.

In addition, biogreases and bio-thermoplastics were developed via the environmentally benign process, which will contribute to further application on the production of new bio-based materials.

Further, this study essays a novel acid functionalized iron/iron oxide nanoparticles catalyst with excellent product yields for epoxide ring opening of oleochemicals for a greener synthetic method of biopolyols, and excellent environmental benefits with life cycle assessment of syntheses. Those functionalized iron/iron oxide core shell nanoparticles catalysts has great potential for biomedical engineering process with the highest magnetization of Fe(0) core among all metals.

DESIGN AND PREPARATION OF PLANT OIL-BASED POLYMERS AND THEIR APPLICATIONS

by

BYUNG-JUN KOLLBE AHN

B.S., Konkuk University, Korea, 2000
M.S., Konkuk University, Korea, 2003

A DISSERTATION

submitted in partial fulfillment of the requirements for the degree

DOCTOR OF PHILOSOPHY

Department of Grain Science and Industry
College of Agriculture

KANSAS STATE UNIVERSITY
Manhattan, Kansas

2011

Approved by:

Major Professor
Xiuzhi Susan Sun

Abstract

Renewable materials are desirable for many applications due to the finite fossil resources and environmental issues. Plant oil is one of the most promising renewable feedstocks. Plant oils and functionalized oleo-chemicals including functionalized soybean oils have become attractive sustainable chemicals for industrial applications. Especially, epoxidized oleo-chemicals such as epoxidized soybean oil (ESO) are one of the most well-known readily available inexpensive functionalized plant oils. In this study, novel polymers and nanocomposites for sustainable materials applications were designed and prepared via ring-opening of epoxide in plant oils, and their chemical and physical properties were characterized.

The novel transparent elastomers derived from functionalized plant oils have a great potential as flexible electronic and biological applications with their inherent low toxicity. Especially, their rheological properties showed a potential for pressure sensitive adhesives (PSAs). The dominant thermal stability and transparency were obtained via green processing: one pot, single step, fast reactions in moderate conditions, or solvent-free UV curing conditions. These oleo-based elastomers presented excellent end-use properties for PSAs application comparable to commercial PSA tapes. Based on the principal chemical studies, the roles of the each component have been identified: polymer derived from the ring-opening of epoxides as an elastomer, and dihydroxylated triglycerides as a tackifier. Their interaction was also elucidated with an element label analysis. The mechanical and rheological properties of the oleo-polymer as PSAs were able to be improved with a rosin ester tackifier.

In addition, biogreases and bio-thermoplastics were developed via the environmentally benign process, which will contribute to further application on the production of new bio-based materials.

Further, this study essays a novel acid functionalized iron/iron oxide nanoparticles catalyst with excellent product yields for epoxide ring opening of oleochemicals for a greener synthetic method of biopolyols, and excellent environmental benefits with life cycle assessment of syntheses. Those functionalized iron/iron oxide core shell nanoparticles catalysts has great potential for biomedical engineering process with the highest magnetization of Fe(0) core among all metals.

Table of Contents

List of Figures

List of Schemes

List of Tables

Acknowledgements

First, I thank God for his blessing. I would like to express my most sincere gratitude and appreciation to my advisor Dr. Xiuzhi Susan Sun. As a role model, she taught me how to be, how to think, and how to behave as a scientist. Without her, I would not realize how meaningful being a good scientist is to the world. My appreciation is also extended to my advisory committee members who are Drs. Stefan Bossmann, Donghai Wang, and Om Prakash. They always encouraged me to do my best in what I believe which increased my motivation and creativity. Special thanks go to Dr. Stefan Kraft who is not only my best friend but also my chemistry tutor and mentor. I would like to thank my lab-mates: Gyangyan Qi, Yonghui Li, Hongzhou Huang, Minjung Kim, Tianjian Tong, and my undergraduate assistants Jonggeun Sung and Namhoon Kim. Also, I would like to thank my awesome collaborators Dr. Hongwang Wang, Myles Ikenberry, and Shona Robinson. Most importantly, I thank my lovely wife Eunmee and my sweet family (brother, sister, mother, father) for their endless support with love. Also, I thank father Park and pastor Jeong for their pray and for helping me try to be a better person every day. I acknowledge the USB (United Soybean Board) and KSC (Kansas Soybean Commission) for financial support of this work, and also acknowledge Dr. Om Prakash and Mr. Alvaro Herrera for conducting NMR.

Chapter 1 - Introduction

1.1. Overview

The finite reserves, non-uniform distribution, volatile prices, and environmental concern such as global warming and climate changes have urged scientists and engineers to develop sustainable materials from renewable resources such as lipid, protein, carbohydrate, cellulose, and lignin (Ahn et al. 2011a; Ahn et al. 2011b; Belgacem and Gandini 2008; Lligadas et al. 2010; Meier et al. 2007; Metzger and Bornscheuer 2006; Xia and Larock 2010). Sustainable materials and renewable energy became a more attractive topic to promise a better world for the next generation, and many studies have conducted in the field of renewable materials and energy derived from agricultural products including first generation biofuels such as bioethanol derived from maize although they have a strong challenge of competition with food supplies. Avoiding competition with food supplies, the development of second generation cellulosic biofuels or third generation algae biofuels has been studied (An et al. 2011). Meanwhile, biobased materials require relatively less amount of energy input compared with the first and second generation biofuels so as to result in positive energy balance in terms of life cycle assessment. Thus, value-added biobased products converted from agricultural products and byproducts are desired for our sustainable economic development (Belgacem and Gandini 2008). Plant oil is one of the most readily available candidates for the renewable materials, and through the various functionalization techniques, oleochemicals has potential to replace petrochemicals with environmental advantages including low toxicity and inherent biodegradability, and many researches about functionalized plant oils have been conducted (Helling and Russell 2009; Lligadas et al. 2010; Meier et al. 2007; Metzger and Bornscheuer 2006; Xia and Larock 2010). In addition, using waste cooking oil for biofuels and biobased products can be more energy efficient (Guzatto et al. 2011; Muralidharan and Vasudevan 2011). However, plant oils often exhibit poor thermal and oxidative stability because of their nature of *E*/*Z*-isomerizations (cis/trans isomerizations) and allylic autoxidation for lubricant applications, and poor mechanical properties for composite applications (Erhan and Asadauskas 2000). To solve these problems, various chemical modifications were undertaken to produce these materials with more favorable characteristics for specific applications.

Though there is increasing in using renewable resources, the most production processes cannot be considered as "green chemistry". The term "green chemistry" was comprehensively answered by Anastas and Warner, "Green chemistry is the utilization of a set of principles that reduces or eliminates the use or generation of hazardous substance in the design, manufacture and application of chemical products (Anastas and Warner 1998)." Sometimes the concept was misunderstood that using renewable resources is "green chemistry", yet it is only one of the 12 principles of green chemistry: 1) prevention, 2) atom economy, 3) less hazardous chemical syntheses, 4) designing safer chemicals, 5) safer solvents and auxilaries, 6) design for energy efficiency, 7) use of renewable feedstocks, 8) reduce derivatives, 9) catalysis, 10) design for degradation, 11) real-time analysis for pollution prevention, 12) inherently safer chemistry for accident prevention (Anastas and Warner 1998). Life cycle assessment (LCA), also known as life cycle analysis, is a important tool to allow the evaluation of environmental benefits of chemicals and materials in a process and its entire life cycle (Helling and Russell 2009; Luterbacher et al. 2009). However, limited researches were reported about the integration of LCA into great chemistry, and still in challenge to progress (Jessop 2011; Luterbacher et al. 2009).

1.2. Objective

The overall objective of this study is to design and prepare oleo-polymers with higher biobased contents via greener chemical syntheses for the applications of value-added agricultural products.

The specific research activities of this study are as follows

1. To reveal the chemistry bias of epoxidized soybean oil (ESO)/dihydroxyl soybean oil (DSO) in presence of phosphoric acid based on the fundamental chemical studies, and accomplished the polymeric matrix for potential pressure sensitive adhesives (PSA) applications. The details of this research are described in Chapter 2.

2. To accomplish a fast curing (drying) process which is essential for industrial applications., and to prepare the soybean oil-based PSA films and tapes which can replace the petro-based PSAs for a broad range of applications including flexible electronics and medical

devices with its thermal stability, transparency, chemical resistance, and potential bio-degradability from triglycerides. The details of this research are described in Chapter 3.

3. To prepare greener DSO using phosphoric acid as a catalyst and create DSO-contained phosphate esters, or phosphate ester functionalized DSO with improved peel strength. The details of this research are described in Chapter 4.

4. To accomplish higher biobased contents (the PSA contains acrylated epoxidized soybean oil (AESO) up to 97%) with simpler functionalization steps, which will save energy and reduce environmental impacts. The details of the PSAs using AESO via free-radical polymerization are described in chapter 5, and the details of the other PSAs using an ESO/DSO blend via cationic polymerization are described in chapter 6.

5. To accomplish solvent-free acid-catalyzed ring-openings of epoxidized oleochemicals using metallic stearates or stearic acid based on the discovery of the catalytic competition of the ring opening of plant oil derived epoxide with Brøsted acid (stearic acid) and Lewis acid (its salts), regarding product yields and conversion rate in the same solvent-free condition. A practical application of this method was attempted using soybean oil to give biogreases and bio-thermoplastics. The details of this research are described in chapter 7.

6. To apply the novel sulfamic acid functionalized APTES coated Fe/Fe3O4 nanoparticles (NPs) for a ring-opening catalyst of the epoxidized methyl oleate, which allows for a convenient recycling and reaction process in a magnetic field for bio-polyol synthetic applications. And, to evaluate environmental risks as a practical application of initial life cycle assessment. The details of this research are described in chapter 8.

1.3. Literature review

1.3.1. Chemistry of plant oils (Oleochemicals)

1.3.1.1. Transesterification

Transesterification of plant oils (triglycerides) are the most well-known straightforward chemistry of plant oils. The basic derivatives of triglycerides have different physical properties depending on the carbon chain length and the distribution and location of unsaturated moieties which result in various areas of application (Behr et al. 2008). For example, fatty acids and

glycerol are obtained from the hydrolysis for pharmaceutical and cosmetic applications, and fatty acid esters are derived from the transesterification for biodiesel and lubricant applications (Kralova and Sjoblom 2010). In addition, several researches on acid functionalized heterogeneous catalysts have been reported for biodiesel process in which the catalysts can be reusable (Melero et al. 2009; Melero et al. 2010; Mo et al. 2008). Beyond biodiesel, many chemical products derived from native fats and oils, called oleochemicals, are currently used such as fatty acids, fatty alcohols, fatty acid esters, and specialties. Behr and Gomes (2010); Behr et al (2008) reviewed the current processes of triglycerides for their applications, classified the oleochemicals such as various fatty acids, fatty acid salts, functionalized plant oils, and their applications. Fatty acids are also applied for linear polymers for PSA (Bunker et al. 2003; Bunker and Wool 2002; Klapperich et al. 2009) and polyol (Lligadas et al. 2006), and applications using oleic acid methyl ester as a starting material. Bunker et al (2003); Bunker and Wool (2002); Klapperich et al (2009) functionalized oleic acid with epoxidation followed by acrylation for PSA applications. Lligadas et al (2006) epoxidized methyl oleate (oleic acid methyl ester) followed by linear polyether polyol from epoxidized methyl oleate for rigid polyurethane composites.

Asakuma et al (2009) studied transesterification and hydrolysis of triglycride under acidic and basic conditions in terms of activation energies to clarify the mechanism. High viscosity of plant oil-based biodiesel is a challenge for its applications. Conceicua et al (2005) investigated rheological behavior of castor oil, and castor oil biodiesel, and their mixture with mineral biodiesel.

1.3.1.2. Fuctionalization of unsaturated sites

Functionalization of unsaturated sites: epoxidation, acrylation, and autooxidation. Soybean is the number one oil seed crop in the US (Behr et al. 2008). Epoxidized soybean oil (ESO), acrylated epoxidized soybean oil (AESO), and drying oils (linseed oil) are commercially available. La Scala and Wool (2005) has reported the rheological behavior of functionalized plant oils in terms of their functional group and quantity of the functionality. Epoxidation of the unsaturated oleochemical is a straightforward reaction; thus, ESO is inexpensive compared to other commercially available functionalized plant oils (Ahn et al. 2011a; Ahn et al. 2011b). The epoxidation of plant oils has been conducted with either meta-chloroperoxybenzoic acid (Ahn et al. 2011a; Ahn et al. 2011b) or hydrogen peroxide and formic acid (Bunker and Wool 2002;

Meier et al. 2007; Xia and Larock 2010). In addition, enzymatic epoxidation of soybean oil methyl ester was also studied to avoid uses of petrochemicals such as volatile organic solvents and toxic catalysts (Lu et al. 2010). The ring openings of the hindered secondary epoxides in oleochemicals were questionable; thus, Rios et al (2005) investigated the ring opening of epoxidized methyl oleate (EMO) by different alcohols using commercial heterogeneous acid resin catalysts such as SAC 13 and Amberlite 15 to form α-hydroxy alkoxylates in terms conversion rate and product selectivity. The conversion rate increased with the acid strength but the selectivity decreased (Rios et al. 2005). Salimon and Salih (2010) reported a α-hydroxy ring opening of the epoxide using isobutanol with sulfuric acid or using various fatty acids with p-toluenesulfonic acid as a catalyst.

Acrylation of oleochemcals was prepared from acrylation of epoxidized oleochemicals using acrylic acid (Bunker et al. 2003; Bunker and Wool 2002; Xia and Larock 2010). Acrylated epoxidized oleochemicals, including AESO, have shown great potential for PSA or coating applications; thus, Pelletier et al investigated UV initiated free radical polymerization using three commercial UV photoinitiators, and demonstrated DAROCUR 1173 (BASF resins, Wyandotte, MI) giving the fastest reaction and highest yields of crosslink (Pelletier et al. 2006).

Drying oil is air-exposure plant oil which contains more linoleic or linolenic acid than oleic acid, such as linseed oil, since auto-oxidation is more likely to happen in between vicinity unsaturated sites (Kumar et al. 2008). This drying oil, often called alkyd resin, has been commonly used as an environmentally friendly oil-based paint, wood finish, and varnish.

1.3.2. Plant oil-based polymers

1.3.2.1. Oil paints, inks, and coatings

Common plant oils (linseed, tung, soybean, rapeseed oils), their derivatives (fatty acid esters), oligomerized linseed oil (drying oil), and alkyd resins for ink additives have been studied in the relation between their chemical structural and rheological properties (Blayo et al. 2001). Kumar et al (2008) synthesized nanoparticles in situ during auto-oxidation of drying oil and developed a sliver of nanoparticles embedded antibacterial paint. Chen et al (2011) reported enhanced performance of UV curable AESO coating by incorporating it with acrylated sucrose and hyperbranched acrylates. Cheong et al (2009) prepared palm olein polyol and reacted it with

acrylic acid via esterification; this acrylated prepolymer showed potential for UV curable coatings. Soybean oil phosphate ester polyols were also presented with a melamine/formaldehyde resin incorporated into solventborne and waterborne bake coating (Zhong et al. 2001).

1.3.2.2. Composites

Currently, the widespread applications of ESO are as a plasticizer. Czub (2006) modified Bisphenol A based epoxy resin with ESO, and it demonstrated excellent mechanical properties compared to commercial grade active diluents in its low water absorption, high chemical resistance, and plasticizing effect. Liang and Chandrashekhara (2006) synthesized epoxidized allyl soyate by the process of transesterification and epoxidation of regular soy bean oil and monitored the curing kinetics and rheology of the epoxy resin. Xu et al (2002) synthesize ESO polymer crosslinked by triethylene glycol diamine, and reported its strong viscoelastic properties similar to synthetic rubbers.

Biopolyol is also one of the biggest markets of functionalizaed plant oils for polyurethane applications. Recently, hydroxyl soybean oil via alcoholysis of ESO called soy polyols has been widely used for PU applications, such as BiOH® (Cargill Inc.) (Lligadas et al. 2010; Meier et al. 2007). Four different biopolyols were derived from a ring-opening of ESO with hydrochloric acid, hydrobromic acid, methanol, and hydrogen, and their chemical physical properties were investigated (Guo et al. 2000a). Meanwhile, Lozada et al (2009) evaluated six different commercial ring-opening catalysts to prepare biopolyol from ESO while avoiding side reactions at a low concentration and temperature. Zhao et al (2008) opened the epoxide of ESO to obtain mono- or diihydroxyl soybean oils and mono- or di-amino soybean oil, which were crosslinked with 1,4-phenylene diisocyanate.

In addition to studies of the ring-opening of ESO, actual polyurethane foams when prepared in various conditions with soypolyol, and their foam properties were investigated (Guo et al. 2000b). The low reactivity of biopolyol was increased by conversion of secondary alcohol sites to the ethoxylation (Ionescu et al. 2007). In addition, Helling and Russell (2009) conducted life cycle assessment on biopolyol derived from soybean or castor oil and demonstrated environmental costs and benefits compared to petrochemical-based polyols.

Meanwhile, Harry-O'kuru et al (2002); Helling and Russell (2009) found an interesting industrial crop, milkweed, which has growing market demand for its hypoallergenic floss for use in pillows, comforters, and etc. The milkweed seed contains 25 w/w % of unsaturated oil. Harry-O'kuru et al (2002) epoxidized and polyhydroxylated the milkweed oils using a currently available single step technique. Finally, Lligadas et al (2010) reviewed recent biopolyols derived from plant oil and its derivatives.

1.3.2.3. Pressure-Sensitive Adhesives

Viscoelasticity of plant-oil based polymers have encouraged materials scientists to pursue developing plant oil-based pressure sensitive adhesives (PSA). The pioneer of oleo-based PSA is Professor Richard Wool at University of Delaware. His research team investigated potential PSAs derived from acrylated methyl oleate (AMO) rather than AEMO, and emulsified AMO showed excellent results with the aid of methyl methacrylate (MMA) or buthyl methacrylate (Bunker et al. 2003; Bunker and Wool 2002; Klapperich et al. 2009). David et al (2009) prepared AESO instead of AMO and copolymerized with buthyl methacrylate, showing its potential for PSA applications.

The inherent biodegradability and low toxicity of functionalized plant oils, such as AMO, enable AMO PSA for biological applications. Klapperich et al (2009) copolymerized AMO with methyl methacrylate (MMA) and etkylene glycol dimethacrylate (EGDMA) to form pressure sensitive adhesives and reported reasonable mechanical properties and cell adhesiveness for use as bioactive adhesives.

1.3.2.4. Lubricants from fatty acid esters

Demand of plant oil-based lubricant with their inherent biodegradability and low toxicity has been desired due to negative environmental impacts of mineral oil-based lubricants, which result in non-biodegradable toxic wastes after their uses. However, the poor thermal properties and oxidative instabilities hinder the practical applications of plant oil-base lubricants. Adhvaryu and Erhan (2002) demonstrated that ESO has better thermal and oxidative stability compared to non-functionalized soybean oil due to the modification of unsaturated sites, which prevent lipid auto-oxidation (Kumar et al. 2008). Campanella et al (2010) reported branched ether and ester

compounds from epoxidized vegetable oils for lubricant application. Biswas et al (2005) reported a solvent-free method for amine-functionalized soybean oil derived from ESO, using Diethylamine and $ZnCl_2$ to obtain anti-oxidation. α-Hydroxy ether from EMO was also reported as a biolubricant via solvent-free condition (Moser et al. 2007; Salimon and Salih 2010). Sharma et al (2006) presented a ring opening of ESO using 1-butanethiol to form antiwear/antifriction lubricants, but its actual antiwear/antifriction properties were not demonstrated in the study. Sharma et al (2008) also reported the ring opening of ESO using an anhydrous solvent for lubricant applications.

Liu et al (2007) studied the cationic polymerization rate of soybean oil related to the amount of initiator (boron trifluoride diethyl etherate), temperature, and pressure of carbon dioxide in a supercritical carbon dioxide medium. This low molecular weight oligomerized soybean oil could be used as a lubricant.

1.4. References

Adhvaryu, A. and Erhan, S. Z. 2002. Epoxidized soybean oil as a potential source of high-temperature lubricants. Industrial Crops and Products 15:247-254.

Ahn, B. K., Kraft, S. and Sun, X. S. 2011a. Chemical pathways of epoxidized and hydroxylated fatty acid methyl esters and triglycerides with phosphoric acid. Journal of Materials Chemistry 21:9498-9505.

Ahn, B. K., Kraft, S., Wang, D. and Sun, X. S. 2011b. Thermally Stable, Transparent, Pressure-Sensitive Adhesives from Epoxidized and Dihydroxyl Soybean Oil. Biomacromolecules 12:1839-1843.

An, H. J., Wilhelm, W. E. and Searcy, S. W. 2011. Biofuel and petroleum-based fuel supply chain research: A literature review. Biomass & Bioenergy 35:3763-3774.

Anastas, P. T. and Warner, J. C. 1998. Green Chemistry: Theory and Practice. Oxford University Press: New York.

Asakuma, Y., Maeda, K., Kuramochi, H. and Fukui, K. 2009. Theoretical study of the transesterification of triglycerides to biodiesel fuel. Fuel 88:786-791.

Behr, A. and Gomes, J. P. 2010. The refinement of renewable resources: New important derivatives of fatty acids and glycerol. European Journal of Lipid Science and Technology 112:31-50.

Behr, A., Westfechtel, A. and Gomes, J. P. 2008. Catalytic processes for the technical use of natural fats and oils. Chemical Engineering & Technology 31:700-714.

Belgacem, M. N. and Gandini, A. 2008. Monomers, Polymers and Composites from Renewable Resources. Elsevier: Oxford.

Biswas, A., Adhvaryu, A., Gordon, S. H., Erhan, S. Z. and Willett, J. L. 2005. Synthesis of diethylamine-functionalized soybean oil. Journal of Agricultural and Food Chemistry 53:9485-9490.

Blayo, A., Gandini, A. and Le Nest, J. F. 2001. Chemical and rheological characterizations of some vegetable oils derivatives commonly used in printing inks. Industrial Crops and Products 14:155-167.

Bunker, S., Staller, C., Willenbacher, N. and Wool, R. 2003. Miniemulsion polymerization of acrylated methyl oleate for pressure sensitive adhesives. International Journal of Adhesion and Adhesives 23:29-38.

Bunker, S. P. and Wool, R. P. 2002. Synthesis and characterization of monomers and polymers for adhesives from methyl oleate. Journal of Polymer Science Part a-Polymer Chemistry 40:451-458.

Campanella, A., Rustoy, E., Baldessari, A. and Baltanas, M. A. 2010. Lubricants from chemically modified vegetable oils. Bioresource Technology 101:245-254.

Chen, Z. G., Wu, J. F., Fernando, S. and Jagodzinski, K. 2011. Soy-based, high biorenewable content UV curable coatings. Progress in Organic Coatings 71:98-109.

Cheong, M. Y., Ooi, T. L., Ahmad, S., Yunus, W. and Kuang, D. 2009. Synthesis and Characterization of Palm-Based Resin for UV Coating. Journal of Applied Polymer Science 111:2353-2361.

Czub, P. 2006. Application of modified natural oils as reactive diluents for epoxy resins. Macromolecular Symposia 242:60-64.

David, S. B., Sathiyalekshmi, K. and Raj, G. A. G. 2009. Studies on acrylated epoxydised triglyceride resin-co-butyl methacrylate towards the development of biodegradable pressure sensitive adhesives. Journal of Materials Science-Materials in Medicine 20:61-70.

Erhan, S. Z. and Asadauskas, S. 2000. Lubricant basestocks from vegetable oils. Industrial Crops and Products 11:277-282.

Guo, A., Cho, Y. J. and Petrovic, Z. S. 2000a. Structure and properties of halogenated and nonhalogenated soy-based polyols. Journal of Polymer Science Part a-Polymer Chemistry 38:3900-3910.

Guo, A., Javni, I. and Petrovic, Z. 2000b. Rigid polyurethane foams based on soybean oil. Journal of Applied Polymer Science 77:467-473.

Guzatto, R., de Martini, T. L. and Samios, D. 2011. The use of a modified TDSP for biodiesel production from soybean, linseed and waste cooking oil. Fuel Processing Technology 92:2083-2088.

Harry-O'kuru, R. E., Holser, R. A., Abbott, T. P. and Weisleder, D. 2002. Synthesis and characteristics of polyhydroxy triglycerides from milkweed oil. Industrial Crops and Products 15:51-58.

Helling, R. K. and Russell, D. A. 2009. Use of life cycle assessment to characterize the environmental impacts of polyol production options. Green Chemistry 11:380-389.

Ionescu, M., Petrovic, Z. S. and Wan, X. M. 2007. Ethoxylated soybean polyols for polyurethanes. Journal of Polymers and the Environment 15:237-243.

Jessop, P. G. 2011. Searching for green solvents. Green Chemistry.

Klapperich, C. M., Noack, C. L., Kaufman, J. D., Zhu, L., Bonnaillie, L. and Wool, R. P. 2009. A novel biocompatible adhesive incorporating plant-derived monomers. Journal of Biomedical Materials Research Part A 91A:378-384.

Kralova, I. and Sjoblom, J. 2010. Biofuels-Renewable Energy Sources: A Review. Journal of Dispersion Science and Technology 31:409-425.

Kumar, A., Vemula, P. K., Ajayan, P. M. and John, G. 2008. Silver-nanoparticle-embedded antimicrobial paints based on vegetable oil. Nature Materials 7:236-241.

La Scala, J. and Wool, R. P. 2005. Rheology of chemically modified triglycerides. Journal of Applied Polymer Science 95:774-783.

Liang, G. and Chandrashekhara, K. 2006. Cure kinetics and rheology characterization of soy-based epoxy resin system. Journal of Applied Polymer Science 102:3168-3180.

Liu, Z. S., Sharma, B. K. and Erhan, S. Z. 2007. From oligomers to molecular giants of soybean oil in supercritical carbon dioxide medium: 1. Preparation of polymers with lower molecular weight from soybean oil. Biomacromolecules 8:233-239.

Lligadas, G., Ronda, J. C., Galia, M., Biermann, U. and Metzger, J. O. 2006. Synthesis and characterization of polyurethanes from epoxidized methyl oleate based polyether polyols as renewable resources. Journal of Polymer Science Part a-Polymer Chemistry 44:634-645.

Lligadas, G., Ronda, J. C., Galia, M. and Cadiz, V. 2010. Plant Oils as Platform Chemicals for Polyurethane Synthesis: Current State-of-the-Art. Biomacromolecules 11:2825-2835.

Lozada, Z., Suppes, G. J., Tu, Y. C. and Hsieh, F. H. 2009. Soy-Based Polyols from Oxirane Ring Opening by Alcoholysis Reaction. Journal of Applied Polymer Science 113:2552-2560.

Lu, H., Sun, S. D., Bi, Y. L., Yang, G. L., Ma, R. L. and Yang, H. F. 2010. Enzymatic epoxidation of soybean oil methyl esters in the presence of free fatty acids. European Journal of Lipid Science and Technology 112:1101-1105.

Luterbacher, J. S., Froling, M., Vogel, F., Marechal, F. and Tester, J. W. 2009. Hydrothermal Gasification of Waste Biomass: Process Design and Life Cycle Asessment. Environmental Science & Technology 43:1578-1583.

Meier, M. A. R., Metzger, J. O. and Schubert, U. S. 2007. Plant oil renewable resources as green alternatives in polymer science. Chemical Society Reviews 36:1788-1802.

Melero, J. A., Bautista, L. F., Morales, G., Iglesias, J. and Briones, D. 2009. Biodiesel Production with Heterogeneous Sulfonic Acid-Functionalized Mesostructured Catalysts. Energy & Fuels 23:539-547.

Melero, J. A., Bautista, L. F., Morales, G., Iglesias, J. and Sanchez-Vazquez, R. 2010. Biodiesel production from crude palm oil using sulfonic acid-modified mesostructured catalysts. Chemical Engineering Journal 161:323-331.

Metzger, J. O. and Bornscheuer, U. 2006. Lipids as renewable resources: current state of chemical and biotechnological conversion and diversification. Applied Microbiology and Biotechnology 71:13-22.

Mo, X. H., Lotero, E., Lu, C. Q., Liu, Y. J. and Goodwin, J. G. 2008. A novel sulfonated carbon composite solid acid catalyst for biodiesel synthesis. Catalysis Letters 123:1-6.

Moser, B. R., Sharma, B. K., Doll, K. M. and Erhan, S. Z. 2007. Diesters from oleic acid: Synthesis, low temperature properties, and oxidation stability. Journal of the American Oil Chemists Society 84:675-680.

Muralidharan, K. and Vasudevan, D. 2011. Performance, emission and combustion characteristics of a variable compression ratio engine using methyl esters of waste cooking oil and diesel blends. Applied Energy 88:3959-3968.

Pelletier, K., Belgacem, N. and Gandini, A. 2006. Acrylated vegetable oils as photocrosslinkable materials. Journal of Applied Polymer Science 99:3218-3221.

Rios, L. A., Weckes, P. P., Schuster, H. and Hoelderich, W. F. 2005. Resin catalyzed alcoholysis of epoxidized fatty esters: Effect of the alcohol and the resin structures. Applied Catalysis a-General 284:155-161.

Salimon, J. and Salih, N. 2009. Preparation and Characteristic of 9, 10-Epoxyoleic Acid α-Hydroxy Ester Derivatives as Biolubricant Base Oil. European Journal of Scientific Research 31:265-272.

Salimon, J. and Salih, N. 2010. Modification of Epoxidized Ricinoleic Acid for Biolubricant Base Oil With Improved Flash and Pour Points. Asian Journal of Chemistry 22:5468-5476.

Sharma, B. K., Adhvaryu, A. and Erhan, S. Z. 2006. Synthesis of hydroxy thio-ether derivatives of vegetable oil. Journal of Agricultural and Food Chemistry 54:9866-9872.

Sharma, B. K., Liu, Z. S., Adhvaryu, A. and Erhan, S. Z. 2008. One-pot synthesis of chemically modified vegetable oils. Journal of Agricultural and Food Chemistry 56:3049-3056.

Xia, Y. and Larock, R. C. 2010. Vegetable oil-based polymeric materials: synthesis, properties, and applications. Green Chemistry 12:1893-1909.

Xu, J. Y., Liu, Z. S., Erhan, S. Z. and Carriere, C. J. 2002. A potential biodegradable rubber-viscoelastic properties of a soybean oil-based composite. Journal of the American Oil Chemists Society 79:593-596.

Zhao, H. P., Zhang, J. F., Sun, X. S. and Hua, D. H. 2008. Syntheses and properties of cross-linked polymers from functionalized triglycerides. Journal of Applied Polymer Science 110:647-656.
Zhong, B., Shaw, C., Rahim, M. and Massingill, J. 2001. Novel coatings from soybean oil phosphate ester polyols. Journal of Coatings Technology 73:53-57.

Chapter 2 - Chemical Pathways of Epoxidized and Hydroxylated Fatty Acid Methyl Esters and Triglycerides with Phosphoric Acid

[This work has been published: Ahn, B. J. K., Kraft, S., & Sun, X. S. (2011). *Journal of Materials Chemistry, 21*(26), 9498-9505.]

2.1. Abstract

The polymerization pathways of epoxidized and hydroxylated triglycerides with phosphoric acid (H_3PO_4) were investigated using model reactions. Involved epoxides and diols were derived from oleic acid methyl ester, which was easily monitored by one- and two-dimensional nuclear magnetic resonance (NMR) techniques as well as electrospray ionization mass spectroscopy (ESI-MS). Phosphoric acid played two key functions: a) as a Brønsted acid catalyst that activated the epoxide toward nucleophilic attack by the diol, thus generating ether (C-O-C) cross-linkages; and b) as a reaction partner establishing phosphate ester linkages [$(RO)_2(O)P$-O-C, R = C or H]. In studies with ^{18}O labeled diol, phosphate esters formed exclusively from H_3PO_4 and epoxide without incorporation of diol whereas diols acted as polymerization initiators in polyether formations.

2.2. Introduction

The limited availability of fossil fuel resources for the manufacturing of new material has spurred great demand for sustainable and renewable raw materials from biomass. Plant oil-derived feedstocks are one of the most inexpensive and readily available sources for biobased and biodegradable polymeric materials (Cakmakli et al. 2005; Tsujimoto et al. 2004). For example, epoxidized plant oils are widely used as additives, plasticizers and stabilizers for polyvinyl chloride (PVC) or as co-reactants for epoxy resins; hydroxylated oleochemicals such as soy polyols also are well known cross-linking agents for polyurethane industry (Chakraborti et al. 2004; Lligadas et al. 2006; Schilling 1986). Epoxidized soybean oil (ESO) was modified using super phosphoric acid and incorporated into coatings mixed with melamine/formaldehyde and other additives (Zhong et al. 2001).

Several successful trials for oleo-based pressure-sensitive adhesives (PSAs) were previously reported using acrylated methyl oleate, but the addition of petrochemicals was still required (e.g., polymethyl methacrylate, butanediol diacrylate, or ethylene glycol dimethacrylate challenges). Overcoming the long curing time is necessary if plant oil-based PSAs are to have broad commercial application (Bunker et al. 2003; David et al. 2009; Klapperich et al. 2009). To address this challenge, we introduced components that provide hydrophilic domains such as OH-groups to establish adhesion and used a model system to establish chemical pathways that may further help design high-performance PSAs. To generate polymeric cross-links, we gravitated toward epoxide-based electrophiles activated in the presence of phosphoric acid (H_3PO_4) and successfully introduced the epoxidized soybean oil (ESO)-based PSA. The chemical reaction mechanism of epoxides in fatty acid esters or plant oils in the presence of H_3PO_4 remained veiled, and contribution of secondary alcohols of hydroxyl moiety in the network was also questionable. Guo et al. provided evidence that epoxides derived from soybean oils react with H_3PO_4 with a significant degree of phosphate ester-based cross-links whereas acid-catalyzed formation of ether-based cross-links was not reported in their IR-studies (Guo et al. 2007). On the other hand, Nyk et al. reported that phosphoric acids with diepoxides can generate not only phosphate ester cross-links but also ether cross-links (Nyk et al. 1991). In this study, we introduced the biobased PSA using ESO and hydroxylated soybean oil (HSO) with H_3PO_4 and clarified the cause of depolymerization of the polymer. In addition, we shed light on the bias of chemical pathways in epoxidized and hydroxylated fatty acid esters in the presence of H_3PO_4 and elucidated the reaction between secondary epoxides and hydroxyl moities in fatty acid esters or triglycerides.

2.3. Experimental

General. NMR analyses. 1D ^{1}H NMR, 2D ^{1}H-^{1}H COSY NMR and ^{31}P NMR spectra for the samples were recorded quantitatively using a Varian S spectrometer (Varian Inc., Palo Alto, CA, USA) at observing frequencies of 500 MHz for ^{1}H and 202.35 MHz for ^{31}P, respectively, on a 3 mm penta probe. The sample solutions were prepared in $CDCl_3$ in 15% v/v concentrations. ^{1}H NMR spectra were obtained with 32 scans at a delay time of 1 s between scans. 2D ^{1}H-^{1}H COSY spectra were obtained with 128 increments and 4 scans for each increment. A sinebell

function was used during processing for both dimensions. ^{31}P NMR spectra were obtained with 1000 scans at a delay time of 3 s between scans.

ESI-MS. Electrospray Ionization spectra were acquired on an LCT Premier (Waters Corp., Milford, MA, USA) time of flight mass spectrometer. The instrument was operated at 10,000 resolution (W mode) with dynamic range enhancement that attenuates large-intensity signals. The cone voltage was 60eV. Spectra were acquired at 16666 Hz pusher frequency covering the mass range of 100 to 1200 u and accumulating data for 2 s per cycle. Mass correction for exact mass determinations was made automatically with the lock mass feature in the MassLynx data system. A reference compound in an auxiliary sprayer was sampled every third cycle by toggling a "shutter" between the analysis and reference needles. The reference mass was used for a linear mass correction of the analytical cycles. Samples were presented in acetonitrile as a 20ul loop injection using an autoinjector (LC PAL, CTC Analytics AG, Zwingen, Switzerland).

9,10-Epoxy Methyl Stearate (5). A solution of methyl oleate (4.5 g, 15 mmol) in 100 mL dichloromethane was stirred at 0°C, and a solution of mCPBA (**4**) (7.9 g, 46 mmol) in 50 mL dichloromethane was added gently. After completion, the temperature was raised to room temperature and the mixture was stirred for another 18 h. Subsequently, the solvent was removed via a rotary evaporator. In a separatory funnel, the crude material was washed with 2 x 120 mL saturated sodium bisulfite solution and extracted with 2 x 150 mL diethyl ether. The ethyl ether solution was separated and washed with 120 mL sodium bicarbonate. The organic layer was dried over anhydrous magnesium sulfate and filtered, and the solvent was removed by a rotary evaporator. The crude material was purified by column chromatography (silica; hexane/ethyl acetate 99:1 to 80:20 gradient), producing 9,10-epoxy methyl stearate (**5**) as a clear oil in 87% yield after drying under high vacuum. ^{1}H NMR ($CDCl_3$, 500 MHz): δ 3.61 (s, 3 H), 2.84 (m, 2 H), 2.25 (t, J = 7.5 Hz, 2 H), 1.57 (m, 2 H), 1.50-1.17 (m, 24 H), 0.83 (t, J = 7.6 Hz, 3 H).

9,10-Dihydroxy Methyl Stearate (6). **5** (3.0 g, 9.6 mmol) was stirred with 15 mL perchloric acid (10% in water) in 150 mL THF/water (3/2) for 20 h. Subsequently, 120 mL diethyl ether was added, and the aqueous layer was removed in a separatory funnel. The organic layer was then washed with 2 x 150 mL saturated sodium bicarbonate, dried over anhydrous magnesium sulfate, and filtered. After the solvent was removed with a rotary evaporator, the crude material was purified by column chromatography (silica; hexane/ethyl acetate 99:1 to

80:20 gradient) and dried under high vacuum to obtain a white powder in 80% yield. O^{18} labeled **6** for mechanistic study was synthesized in 1/10 scale. ^{1}H NMR ($CDCl_3$, 500 Mhz): δ 3.66 (s, 3 H), 3.39 (m, 2 H), 2.29 (t, *J* = 7.5 Hz, 2 H), 2.1 (bs, 2 H), 1.57 (m, 2 H), 1.55-1.20 (m, 24 H), 0.87 (t, *J* = 7.6 Hz, 3 H).

Reaction of Epoxide 5 and Diol 6 in the Presence of CF_3SO_3H. A 2:1 mixture of **5** (0.06 g, 0.192 mmol) and **6** (0.0317g, 0.096 mmol with 10 w/w % of trifluoromethanesulfonic acid (0.006 g, 0.039mmol) in $CDCl_3$ (200μL) in an NMR tube (3 mm). ESI-MS, ^{1}H NMR and ^{1}H-^{1}H COSY in $CDCl_3$ (500 MHz) were acquired. Key signals were identified for **7**: δ 3.22 and 3.31 (R"R'HCOC(R_2)-$H_{alcohol}$ for various R' and R"); δ 3.53 (broad) for various HOC(R_2)-H_{ether}. A side product [9(10)-hydroxy-10(9)-di (or tri) stearate (**8**)] resulting from transesterification was detected: δ 4.81 $RCO_2CR'R"$ and alcohol signal coupling with ester at δ 3.57 in **8**.

Reaction of Epoxide 5 in the Presence of H_3PO_4. Compound **5** (0.06g, 0.192 mmol) with 10 w/w % H_4PO_3 (85% solution in water) (0.006 g, 0.06mmol) in $CDCl_3$ (200μL) in an NMR tube (3 mm). ESI-MS, ^{1}H NMR and 2D ^{1}H-^{1}H COSY in $CDCl_3$ (500 MHz) were acquired.

Reaction of Epoxide 5 and Diol 6 in the Presence of H_3PO_4. A 2:1 mixture of **5** (0.06 g, 0.192 mmol) and **6** (0.0317 g, 0.096 mmol) together with 10 w/w % (0.006 g, 0.06mmol) of H_3PO_4 were agitated in $CDCl_3$ (200 μL) within an NMR tube (3 mm). ESI-MS, ^{1}H NMR and 2D ^{1}H-^{1}H COSY in $CDCl_3$ (500 MHz) were acquired. For a kinetic NMR experiment that avoided unclear analysis interrupted by water signal in spectrum, 99.99% phosphoric acid was used. Disappearance of the epoxide chemical shift in the mixture of starting materials [**5**: δ 2.84 ($CH_{epoxide}$); **6**: δ 3.39 (HOC-$H_{alcohol}$] as well as appearance of product **7** and **9-17** [δ 3.53-3.63 (COC(R_2)-H_{ether}); δ 4.09-4.32 [(R'-O)$_2$(O)POC(R_2)-$H_{phosphate}$)] was monitored by ^{1}H NMR spectroscopy at room temperature.

Reaction of 5 with *i*-Propanol in the Presence of H_3PO_4. A solution of 9,10-epoxy methyl stearate (**5**) (0.50 g, 1.66 mmol) and 10 wt% (0.05g) phosphoric acid (85% solution in water) in isopropanol (10mL, 130.78mmol) was stirred continuously at room temperature for 12 h. After purification by column chromatography (hexane/ethyl acetate gradient 99/1 to 90/10), **9a,b** was obtained as a light yellow oil (yield: 0.36 g, 0.96 mmol). ^{1}H NMR ($CDCl_3$, 500 MHz, integrals were set for a 1:1 mixture of **9a** and **9b**): δ 3.66 (m) and 3.65 (s) (both signals have a combined integral of 8 H), 3.55 (m, 2 H), 3.44 (m, 2 H) 3.16 (m, 2 H), 2.29 (t, *J* = 7.3 Hz, 4 H), 1.60 (m, 4 H), 1.50-1.17 (m, 48 H), 1.15 (d, *J* = 6.1 Hz, 3 H), 1.13 (d, *J* = 6.1 Hz, 3 H), (t, *J* = 6.8

Hz, 6 H). Diol **6** was isolated as a side product that eluted after **9a**/**9b** from the silica column (yield: 0.12 g, 0.36 mmol, white powder).

Reaction of Epoxide 5 and Diol 6-(^{18}O) in the Presence of H_3PO_4. (**a**) 2:1 mixture of **5** (0.6 g, 1.92 mmol) and **6** (0.317 g, 0.96 mmol) with 10 w/w % phosphoric acid (85% in water, 0.06 g), and (**b)** 2:1 mixture of **5** (0.6 g) and **6-(^{18}O)** (0.0317 g) with 10 w/w % phosphoric acid (85% in water, 0.06 g) were stirred in a round-bottom flask in CH_2Cl_2 (0.3ml) at room temperature for 12 h. ESI-MS and ^{1}H NMR spectra were acquired.

Peel strength of the PSAs. The 90 ° peel adhesion test was conducted according to ASTM method D3330/D3330M-04 (ASTM, 2004). The glass specimen was placed on a fixture clamped to the moving steel panel of the peel adhesion tester (Vertical Motorized Test Stand, MV-110-S). The non-adhesive-coated end of each strip was doubled back at a 90 ° angle and clamped into the moving jaw to ensure a peel angle of 90 ° during peel testing.

2.4. Results and discussion

After treating mixtures of ESO (**1**) and HSO (**2**) in methylene chloride (50 w/w % solution) with H_3PO_4 (10 w/w % of ESO) for 10 min, we noticed an increase in viscosity and stickiness. After overnight drying at room temperature on a polyterephthalate (PET) film, the ESO/HSO polymer formed and had considerable peel strength. Peel strength was affected by the ratio of **1** to **2**. By using a 2:1 mixture of **1** and **2**, we obtained a stronger peel adhesion strength than commercial Scotch Magic Tape® (**Fig. 2.1**). Changing the ratio to 4:1 and reducing the amount of H_3PO_4 to 5% (w/w) resulted in decreased peel strength.

However, despite outstanding peel strength of 2:1 (ESO:HSO) with 10 w/w % H_3PO_4, the adhesive disintegrates noticeably, rendering an oil, in 1 month. A newly appeared carboxylic peak at 1710 and increase of broad hydroxyl band at 3200-3550 from glycerol on Fourier transform infrared (FTIR) spectra (**Fig. 2.2a**) demonstrate that triglyceride ester linkages were broken in the presence of moisture via acid-catalyzed ester hydrolysis (Smith and March 2001). To enhance the adhesive's shelf life, liquid-liquid extraction was conducted; however, the polar tackifier (HSO) was washed out with the water layer even after several centrifuge trials at 3000 rpm for 15 min. This loosened adhesion properties to a degree that was easily noticed by hand after drying. Therefore, we reduced the amount of H_3PO_4 available to be consumed by

establishing phosphate cross-linkage (Guo et al. 2007). Tracking the progression of reducing epoxide [δ 2.84 ($CH_{epoxide}$)] monitored by ^{1}H NMR spectroscopy revealed that reducing the amount of phosphoric acid resulted in its complete consumption (**Fig. 2.2b**). Concentrations of epoxide were determined for each data point by ^{1}H NMR integration of the CH-epoxide signal. Based on this result, we obtained a much longer shelf life of PSA with 5% (w/w) H_3PO_4; we found no degradation into oil in atmosphere for more than 6 months.

To understand the nature of the underlying polymeric networks on a chemical level, we invoked the possibility of both phosphate ester and polyether linkages. (**Scheme 2.1**). The formation of 2-hydroxyphosphates from epoxides and phosphoric acid consistent with pathway a is well documented (Aberathy and Laurent 1993; Long and Pritchard 1956; Moghadam et al. 2004). Furthermore, ample precedence has been provided for the establishment of ether networks from the acid-catalyzed reaction of epoxides with nucleophilic alcohols via an activated monomer mechanism (AM) (Nyk et al. 1991; Penczek et al. 1986) consistent with pathway b (Kwart and Goodman 1960; Parker and Isaacs 1959). If pathway b contributes to the overall polymeric network at least in part, calculated addition of polyols to the reaction mixture would amplify initiation events during polymerization. This would allow for the control of molecular weight at a level suitable for generation of PSAs.

To understand and manipulate polymer formation from **1** and **2** in the presence of H_3PO_4, we embarked on mechanistic investigations into the establishment of chemical connections in the cross-links. In so doing, we substituted soybean oil derivatives **1** and **2**, which constitute *mixtures* of triglyceride esters, with less complex single-chain model compounds **5** and **6**; compound **5** was derived from epoxidation of methyl oleate (**3**) with meta-chlorobenzoic acid, (**4**) (**Scheme 2.2a**).

To probe for the possibility of an acid-catalyzed polymerization analogous to pathway a (**Scheme 2.1**), we mixed **5** and **6** in the presence of the strong acid trifluoromethanesulfonic acid (CF_3SO_3H), which, unlike phosphoric acid (H_3PO_4), is not as not prone to form esters easily with alcohols or epoxides. A rapid gelation occurred within 1-2 s of adding CF_3SO_3H, and subsequent ^{1}H NMR analysis revealed the formation of **Polymer-5-6-T** (**Scheme 2.2b**), containing a mixture of short chain polyethers (**7**). Their structural identity was confirmed by 2D ^{1}H-^{1}H COSY nuclear magnetic resonance (NMR) (**Fig. 2.3a**); the cross-peaks between two alcoholic C-H signals (H_{alc-1}, **Scheme 2.1**) at δ 3.31 and 3.22 that were residing in the direct vicinity of ether

linkages (H_{ether}) at δ 3.51 (**Scheme 2.1**) were particularly revealing. During the reaction, 9(10)-hydroxy-10(9)-di (or tri) stearate (**8**) (**Scheme 2.1**) was produced as a by-product from acid-catalyzed transesterification (Saravanan et al. 2010); this was verified by a cross-peak between an esterified secondary alcohol signal (H_{ester}, δ 4.81) and a separate alcohol signal (H_{alc-3}, δ 3.57) (**Fig. 2.3**).

Electrospray ionization mass spectroscopy (ESI-MS) of **Polymer-5-6-T** revealed the presence of oligomer **7a-b**, which contained 2-3 repeat units (m/z = 665.5, 977.8). No incorporation products containing the CF_3SO_3-moieties was observed by ESI-MS.

The formation of **Polymer-5-6-P** from 2:1 mixtures of **5** and **6** in the presence of H_3PO_4 was followed by ^{1}H NMR spectroscopy in $CDCl_3$. Product signals at δ 3.5 (H_{ether}, **Fig. 2.4**), δ 3.31, and 3.22 (H_{alc-1}) were nearly identical to ^{1}H NMR signals from **Polymer-5-6-T** (**Scheme 2.2b**) and indicate that polyether formation does, in fact, occur in the reaction of **5** and **6** in the presence of H_3PO_4. In addition, we detected phosphate ester ($H_{phosphate}$) signal at δ 4.04 and its vicinity alcohol signal at δ 3.5 (H_{alc-2}) overlapped with the ether signal as well as cyclic phosphate ($H_{phosphate}$) signal overlapped with phophate ester; we attributed this to the presence of phosphoric acid (**Scheme 2.1**) (Derouet et al. 2001; Maffei and Buono 2003; Pouchert and Behnke 1993). Rapid early growth of the signal at δ 4.04 was interpreted as the initial buildup of a monophospate-moieties (**Scheme 2.3a**, m = 1).

The ESI-MS spectra of **Polymer-5-6-P** in the positive ion mode showed Na^+-adducts of polyethers **7a-c** (**Scheme 2.2b**) as well as tertiary phosphate esters **10-12**. Compound **11** represents a hybrid system that contains ethers and phosphate linkages. In contrast, acidic primary and secondary phosphate esters **13-17** were detected in the negative ion mode as [M-H^+] phosphate anions. In comparison, **Polymer-5-6-T** (formed from **5** and **6** and trifluoromethanesulfonic acid) displayed peaks from polyethers **7a-b** (as Na^+ adducts). This highlights that phoshate ester formation occurs *parallel* with polyether formation. The reaction of **5** with H_3PO_4 in the absence of **6** produced the expected signals associated with phosphate ester cross-linkages δ 4.09 ($H_{phosphate}$) and ether moieties at δ 3.51 (H_{ether}).(**Fig. 2.5**) Moreover, the appearance of diol **6 (**δ 3.39) from apparent epoxide hydrolysis was detected. This demonstrates that the nature of cross-links is identical in both **Polymer-5-P** and **Polymer-5-6-P**. Apparently, their different material properties are consequences of different molecular weights,

which, in turn, are modulated by the relative abundances of epoxide **5** and diol **6** in the original mixture.

Tracking the formation of **Polymer-5-6-P** from epoxide **5,** diol **6,** and H_3PO_4 by ^1H NMR spectroscopy (**Fig. 2.6**) revealed a near-constant ratio of total ether integral to total phosphate ester integral over the course of the reaction (1:1.4). We also found that diol **6**, which was absent at the beginning of the reaction, was built up over time, presumably from hydrolysis of **5** and residual water from the 85% H_3PO_4 solution. Two possible routes (Pathways 1 and 2, **Scheme 2.3b**) could explain the formation of (poly) ethers under the reaction conditions. In pathway 1, diol **6** acts as the nucleophile to attack an activated oxonium species **A** (derived from O-protonation of **5**) in an *alcoholysis* reaction. The formed 'dimer' **7** would engage in further attacks on **A** in the context of a living polymerization. This route would therefore incorporate exactly one molecule **6** into the growing chain. In the alternative pathway 2, intermediate **A** is nucleophilically attacked by another epoxide molecule **5** to form trialkyloxonium species **B**. Polymerization would continue in this manner until hydrolysis occurs in the termination step. Unlike Pathway 1, no incorporation of diol **6** into the growing chain would be expected in Pathway 2.

To assess the general viability of alcoholysis reactions involving epoxide **5** (in accordance with pathway 1 in **Scheme 2.3b**), we substited diol **6** in an exploratory experiment with the secondary alcohol *i*-propanol, which has spectroscopically distinct features. Mixing one equvalent of epoxide **5** with a 78-fold excess of *i*-propanol in 10 wt.% of H_3PO_4 (85 % solution in water) produced the regioisomeric alcoholysis products **9a-b** in 60 % isolated yield (**Fig. 2.7a**), whereas diol **6** was formed in 22.5% due to hydrolysis. ^1H NMR spectroscopy of **9a-b** revealed the presence of both alcoholic and ethereal C-H bonds in a 1:1 ratio by integration (**Fig. 2.8a**). With the help of ^1H-^1H COSY NMR (**Fig. 2.7c**), we were able unambiguously to identify the signal for the isopropyl-ether proton (C-H^k in **Fig. 2.7**) at δ 3.64 due to its its cross-peaks with characteristic isopropyl methyl signals at δ 1.10 and δ 1.07. Further analysis of the ^1H-^1H COSY NMR spectrum revealed the occurrence of a set of diastereotopic protons for either H^e or H^h with a combined total of three different signals. This indicates the proximity of H^e and H^h to a nearby stereocenter(s) consistent with the chiral nature of **9a-b**. A similar splitting also occurred for the diastereotopic methyl groups bearing H^l. This observation confirms the stereospecific attachment of the isopropyl group to a chain that already contains stereocenters, which is expected for an

S_N2 attack of the alcohol to a *cis*-epoxide **5**. The complete chemical shift assignment can be found in Scheme 3. A silent ^{31}P NMR spectrum (**Fig. 2.8b**) for **9a-b** confirms the notion that phosphate esters are *not* part of this covalent scaffold. To spike the absent of phosphate ester linkages, triphenyl phosphate (0.04 mg) was added in **9a-b** solution in $CDCl_3$ (0.6 mL) as a dection limit, then there was merely phosphate signal of tripheny phosphate was detected in 31P NMR spctrum. The formation of hydroxyethers **9a-b** is in support of the general feasibility of an alcoholysis reaction (pathway 1, **Scheme 2.3b**). The 3:1 product ratio of alcoholysis adducts **9a-b** and hydrolysis product **6** compared to a 311:1 ratio of *i*-propanol and water (from the 85% aqueous solution of H_3PO_4) mean that the relative rate of alcoholysis to hydrolysis is 1:103.

Although alcoholysis is possible in principle with **5** and an excess of a secondary alcohol, we still needed to differentiate unambiguously between pathway 1 and pathway 2 during polyether formation in **Polymer-5-6-P** (**Scheme 2.3b**). Using isotopically labeled starting materials of diol **6-(^{18}O)** would allow us to use mass spectroscopy to determine the potential incorporation of the diol into polymeric products (**Scheme 2.4**).

For that purpose, we synthesized the mono-^{18}O-enriched diol **6-(^{18}O)** from acid-catalyzed hydrolysis of epoxide **5** and $H_2{}^{18}O$. Subsequently, a 2:1 mixture of **5** and **6-(^{18}O)** was reacted in the presence of 10 wt.% H_3PO_4 (*5 % solution in water), and the resultant product mixture [**Polymer-5-6-(^{18}O)-P]** was analyzed by ESI-MS (**Scheme 2.4b**). Compounds **7a-(^{18}O)** and **7b-(^{18}O)** were identified as mono-labeled ethers with isotopic enrichments of ≥95%. Interestingly, the trimeric bis-ether **7b-(^{18}O)** also carried only one ^{18}O-label. The formation of **7a-(^{18}O)** and **7b-(^{18}O)** provides strong evidence for an alcoholysis mechanism (Pathway 1, **Scheme 2.3b**) based on the nucleophilic attack of **6-(^{18}O)** to unlabeled intermediate **A** to form **7a-(^{18}O)** in the initiation step. Addition of 'dimer' **7a-(^{18}O)** to another unlabeled molecule **A** produced *mono*-labeled trimer **7b-(^{18}O)**, underscoring a living polymerization mechanism. This is consistent with the view that **6-(^{18}O)** is an initiator but not a propagator.

The ESI-MS spectrum of **Polymer-5-6-(^{18}O)-P** in the negative ion mode produced peaks for **13**, **14**, and **15** as the phosphate-containing species in this run (**Scheme 2.4b**). None of these signals displayed appreciable ^{18}O-incorporation (<5%). This finding supports the notion that phosphate ester cross-links are generated from **5** and H_3PO_4 but *not* from potential condensation reactions between **6-(^{18}O)** and H_3PO_4.

2.5. Conclusions

Copolymerization of epoxidized and hydroxylated soybean oils (**1** and **2**) in the presence of phosphoric acid produced a substance with potential for PSA applications. To elucidate the chemistry bias and understand the chemical nature of the PSA, mechanistic studies of this reaction were conducted on an analogous single-chain epoxide and diol model systems **5** and **6**. In the reaction of **5** with H_3PO_4 (85% in water), the phosphate ester cross-linkages in the resultant product were formed in the absence of added alcohols. However, partial hydrolysis of **5** with residual water from the aqueous H_3PO_4 produced **6** in situ, leading to additional ether-moieties in the polymeric network. Similarly, the reaction of **5**, **6**, and H_3PO_4 produced a polymer that contained both ether-moieties as well as phosphate ester units in the polymer backbone. In contrast, polymerizations of **5** and **6** in the presence of CF_3SO_3H produced only the expected polyether network. In studies with model compound **5** and excess isopropanol with H_3PO_4, acid-catalyzed alcoholysis was the main reaction in the epoxide functionalization. This result highlights that alcoholysis reactions can become the main reaction pathway (at the expense of phosphate ester formation) if ratios of alcohol and H_3PO_4 are adjusted.

The role of **6** as a nucleophilic initiator in the formation of polyethers from **5** and **6** (and by analogy **1** and **2**) was confirmed in studies with the mono-^{18}O-labeled compound **6-(^{18}O)**, which produced mono-^{18}O-labeled ether dimer **7a-(^{18}O)** and mono-^{18}O-labeled ether trimer **7b-(^{18}O)**. Mechanistically, a picture arises in which *O*-protonated oxonium ion **A** is subjected to nucleophilic attack by either diol **6** or its counter-anion $H_2PO_4^-$ (**Scheme 2.5**).

The former pathway produces a dimeric diol **7a** that can subsequently react with another epoxide molecule **5** (without any further involvement of **6**). The latter pathway can produce mono-, di-, and tri-phosphate esters with **5**. Phosphoric acid and diol **6** do not form covalent bonds with each other.

In summary, the model system study confirmed the reaction pathways and provided better understanding of ESO (**1**) and HSO (**2**). We believe that this principle study on the identification of chemical pathways of epoxidized and hydroxylated fatty acid monoester and triglycerides with phosphoric acid can provide a rational platform for optimization of their properties and a reaction methodology
for versatile applications.

Figure 2.1. Peel adhesion strength of commercial tapes and the bio-based PSAs controlled by ratio of ESO (1) to HSO (2) and H_3PO_4.

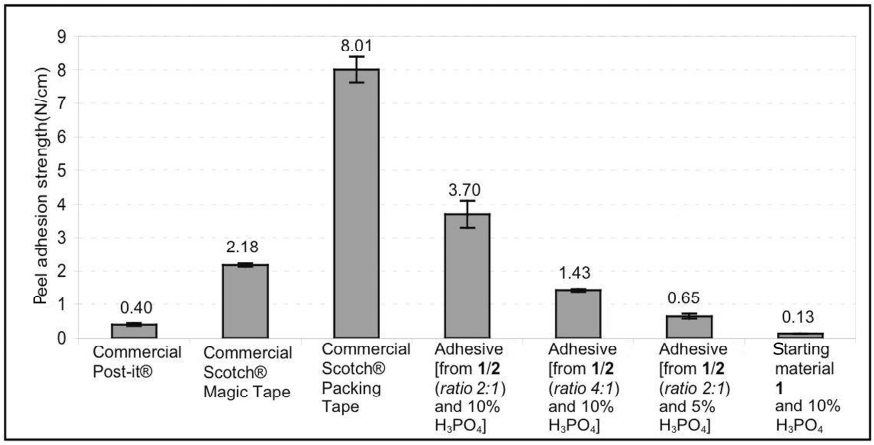

Figure 2.2. a: FTIR spectra of Polymer-1-2-P after one day (bottom) and one month (top), b: Concentration of epoxide in Polymer-5-6-P with 5 w/w % and 10 w/w % tracked by NMR integration

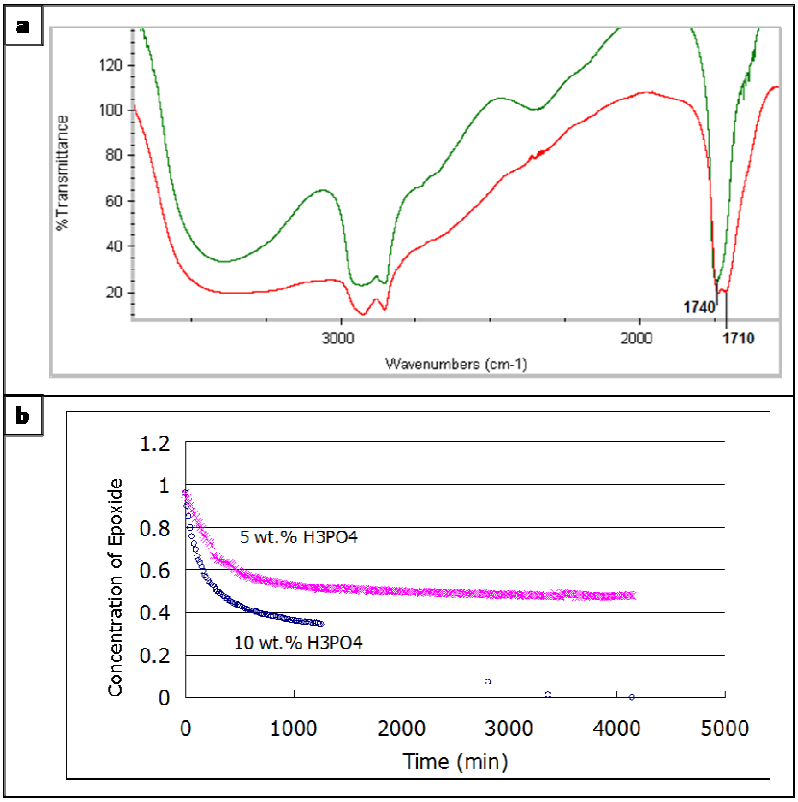

Figure 2.3. a: ^{1}H NMR, b: ^{1}H -^{1}H COSY NMR of Polymer-5-6-T: cross peaks at δ 3.22 and 3.31 respectively coupling with δ 3.51 of 7 and cross peaks at δ 3.57 and 4.81 of side product 8

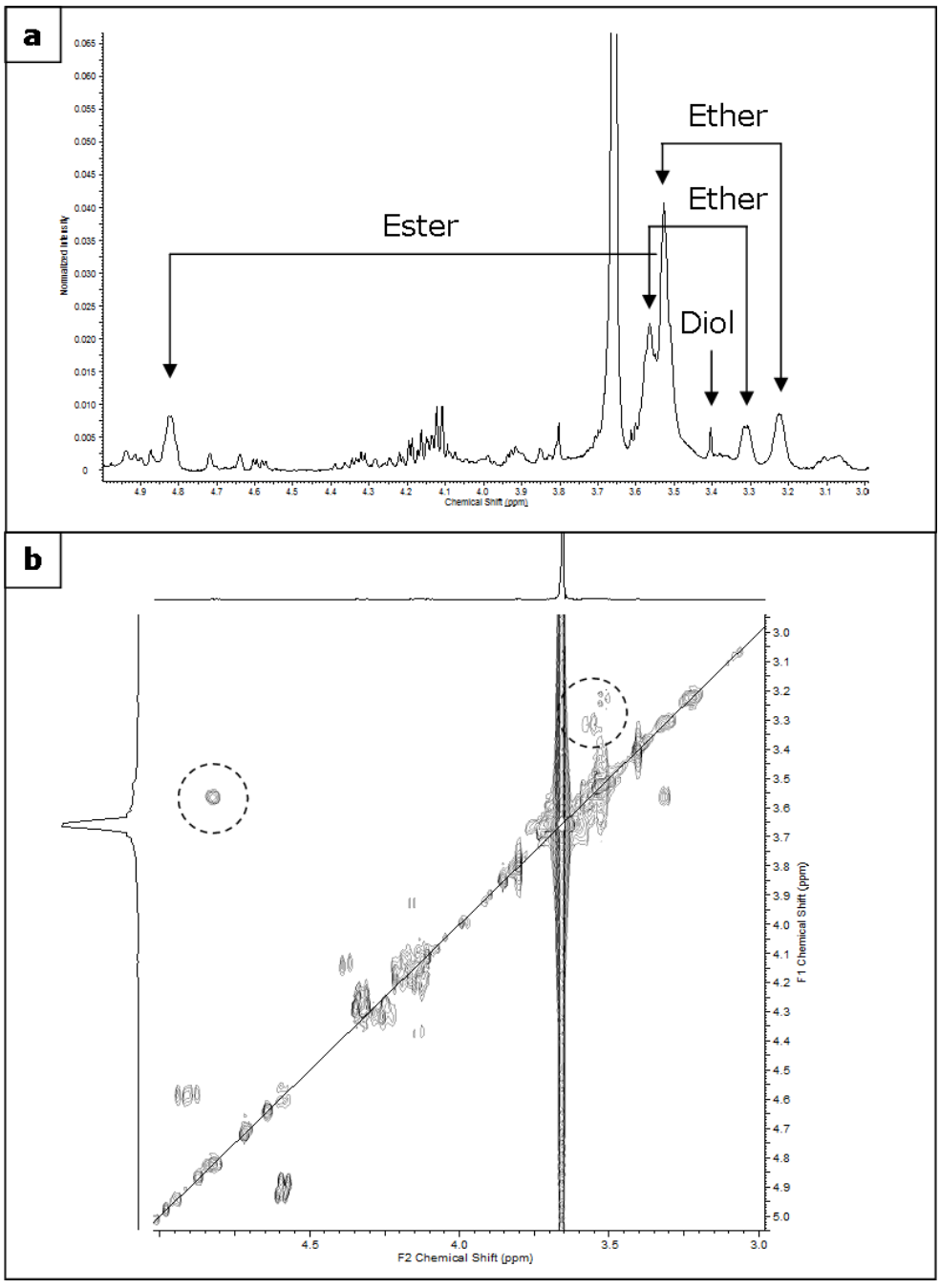

Figure 2.4. a: ^{1}H NMR, b: ^{1}H -^{1}H COSY NMR of Polymer-5-6-P; cross-peaks between at δ 4.04 and 3.5 from phosphate ester and its vicinity alcohol; between δ 3.5 and 3.31, 3.22 from ether and its vicinity alcohols

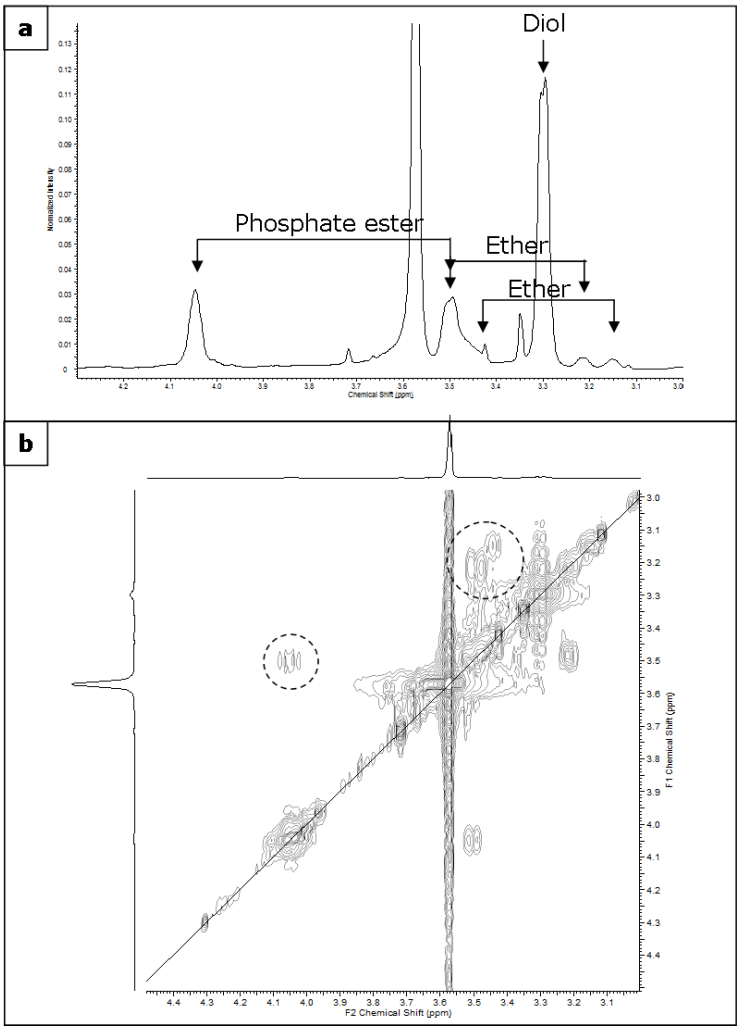

Figure 2.5. ^{1}H NMR of phosphate esters (δ 4.09), ethers (δ 3.51), and dihydroxide 6 (δ 3.39) in Polymer-5-P

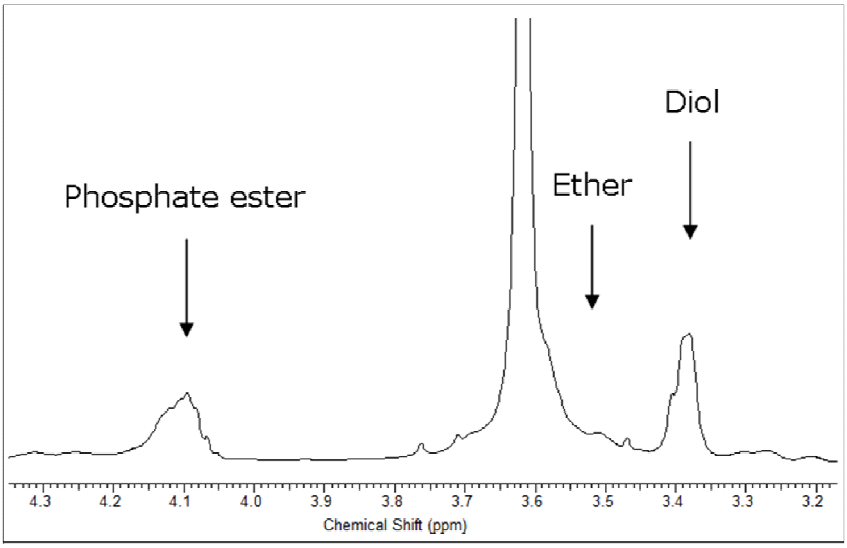

Figure 2.6. Concentrations of epoxides, phosphate esters, ethers, and dihydroxide 6 in Polymer-5-6-P from NMR integration using a methyl group (δ 0.88) as a quantitative internal standard

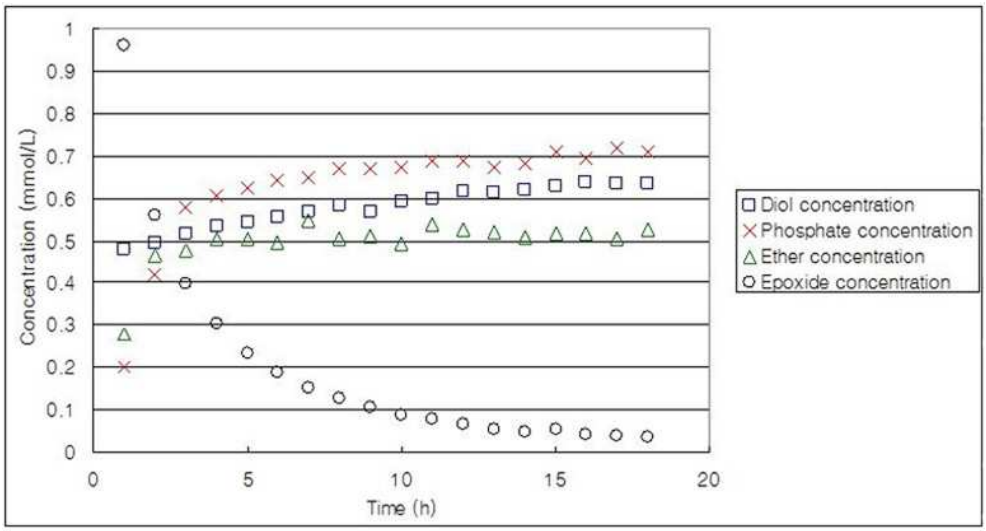

Figure 2.7. a: Isopropyl alcoholysis of 5 and chemical shift assignment for protons in the mixture of regioisomers 9a-b), b: ^{1}H NMR spectrum of isolated compound 9a-b formed from alcoholysis of 5 and isopropanol with labeling of all pertinent protons H^{a-l}, c: ^{1}H-^{1}H COSY experiment of 7; highlighted are key cross-peaks for the coupling between an ethereal C-H bond (H^{f}, $H^{g'}$) at δ 3.38 and vicinal alcoholic C-H bond ($H^{f'}$, H^{g}) at δ 3.1, and (H^{k}, H^{l})/($H^{k'}$, $H^{l'}$) for the coupling between the isopropyl ether proton at δ 3.68 and adjacent methyl groups at δ 1.07 and δ 1.10

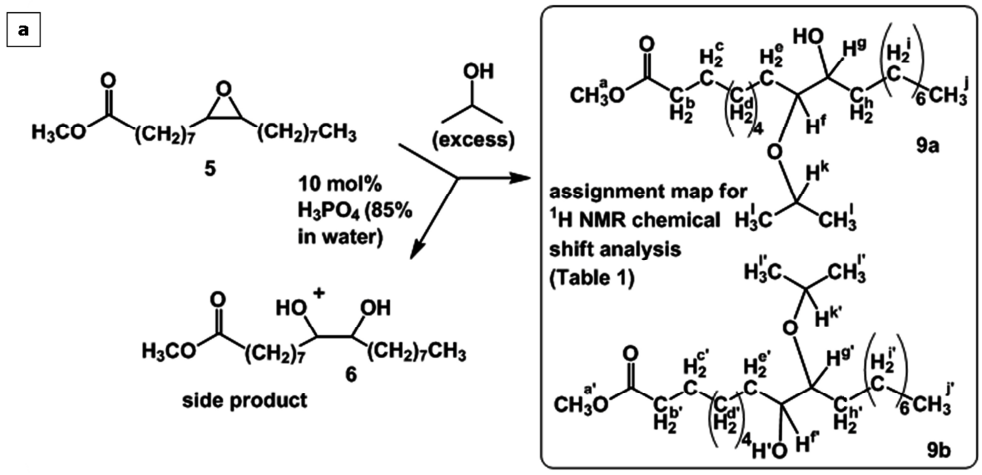

Set of protons	H^{a} $H^{a'}$	H^{b} $H^{b'}$	H^{c} $H^{c'}$	H^{d} $H^{d'}$ H^{i} $H^{i'}$	H^{e} $H^{e'}$ H^{h} $H^{h'}$	H^{f} $H^{g'}$	H^{g} $H^{f'}$	H^{j} $H^{j'}$	H^{k} $H^{k'}$	H^{l} $H^{l'}$	OH OH′
Chemical shift	3.63	2.29	1.60	1.24	1.40 1.35 1.32	3.38	3.1	0.87	3.64	1.07 1.10	3.55

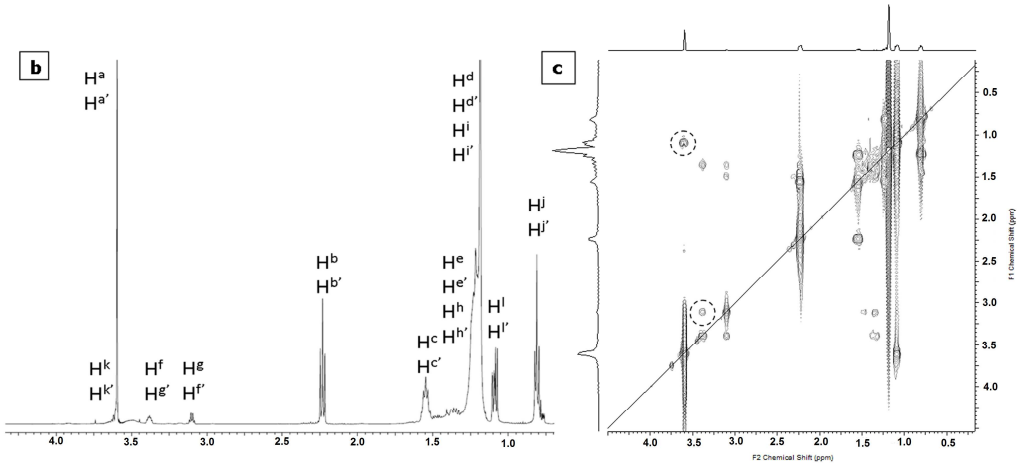

Figure 2.8. a: The alcoholic and ethereal C-H bonds integration of ^{1}H NMR of isolated compound 9a-b, b: ^{31}P NMR of 9a-b

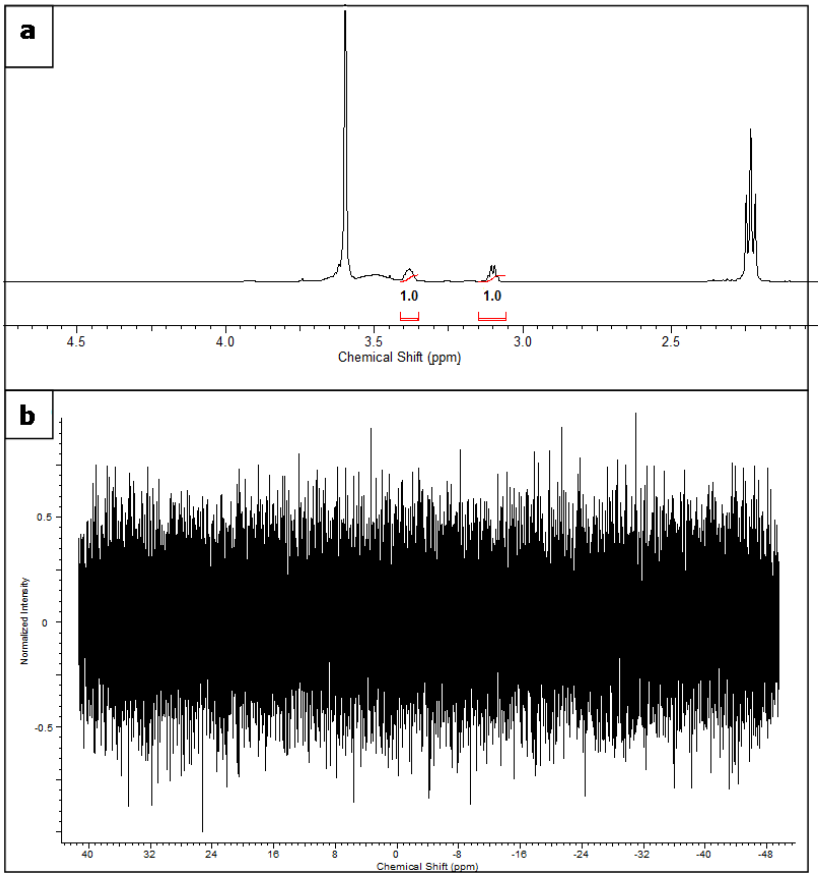

Scheme 2.1. Proposed chemical pathway a and b in Polymer-1-2-P formed from epoxidized soybean oil (1) and hydroxylated soybean oil (2) in the presence of H_3PO_4

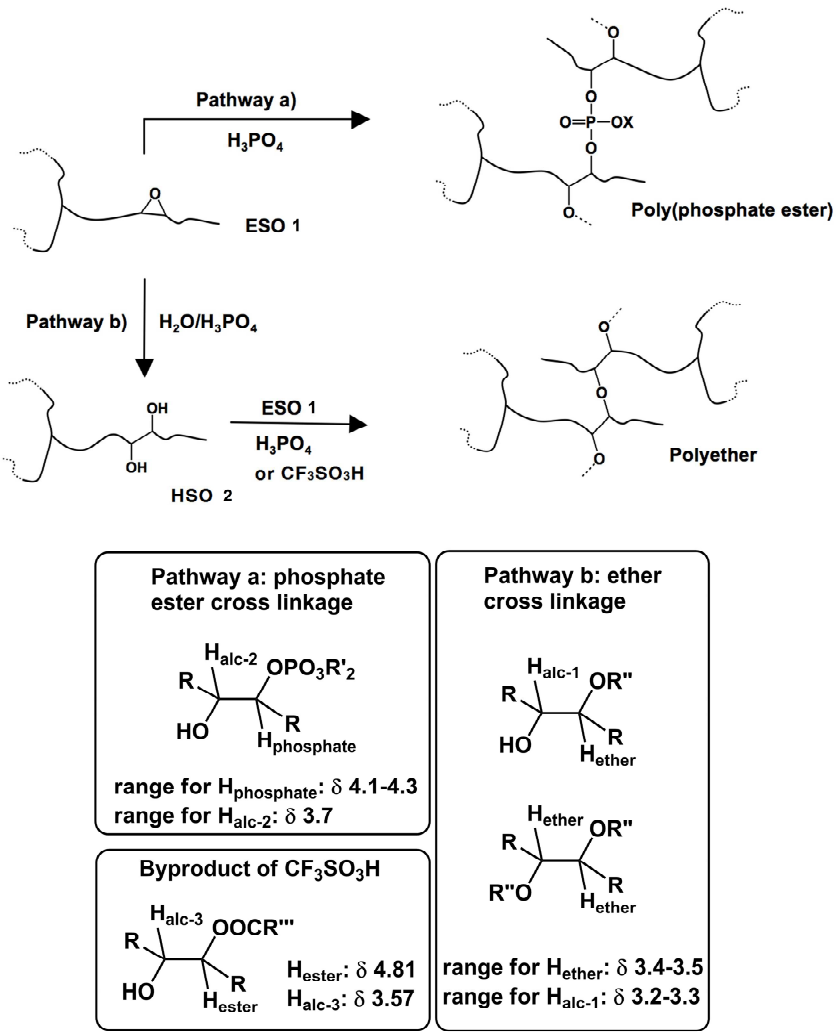

Scheme 2.2. a: Model systems 5 and 6 forming Polymer-5-6-P, b: Polymerization of 5 and 6 (2:1 ratio) in the presence of CF_3SO_3H.

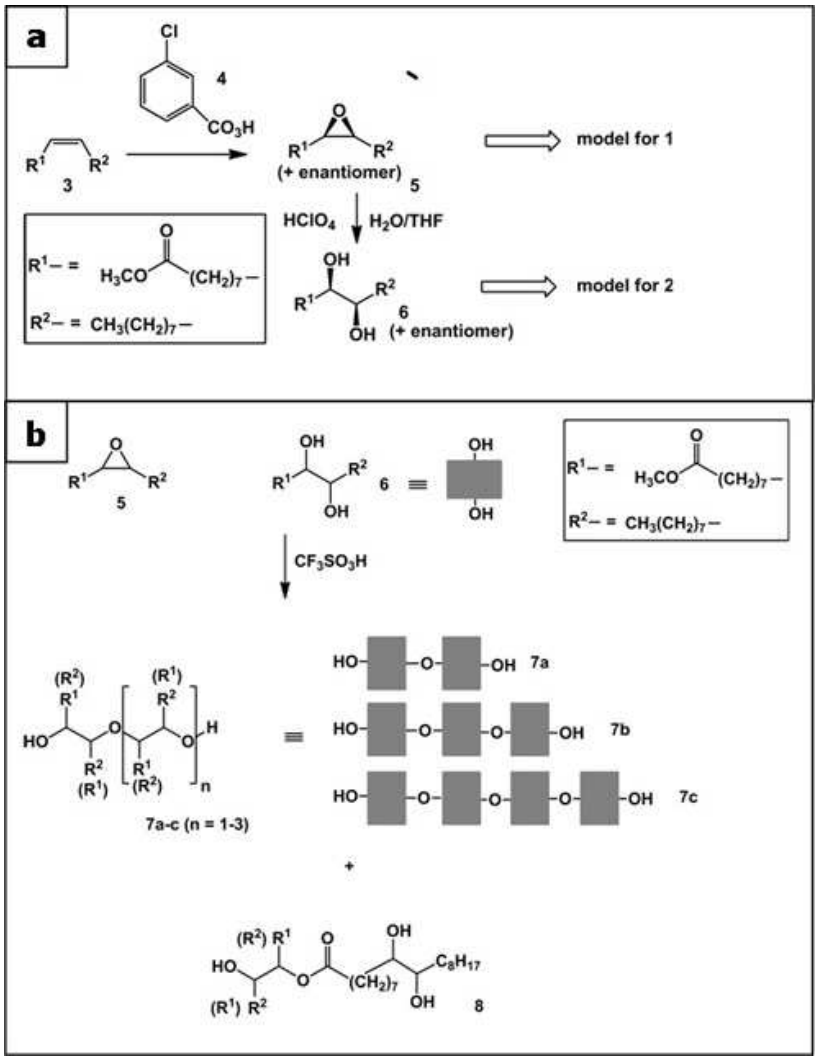

Scheme 2.3. a: Proposed cross-linkages b: proposed polymerization pathway 1 and 2.

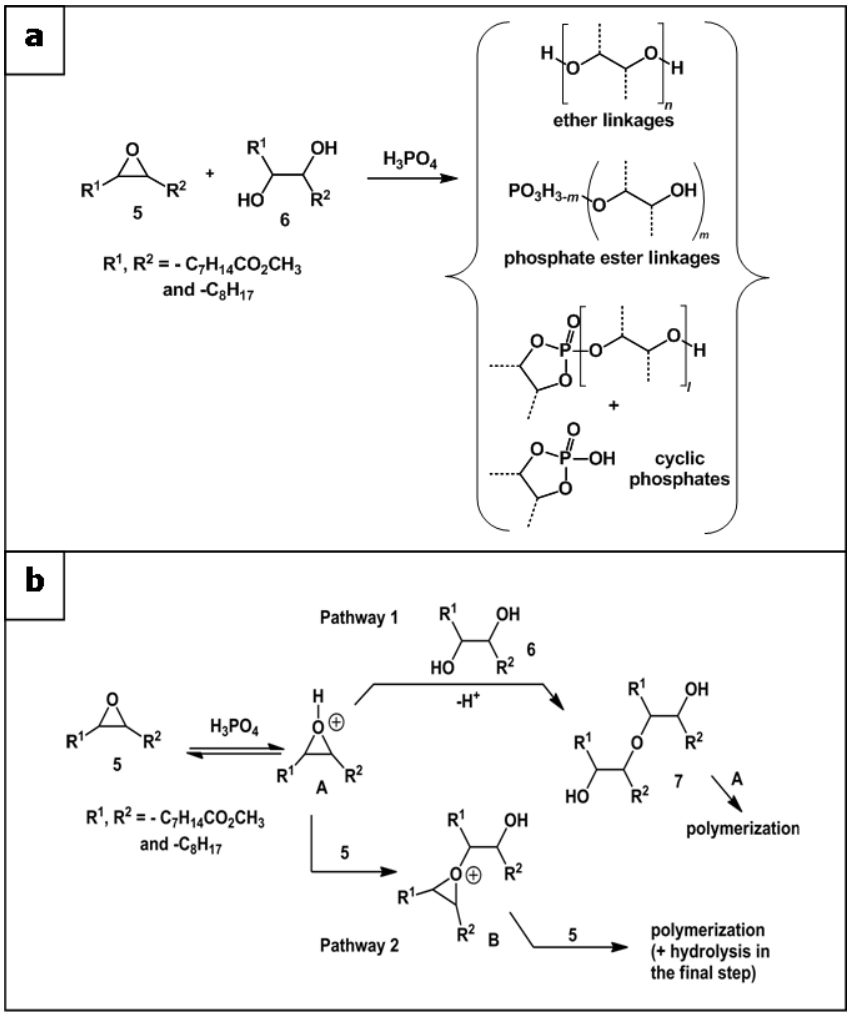

Scheme 2.4. a: Reactions of 5 and 6 in the presence of H_3PO_4: Main product distribution in Polymer-5-6-P, b: Product distribution in polymer-5-6-(^{18}O)-P in the reaction of 5 with 6-(^{18}O) and H_3PO_4

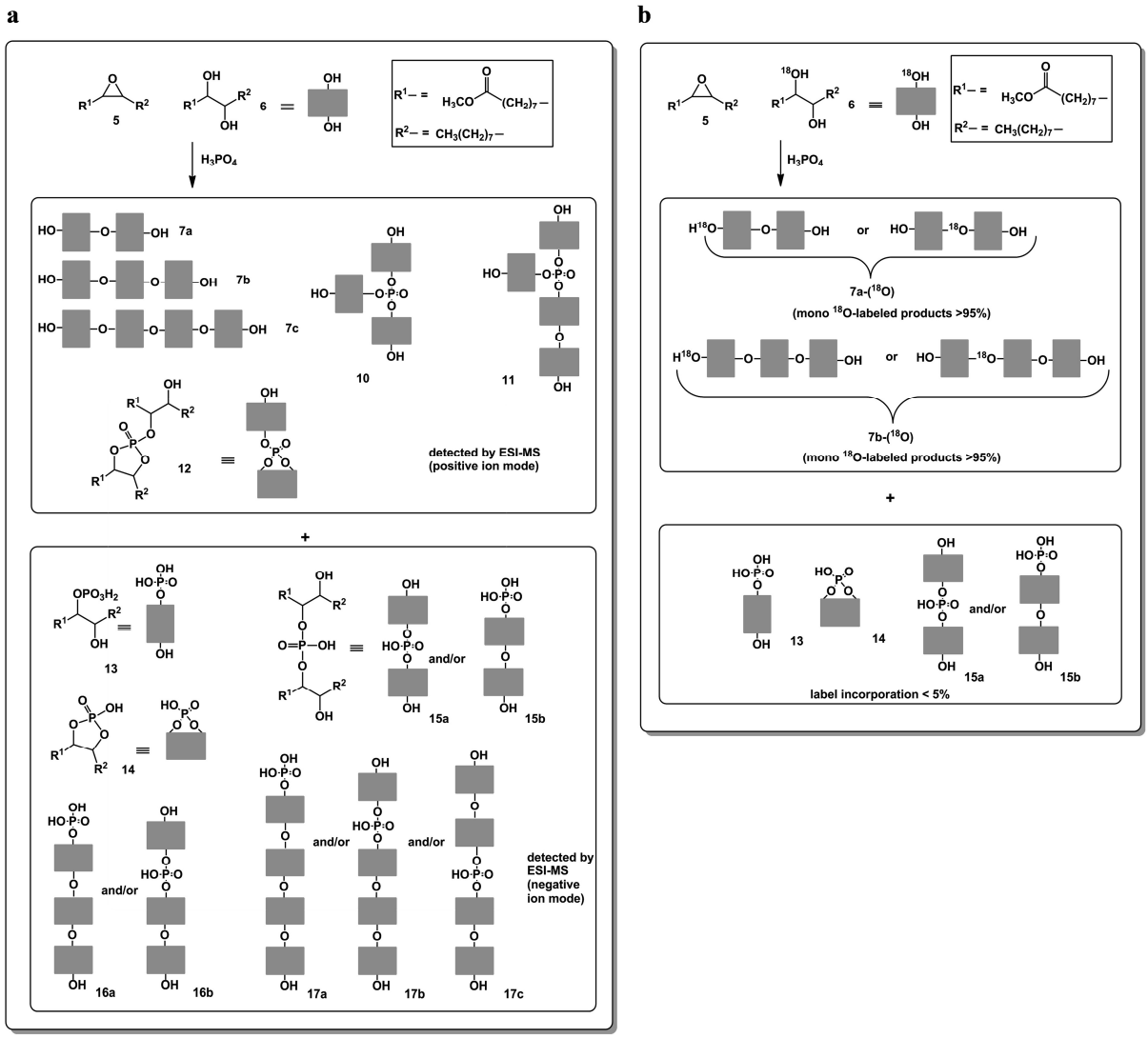

Scheme 2.5. Proposed mechanism of ether and phosphate ester cross-link formation

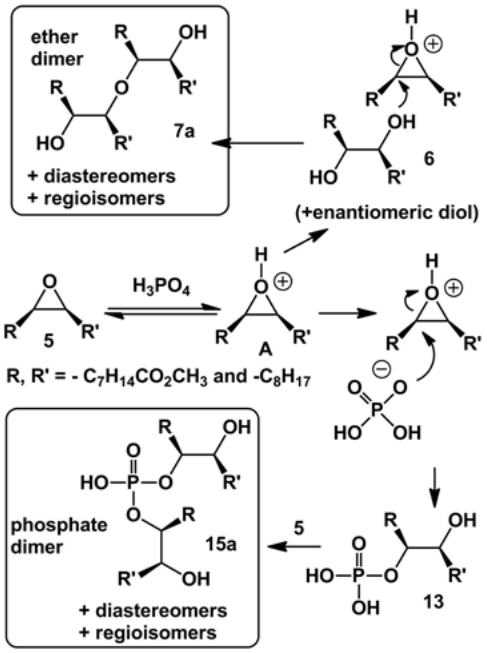

2.6. References

Aberathy, S. M. and Laurent, J. W. 1993. Hydrolysis of phosphate-based aviation hydraulic fluids. Journal of Synthetic Lubrication 10:107-118.

Bunker, S., Staller, C., Willenbacher, N. and Wool, R. 2003. Miniemulsion polymerization of acrylated methyl oleate for pressure sensitive adhesives. International Journal of Adhesion and Adhesives 23:29-38.

Cakmakli, B., Hazer, B., Tekin, I. O. and Comert, F. B. 2005. Synthesis and characterization of polymeric soybean oil-g-methyl methacrylate (and n-butyl methacrylate) graft copolymers: Biocompatibility and bacterial adhesion. Biomacromolecules 6:1750-1758.

Chakraborti, A. K., Rudrawar, S. and Kondaskar, A. 2004. European Journal of Organic Chemistry:3597.

David, S. B., Sathiyalekshmi, K. and Raj, G. A. G. 2009. Studies on acrylated epoxydised triglyceride resin-co-butyl methacrylate towards the development of biodegradable pressure sensitive adhesives. Journal of Materials Science-Materials in Medicine 20:61-70.

Derouet, D., Morvan, F. and Brosse, J. C. 2001. Chemical modification of 1,4-polydienes by di(alkyl or aryl)phosphates. European Polymer Journal 37:1297-1313.

Guo, Y. Z., Hardesty, J. H., Mannari, V. M. and Massingill, J. L. 2007. Hydrolysis of epoxidized soybean oil in the presence of phosphoric acid. Journal of the American Oil Chemists Society 84:929-935.

Klapperich, C. M., Noack, C. L., Kaufman, J. D., Zhu, L., Bonnaillie, L. and Wool, R. P. 2009. A novel biocompatible adhesive incorporating plant-derived monomers. Journal of Biomedical Materials Research Part A 91A:378-384.

Kwart, H. and Goodman, A. L. 1960. The Acid-catalyzed ring openeing of epichlorohydrin. Journal of the American Chemical Society 82:1947-1949.

Lligadas, G., Ronda, J. C., Galia, M., Biermann, U. and Metzger, J. O. 2006. Synthesis and characterization of polyurethanes from epoxidized methyl oleate based polyether polyols as renewable resources. Journal of Polymer Science Part a-Polymer Chemistry 44:634-645.

Long, F. A. and Pritchard, J. G. 1956. Hydrolysis of substituted ethylene oxides in H2O18 solutions. Journal of the American Chemical Society 78:2663-2667.

Maffei, M. and Buono, G. 2003. A two step synthesis of 2-oxo-2-vinyl 1,3,2-dioxaphospholanes and -dioxaphosphorinanes. Tetrahedron 59:8821-8825.

Moghadam, M., Tangestaninejad, S., Mirkhani, V. and Shaibani, R. 2004. Rapid and efficient ring opening of epoxides catalyzed by a new electron deficient tin(IV) porphyrin. Tetrahedron 60:6105-6111.

Nyk, A., Klosinski, P. and Penczek, S. 1991. Water-swelling hydrolyzable gels through polyaddition of H3PO4 to diepoxides. Makromolekulare Chemie-Macromolecular Chemistry and Physics 192:833-846.

Parker, R. E. and Isaacs, N. S. 1959. Mechanisms of epoxide reactionas. Chemical Reviews 59:737-799.

Penczek, S., Kubisa, P. and Szymanski, R. 1986. Activated monomer propagation in cationic polymerizations. Makromolekulare Chemie-Macromolecular Symposia 3:203-220.

Pouchert, C. J. and Behnke, J. 1993. The Aldrich library of ^{13}C and ^{1}H FT NMR spectra. Aldrich Chemical Co.: Milwaukee.

Saravanan, N., Puhan, S., Nagarajan, G. and Vedaraman, N. 2010. An experimental comparison of transesterification process with different alcohols using acid catalysts. Biomass & Bioenergy 34:999-1005.

Schilling, P. 1986. Cationic bituminous emulsions and emulsion aggregate slurries, C08K 5/20 (20060101) B01F 17/00 (20060101) C08K 5/00 (20060101): US Patent 4597799.

Smith, M. B. and March, J. 2001. March's Advanced Organic Chemistry: Reactions, Mechanisms and Structure. Wiley Interscience: New york.

Tsujimoto, T., Uyama, H. and Kobayashi, S. 2004. Synthesis and curing behaviors of cross-linkable polynaphthols from renewable resources: Preparation of artificial urushi. Macromolecules 37:1777-1782.

Zhong, B., Shaw, C., Rahim, M. and Massingill, J. 2001. Novel coatings from soybean oil phosphate ester polyols. Journal of Coatings Technology 73:53-57.

Chapter 3 - Thermally Stable Transparent Pressure Sensitive Adhesives from Epoxidized and Dihydroxyl Soybean Oil

[This work has been published: Ahn, B. K., Kraft, S., Wang, D., & Sun, X. S. (2011). *Biomacromolecules*, *12*(5), 1839-1843]

3.1. Abstract

Thermal stability and optical transparency are important factors for flexible electronics and heat-related applications of pressure sensitive adhesives (PSAs). However, current acryl- and rubber-based PSAs cannot attain the required thermal stability, and silicon-based PSAs are much more expensive than the alternatives. Oleo-chemicals including functionalized plant oils have great potential to replace petrochemicals. In this study, novel bio-based PSAs from soybean oils were developed with excellent thermal stability and transparency as well as peel strength comparable to current PSAs. In addition, the fast curing (drying) property of newly developed bio-based PSAs is essential for industrial applications. The results show that soybean oil-based PSA films and tapes have great potential to replace petro-based PSAs for a broad range of applications including flexible electronics and medical devices because of their thermal stability, transparency, chemical resistance, and potential biodegradability from triglycerides.

3.2 Introduction

Limited fossil fuel resources have necessitated the engineering of affordable and durable materials from renewable natural resources (Belgacem and Gandini 2008; Bozell and Patel 2006; Crivello and Narayan 1992; Lligadas et al. 2006b; Park et al. 2004). Vegetable oils and modified vegetable oils have become attractive sustainable alternatives to petroleum-based materials for industrial applications such as soaps, lubricants, coatings, paints, and, more recently, bioplastics and composites due to their biodegradability and low toxicity (Andjelkovic and Larock 2006; Liu et al. 2007; Robertson et al. 2010; Xia and Larock 2010). Epoxidation of plant oils is inexpensive and efficient, with conversion rates of up to 98% because of their built-in double bonds (Holland et al. 2003; Lligadas et al. 2007; Sharma et al. 2006). Epoxidized triglycerides or

fatty acid esters have been used as plasticizers and stabilizers for polyvinyl chloride (PVC) or as co-reactants for epoxy resins (Chakraborti et al. 2004; Schilling 1986). Epoxidized plant oils were cross-linked recently with inorganic chemicals to obtain organic-inorganic hybrid materials (Ballard et al. 1999; Lligadas et al. 2006b; 2007; Sharma et al. 2006; Uyama et al. 2003). Furthermore, various cationic polymerizations and radical reactions of epoxidized triglycerides or epoxidized methyl oleate (EMO) can be achieved by photo-initiation (Crivello and Narayan 1992), latent catalysts (Park et al. 2004), or strong acid catalysts ($HSbF_6$) (Andjelkovic and Larock 2006; Ballard et al. 1999; Lligadas et al. 2006a; Uyama et al. 2003). Epoxidized soybean oil (ESO) has been used to prepare hydrogels using Lewis acid (BF_3) (Xu et al. 2008) and coatings using phosphoric acid (Zhong et al. 2001). Research efforts have been made to use EMO for pressure sensitive adhesives (PSAs) using acrylated methyl oleate with about 10% petro-based additives [e.g., methyl methacrylate (MMA)] (Bunker et al. 2003; Bunker and Wool 2002; Klapperich et al. 2009). Copolymer derived from acrylated epoxidized triglyceride resin and butyl methacrylate was studied for biodegradable medical PSA applications (David et al. 2009). The main challenge in commercializing these Oleo-based PSA technologies is longer curing time (i.e., Bunker et al (2003); Bunker and Wool (2002) and Klapperich et al (2009) did not clearly report, and David et al (2009) denoted 15 to 60 min at 100 °C), which is not acceptable to industry. In addition, petrochemicals such as 1,4-butanedial diacrylate (BDDA) and MMA are needed to facilitate cross-links (Bunker et al. 2003; Bunker and Wool 2002; Klapperich et al. 2009). In this study, we designed and synthesized a fast-curing copolymer from ESO and dihydroxyl soybean oil (DSO) for PSA applications without using petrochemicals.

ESO PSAs are particularly good candidates for application in advanced flexible electronic devices because of their thermal properties. Organic materials have become attractive over current silicon-based systems not only to reduce cost but also to allow roll-to-roll processing. However, most current flexible petroleum-based plastics and PSAs (e.g., acrylates and rubbers) have fairly low thermal stability as indicated by a glass transition temperature (T_g) range from 80 to 160 °C, a melting point (T_m) from 120 to 160 °C, and large coefficient of thermal expansion (CTE) above 50 ppm K^{-1} (e.g., acryl resin 86 ppm K^{-1} and rubber 231 ppm K^{-1}), all of which limit their uses for flexible electronics or other heat-related applications (Bettinger and Bao 2010; Cheng et al. 2009; Nogi et al. 2009; Nogi and Yano 2008). The high transparency of the ESO PSA is especially useful for e-paper or digital display applications. In

this study, we demonstrated attractive thermal properties (low T_g, high T_m, and low CTE) and transparency of ESO PSA I.

3.3. Materials and Methods

Model system (EMO) for NMR analysis: 9,10-epoxidized methyl oleate (EMO) was prepared following the method described by Holland et al (2003). Then the EMO polymer was prepared: EMO (0.06 g, 0.192 mmol) was agitated with 5 w/w % (0.003 g, 0.03 mmol) H_4PO_3 (85% solution in water) in $CDCl_3$ (200 µL) for 1 min then transferred to an NMR tube (3 mm).

NMR analyses. ^{1}H NMR spectra for the EMO polymer were recorded quantitatively using a Varian S spectrometer (Varian Inc., Palo Alto, CA) at observing frequencies of 500 MHz for ^{1}H on a 3 mm penta probe. The sample solutions were prepared in $CDCl_3$ at 25 °C. ^{1}H NMR spectra were obtained with 32 scans at a delay time of 1 s between scans. 2D ^{1}H-^{1}H COSY spectra for the EMO polymer were obtained with 128 increments and 4 scans for each increment. A sine bell function was used during processing for both dimensions.

Preparation of ESO PSA film. ESO PSA film without addition of DSO was prepared in a petri dish for CTE, DSC, TGA, transmittance, and photo image characterization. ESO (1.0 g, 10 mmol) was dissolved in methyl acetate (1 mL) and cooled to 0 °C, then 5 % (w/w) H_3PO_4 (0.005 g, 0.51 mmol) was added to the ESO solution. The solution was agitated in a warmed sonicator bath (50 °C) and on a vortex for 5 min, then poured into a petri dish and kept in atmosphere for 24 h. The ESO was purchased from Scientific Polymer Products, Inc., Ontario, NY. non-crosslinked ESO was slightly viscous than unmodified soybean oils at room temperature (La Scala and Wool 2005).

Fourier transform infrared spectroscopy (FTIR). FTIR of ESO PSA film and non-cross-linked ESO were obtained using FT-IR/FT-NIR spectrometer (Perkin Elmer Spectrum 400).

Static mechanical tensile test. The tensile test was conducted with dynamic mechanical analysis (Perkin Elmer DMA 7e) based on ASTM standard (ASTM D882-10). All tests were conducted with a preload of 100 mN and a force ramp rate of 10 mNm^{-1}. The sample width and thickness were measured using standard calipers (Mitutoyo).

Thermal properties of ESO PSA film. The CTEs of ESO PSA film (10 mm x 5 mm) were measured using dynamic thermomechanical analysis (Perkin Elmer DTMA 7e) following ISO,

ASTM standard (ISO 11359, ASTM E831) and the method of Nogi et al.[20] at a heating rate of 5 °C min^{-1} in helium atmosphere under tensile mode with 1 mN load. The CTE values were the mean values at 20 to 150 °C. Thermal transitions (T_g and T_m) were obtained with a TA DSC Q200 instrument. About 5 mg of ESO PSA film sample was sealed in a hermetic pan. The sample was heated from -80 to 250 °C at a rate of 10 °C/min, isothermally conditioned at -80 °C for 5 min, and the freeze-dried sample was heated at the same rate. The samples were characterized in an inert environment by using nitrogen with a gas flow rate of 50 mL/min. Decomposition characteristics were determined with a Perkin-Elmer Pyris1 TGA (Norwalk, CT). About 5 mg of each sample was placed in the pan and heated from 40 to 800 °C at a heating rate of 20 °C/min under air atmosphere.

Transmittance. Light transmittances were measured by UV spectrometer (Hewlett-Packard 8453). The thickness of specimens was 0.36 mm for ESO PSA, 0.91 mm for glass, 0.27 mm for PP, and 0.1 mm for PE.

DSO synthesis. ESO (20 g, 20 mmol) was stirred in 500 mL THF/water (300 mL:200 mL) with 1% (v/v) of perchloric acid for 20 h at room temperature. Subsequently, diethyl ether (150 mL) was added, and perchloric acid was removed in aqueous layer via repeated washing in a separatory funnel with saturated sodium bicarbonate until a pH test litmus paper strip read 7.0. The organic layer was dried over anhydrous magnesium sulfate and celite-filtered. The solvent was removed with a rotary evaporator and dried under high vacuum to obtain sticky clear oils in 80% yield (colorless oil). ^{1}H NMR ($CDCl_3$, 500 MHz): δ 5.23 (m, 1H), 4.26 (m, 2H), 4.11 (dd, *J* = 11.7 Hz, *J* = 6.2 Hz, 2H), 4.20, 3.99, 3.91, 3.71, 3.57, 3.43, 3.34 (a total of hydroxyl multiplets; the combined integral was approx. 10H), 2.25 (t, *J* = 7.5 Hz, 2H), 1.68-1.17 (m, approx. 46.5H), 0.86 (m, 9H).

Preparation of ESO PSA tapes. Mixtures of ESO (1 g, 1.5 g, 2 g) and DSO (1 g) at ratio of 1:1, 1.5:1, and 2:1 by weight, respectively, were dissolved in methyl acetate (2 mL) to obtain a dilute solution, then cooled to 0 °C. Then H_3PO_4 was added to the solution at 4, 5, and 6% (w/w), respectively, based on ESO concentration. The solution was agitated in a sonicator bath at 50 °C for 30 s and then on a vortex mixer at room temperature for 30 s; this agitating was repeated 5 times (for 5 min). An appropriate amount of methyl acetate (4 mL) was added to the solution to facilitate easy spreading over a 75 cm^2 carrier, either PET film (200 gauge, adhesive-treated side) or aluminum foil (non-shiny side). The ESO PSAs were then dried at 75 °C and

110 °C for 15, 30, 45, and 60 s, respectively, with a hair dryer (Revlon 1875 W) at low or high rate. The distance between tape and dryer was 3.5 mm.

Peel strength of ESO PSAs. The 90 ° peel adhesion test was conducted according to ASTM method D3330/D3330M-04 (ASTM, 2004). The glass specimen was placed on a fixture clamped to the moving steel panel of the peel adhesion tester (Vertical Motorized Test Stand, MV-110-S). The non-adhesive-coated end of each strip was doubled back at a 90 ° angle and clamped into the moving jaw to ensure a peel angle of 90 ° during peel testing. The speed of the moving jaw for the peel test was 5.0 ± 0.2 mm/s. Data were collected after the first 25 mm of tape was peeled, and average peel adhesion strength was obtained for peeling the rest of the tape. Reported values are the average of the three replications for each treatment.

3.4. Results and Discussion

To create a strong scaffold with adhesive properties that has potential PSA applications, introduced functional groups have to both establish polymeric networks and provide polar functional groups. We proposed a chemical scaffold using ESO as the starting material. ESO was polymerized in the presence of phosphate acid to form a co-polymeric matrix consisting of phosphoric ester and ether cross-linkages; DSO synthesized from the ESO was added to ESO at a designed ratio to improve tackiness, thus providing more hydroxyl moieties (Fig. 3.1).

Functional groups of ESO PSA were confirmed by FTIR. Epoxide band (Guo et al. 2007; Lligadas et al. 2006b) at 824 cm^{-1} almost disappeared while new bands appeared at 3500 cm^{-1} (alcohol groups (Lligadas et al. 2006b)), at 1075 cm^{-1} (ether cross-linkage (Lligadas et al. 2006b)), and at 1002 cm^{-1} (phosphate ester (Guo et al. 2007)), maintaining triglycerides at 1740 cm^{-1} (Fig. 3.2).

This chemistry was confirmed by using one- and two-dimensional NMR studies (Fig. 3.3) with a model system using epoxidized methyl oleate (EMO) to avoid the influence of the complexity of multiple functional moieties in triglycerides. NMR spectra indicated dihydroxyl sites [RC(*H*)(OH)C(*H*)(OH)R'] doublet signal in ^{1}H NMR at δ 3.38, 3.39 coupled each other in ^{1}H-^{1}H COSY NMR, ethers [RR'C(*H*)O-ether] signal at δ 3.50 and δ 3.55 coupled respectively with vicinity alcohol [RC(*H*)(OH)C(H)(R')O-ether] signal at δ 3.20 and δ 3.30 and phosphate ester [RR'C(*H*)O-phosphate ester] triplet signal (mono-, di-, tri-ester (Guo et al. 2007)) at δ 4.10-

4.30 coupled with vicinity alcohol signal [RC(*H*)(OH)C(H)(R')O-phosphate ester] at δ 3.60 (Fig. 3.3). This chemical structural NMR analysis of EMO/H_3PO_4 demonstrated that the EMO polymer from EMO/H_3PO_4 consists of diol, ether, ester and alcohol corresponding to the functional sites of ESO/ H_3PO_4 revealed in FTIR (Fig. 3.2).

The newly developed ESO PSA had small linear CTE (14.08 ppm K^{-1}) comparable to the CTE of glass (8.5 ppm K^{-1}), and much lower than that of most flexible plastics (approx. 50 ppm K^{-1}). This is a great advantage of ESO PSA for heat-relative application compared to current acryl- and rubber PSAs. But we should limit its application in PSA uses with a carrier instead of plastic or thin film because it is unable to stand itself as a thin film due to its low young's modulus (2.05 MPa) and tensile strength (0.16 MPa). The mechanical strength of the ESO PSA film may be improved by several recently developed reinforcement techniques, but in this study we focused on the PSA application. The differential scanning calorimetry (DSC) (Fig. 3.4) indicated the ESO PSA has great thermal stability (e.g., T_g was -34.29 °C and T_m of ESO PSA were above 250 °C) compared to other PSAs and flexible plastics including polyisoprene, polyacrylate (PMMA) (T_m is about 160 °C), polyethylene (PE) (T_m is about 120-150 °C), and polypropylene (PP) (T_m is about 160 °C). After freeze-drying ESO PSA, water moieties trapped in its matrix were decreased, the T_g was reduced to -39.23 °C and crystallization was observed at 160 °C (Fig. 3.4). This demonstrates that the ESO PSA film contained moisture with multiple -OH groups in its matrix. Thermogravimetric Analysis (TGA, Fig 3.5) indicated that the thermal degradation of the ESO PSA was 388 °C.

The light transmittance of the elastomer was above 90% in visible range (390 to 750 nm), which is comparable to glass (microscope slide) transparency and much higher than PE and PP. In addition, the ESO PSA was more optically stationary than other flexible plastics. At 300 nm, above 80% of light passed through the ESO PSA while glass blocked above 90% of light (Fig. 3.6).

In designing the ESO PSA, ensuring desirable properties by balancing the resin ratio of tacky groups and the degree of cross-linking is important. A strong cross-link makes the film too stiff, or cohesion failure occurs if the cross-link is not stronger than the adhesion force (Pocius 1997). DSO was added as a tackifier to provide more tacky sites to ESO PSAs. Because obtaining a fast reaction and short curing time was essential for commercialization in terms of manufacturing process, we targeted a curing time of no more than 60 s, which we achieved by air

drying to remove the solvent. The ESO PSAs were dried on the adhesive-treated side of polyethylene terephthalate (PET) film. Various conditions (ratio, time, temperature) were adjusted for optimum peel strength of PSAs. Based on a preliminary peel strength test, we selected several samples with varied ratios of ESO/DSO/H_3PO_4 mixture using PET plastic film as a carrier. The ESO PSA of 1.5:1 [ESO/DSO (w/w)] with 5% (w/w) H_3PO_4 (ESO PSA I) showed the fastest drying time (30 s) at 110 °C and had comparable peel strength without cohesion failure (clear removal) (Fig. 3.7). The ESO PSA I dried at 110 °C for 45 s had an optimum peel strength of 0.77 N/cm (Fig. 3.7) with glass as a substrate.

The ESO PSA I was selected and evaluated using aluminum foil as carrier, and the peel strength on glass substrate was 2.18 N/cm at 30 s drying, which was comparable to Scotch Magic Tape and much stronger than Post-it Notes (3M, St. Paul, MN; Fig. 3.8). Reusability of the ESO PSA I with PET film as a carrier on glass substrate had comparable peel strength to Post-it Notes during 10 repetitions (Fig. 3.9).

In addition, the ESO PSA I was tolerant to organic solvents as well as water; after it dried, it was not soluble with most organic solvents including chloroform, methane chloride, tetrahydrofuran, ethyl acetate, methyl acetate, acetone, ethyl ether, dimethylformamide and hexane.

3.5. Conclusion

We designed and synthesized the ESO PSA I formula via one-pot, single-step, fast reaction (5 min) at moderate temperature (50 °C) and the ESO PSA tapes were produced at 110 °C within 30 s through a simple air-drying process. The peel strength of the ESO PSA tapes was comparable to commercial PSA tapes such as Post-it Notes and Scotch Magic Tape.

More interestingly, the ESO PSA I had attractive thermal stability: T_g of -34.29 °C, T_m of above 250 °C, and CTE of 11.5 ppm K^{-1}. Furthermore, the ESO PSA I exhibited transparency (above 90% transmittance in visible range) similar to glass. In addition, the ESO PSAs had no interactions with most organic and inorganic chemicals. The newly developed ESO PSAs have great potential to replace the petro-based PSAs in a broad range of applications such as transparent tapes for labeling and packaging, reusable tapes, and flexible electronics such as displays, semiconductors, and solar cells as well as medical and pharmaceutical devices such as

skin wound care treatments and biological adhesives (Lee et al. 2007; Mahdavi et al. 2008). ESO PSAs have thermal stability, optical transparency, chemical resistance, and are potentially biodegradable with triglycerides. We are exploring this biobased material for further applications in our laboratory.

Figure 3.1. Chemical structure of ESO, DSO, and co-polymeric matrix of ESO PSA

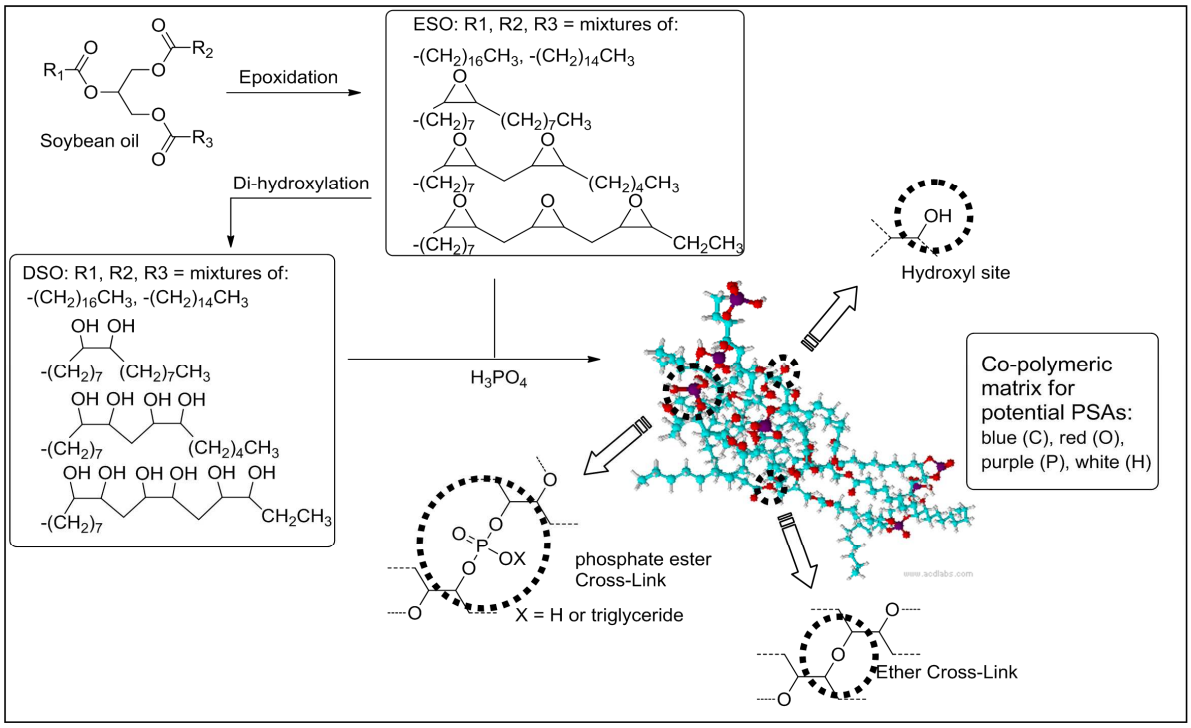

Figure 3.2. FTIR spectrum of ESO PSA and non-cross-linked ESO

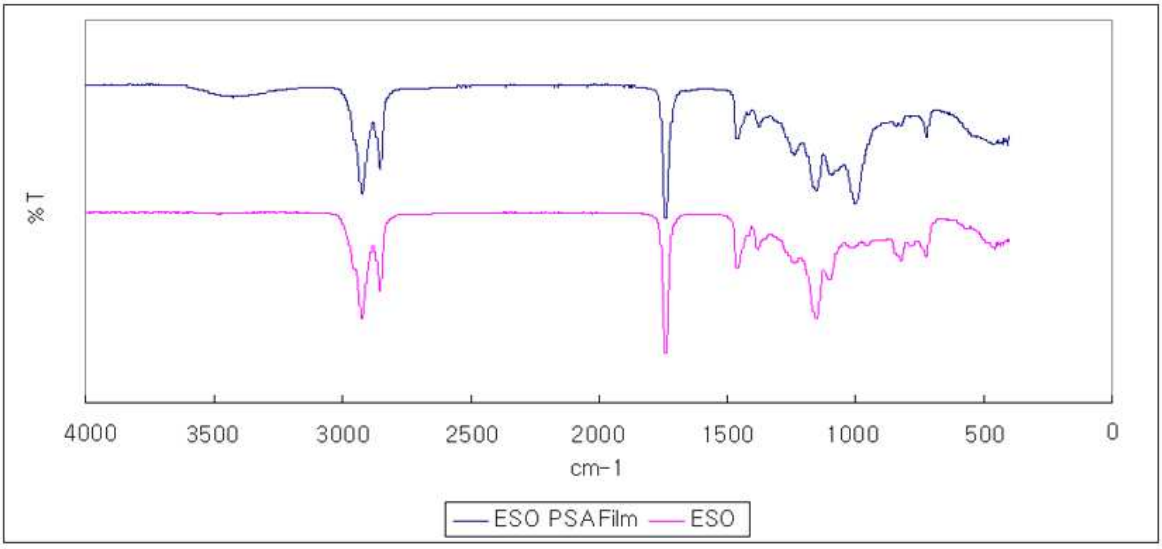

Figure 3.3. ^{1}H NMR (left) and ^{1}H-^{1}H COSY NMR (light) of EMO polymer (EMO/ H_3PO_4)

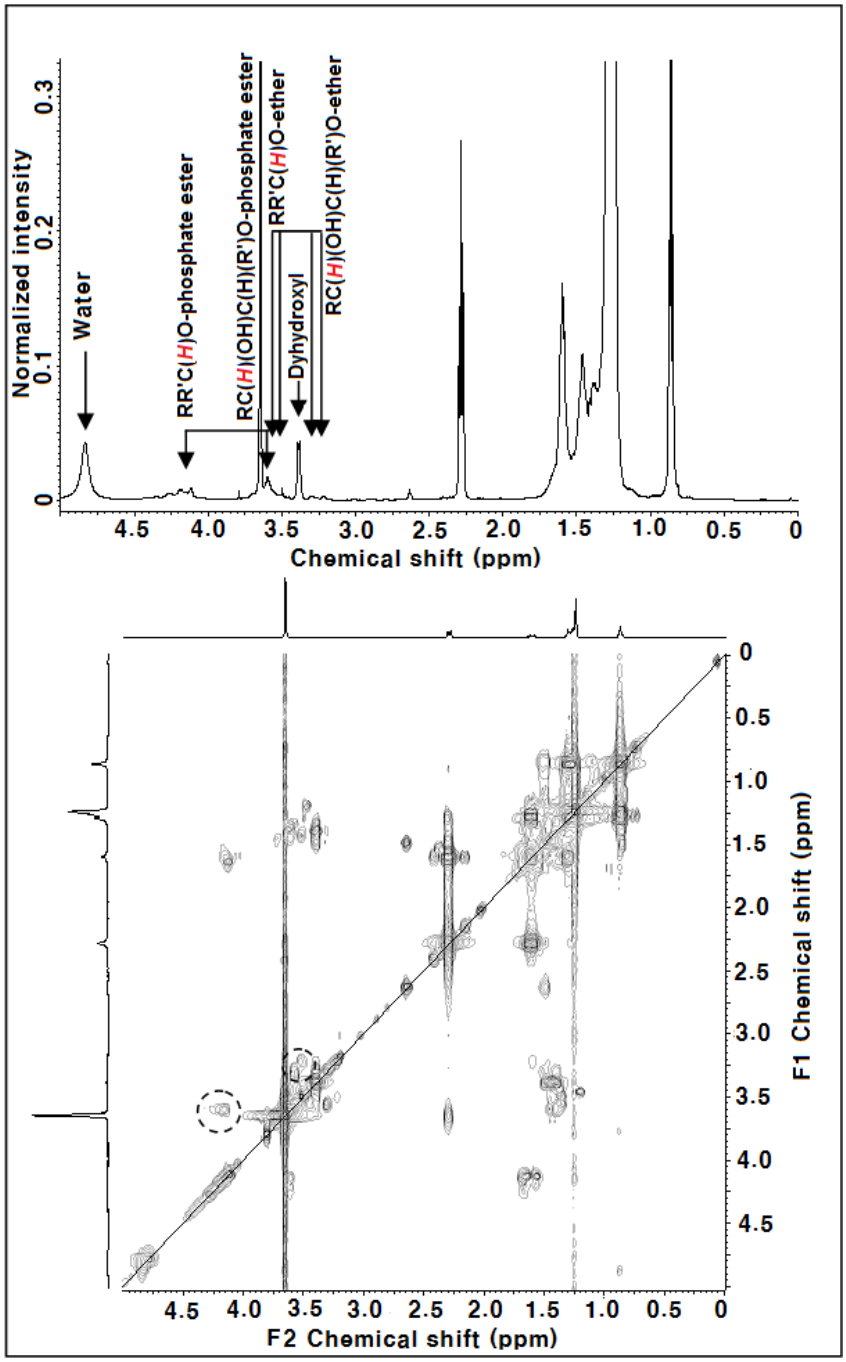

Figure 3.4. DSC curves of the ESO PSA

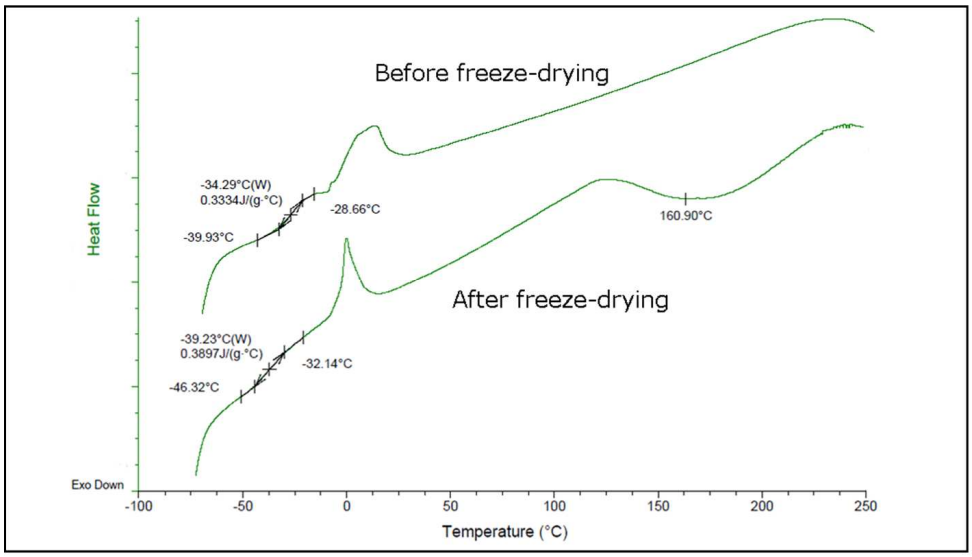

Figure 3.5. TGA curve of the ESO PSA

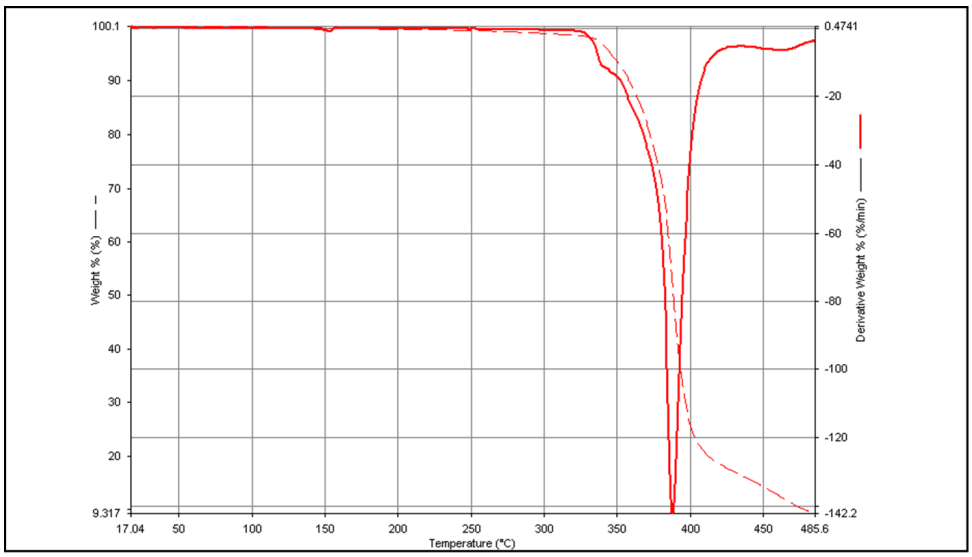

Figure 3.6. Transmittance of the ESO PSA compared to glass, PP, and PE

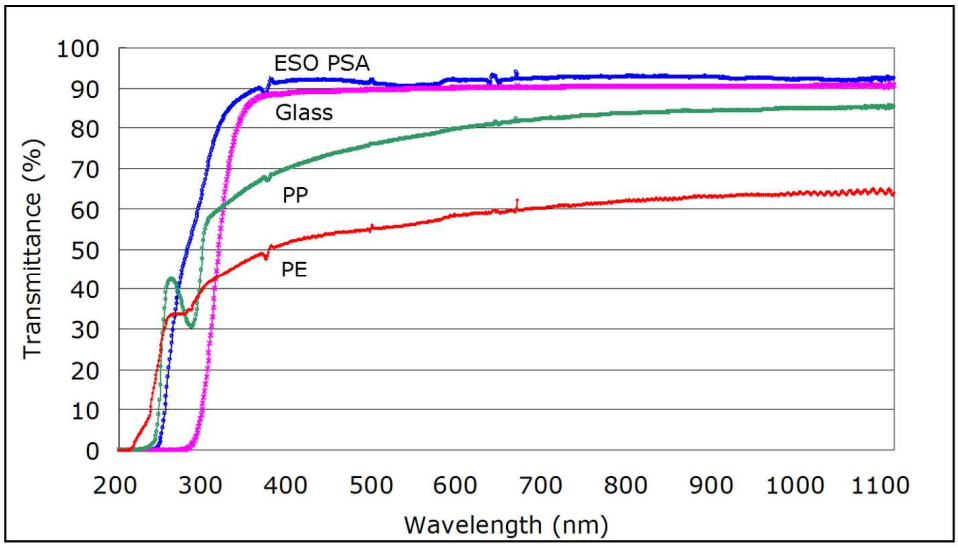

Figure 3.7. Peel strength of ESO PSAs in terms of drying temperature and time regarding clear removal

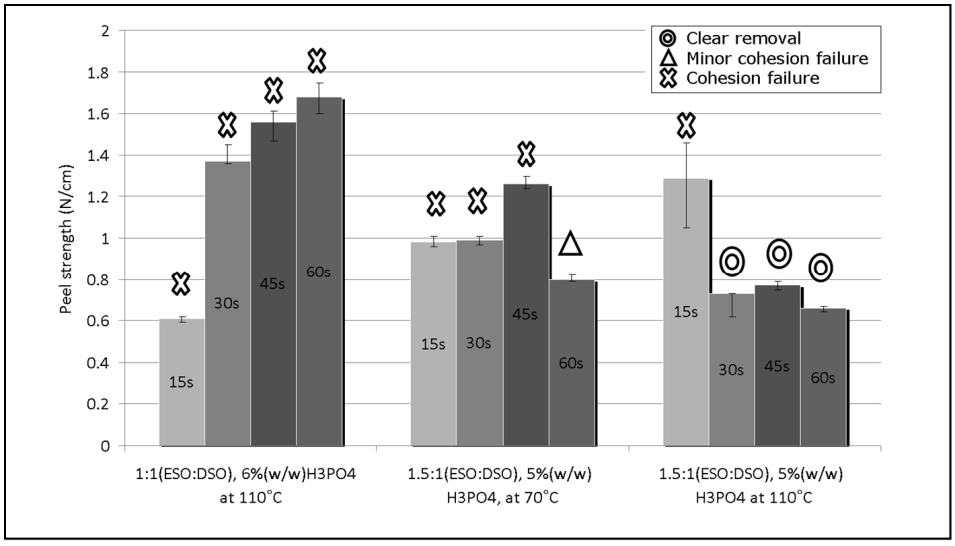

Figure 3.8. ESO PSA on aluminum foil carrier in terms of drying time vs. Scotch Magic Tape and Post-it Notes

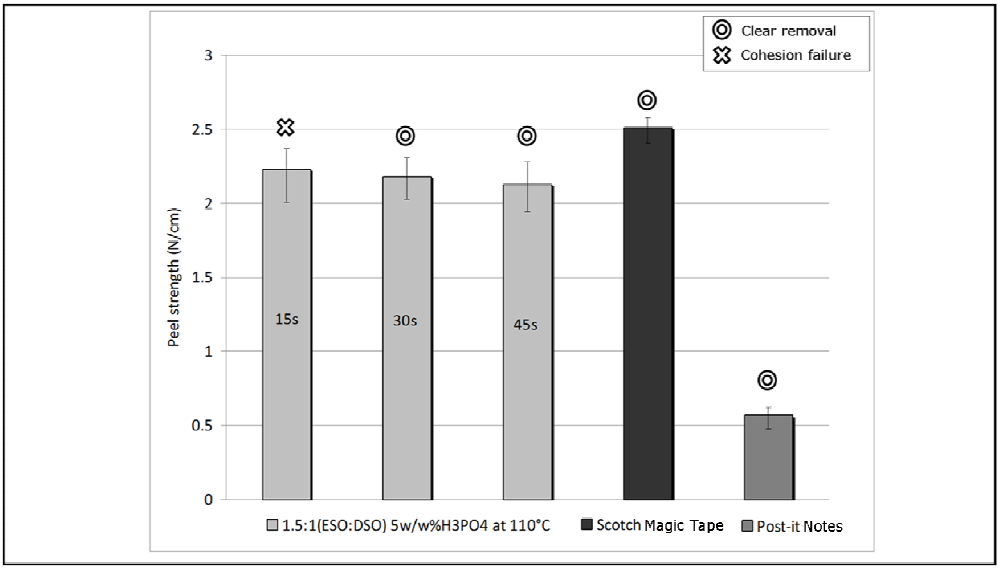

Figure 3.9. Peel strength of the ESO PSAs vs. Post-it Notes regarding reusability

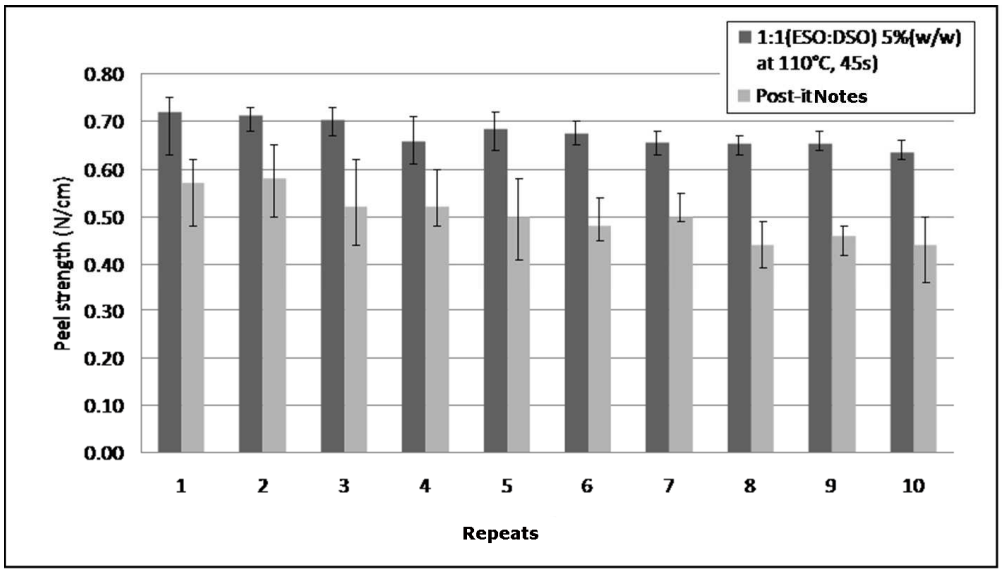

3.6. References

Andjelkovic, D. D. and Larock, R. C. 2006. Novel rubbers from cationic copolymerization of soybean oils and dicyclopentadiene. 1. Synthesis and characterization. Biomacromolecules 7:927-936.

Ballard, R. L., Tuman, S. J., Fouquette, D. J., Stegmiller, W. and Soucek, M. D. 1999. Effects of an acid catalyst on the inorganic domain of inorganic-organic hybrid materials. Chemistry of Materials 11:726-735.

Belgacem, M. N. and Gandini, A. 2008. Monomers, Polymers and composites from renewable resources. Elsevier: Oxford.

Bettinger, C. J. and Bao, Z. A. 2010. Organic thin-film transistors fabricated on resorbable biomaterial substrates. Advanced Materials 22:651-+.

Bozell, J. J. and Patel, M. E. 2006. Feedstocks for the Future: Renewable for the production of chemicals and materials. American Chemical Society: Washington, DC.

Bunker, S., Staller, C., Willenbacher, N. and Wool, R. 2003. Miniemulsion polymerization of acrylated methyl oleate for pressure sensitive adhesives. International Journal of Adhesion and Adhesives 23:29-38.

Bunker, S. P. and Wool, R. P. 2002. Synthesis and characterization of monomers and polymers for adhesives from methyl oleate. Journal of Polymer Science Part a-Polymer Chemistry 40:451-458.

Chakraborti, A. K., Rudrawar, S. and Kondaskar, A. 2004. European Journal of Organic Chemistry:3597.

Cheng, Y., Chen, C., Cheng, C. and Lee, M. M. 2009. Demonstration of organic light emitting diodes: fabricated on flexible Al2O3-embedded poly(dimenthylsiloxane) substrates. Japanese Journal of Applied Physics 48:1-5.

Crivello, J. V. and Narayan, R. 1992. Epoxidized triglycerides as renewable monomers in photoinitiated cationic polymeriztion. Chemistry of Materials 4:692-699.

David, S. B., Sathiyalekshmi, K. and Raj, G. A. G. 2009. Studies on acrylated epoxydised triglyceride resin-co-butyl methacrylate towards the development of biodegradable pressure sensitive adhesives. Journal of Materials Science-Materials in Medicine 20:61-70.

Guo, Y. Z., Hardesty, J. H., Mannari, V. M. and Massingill, J. L. 2007. Hydrolysis of epoxidized soybean oil in the presence of phosphoric acid. Journal of the American Oil Chemists Society 84:929-935.

Holland, J. M., Lewis, M. and Nelson, A. 2003. Desymmetrization of a centrosymmetric diepoxide: Efficient synthesis of a key intermediate in a total synthesis of hemibrevetoxin B. Journal of Organic Chemistry 68:747-753.

Klapperich, C. M., Noack, C. L., Kaufman, J. D., Zhu, L., Bonnaillie, L. and Wool, R. P. 2009. A novel biocompatible adhesive incorporating plant-derived monomers. Journal of Biomedical Materials Research Part A 91A:378-384.

La Scala, J. and Wool, R. P. 2005. Rheology of chemically modified triglycerides. Journal of Applied Polymer Science 95:774-783.

Lee, H., Lee, B. P. and Messersmith, P. B. 2007. A reversible wet/dry adhesive inspired by mussels and geckos. Nature 448:338-U4.

Liu, Z. S., Sharma, B. K. and Erhan, S. Z. 2007. From oligomers to molecular giants of soybean oil in supercritical carbon dioxide medium: 1. Preparation of polymers with lower molecular weight from soybean oil. Biomacromolecules 8:233-239.

Lligadas, G., Ronda, J. C., Galia, M., Biermann, U. and Metzger, J. O. 2006a. Synthesis and characterization of polyurethanes from epoxidized methyl oleate based polyether polyols as renewable resources. Journal of Polymer Science Part a-Polymer Chemistry 44:634-645.

Lligadas, G., Ronda, J. C., Galia, M. and Cadiz, V. 2006b. Bionanocomposites from renewable resources: Epoxidized linseed oil-polyhedral oligomeric silsesquioxanes hybrid materials. Biomacromolecules 7:3521-3526.

Lligadas, G., Ronda, J. C., Galia, M. and Cadiz, V. 2007. Poly(ether urethane) networks from renewable resources as candidate biomaterials: Synthesis and characterization. Biomacromolecules 8:686-692.

Mahdavi, A., Ferreira, L., Sundback, C., Nichol, J. W., Chan, E. P., Carter, D. J. D., Bettinger, C. J., Patanavanich, S., Chignozha, L., Ben-Joseph, E., Galakatos, A., Pryor, H., Pomerantseva, I., Masiakos, P. T., Faquin, W., Zumbuehl, A., Hong, S., Borenstein, J., Vacanti, J., Langer, R. and Karp, J. M. 2008. A biodegradable and biocompatible gecko-inspired tissue adhesive. Proceedings of the National Academy of Sciences of the United States of America 105:2307-2312.

Nogi, M., Iwamoto, S., Nakagaito, A. N. and Yano, H. 2009. Optically transparent nanofiber paper. Advanced Materials 21:1595-+.

Nogi, M. and Yano, H. 2008. Transparent nanocomposites based on cellulose produced by bacteria offer potential innovation in the electronics device industry. Advanced Materials 20:1849-+.

Park, S. J., Jin, F. L. and Lee, J. R. 2004. Synthesis and thermal properties of epoxidized vegetable oil. Macromolecular Rapid Communications 25:724-727.

Pocius, A. V. 1997. The chemistry and physical properties of elastomer-based adhesives. Adhesion and adhesives technology:216-245.

Robertson, M. L., Chang, K. H., Gramlich, W. M. and Hillmyer, M. A. 2010. Toughening of Polylactide with Polymerized Soybean Oil. Macromolecules 43:1807-1814.

Schilling, P. 1986. Cationic bituminous emulsions and emulsion aggregate slurries, C08K 5/20 (20060101) B01F 17/00 (20060101) C08K 5/00 (20060101): US Patent 4597799.

Sharma, B. K., Adhvaryu, A. and Erhan, S. Z. 2006. Synthesis of hydroxy thio-ether derivatives of vegetable oil. Journal of Agricultural and Food Chemistry 54:9866-9872.

Uyama, H., Kuwabara, M., Tsujimoto, T., Nakano, M., Usuki, A. and Kobayashi, S. 2003. Green nanocomposites from renewable resources: Plant oil-clay hybrid materials. Chemistry of Materials 15:2492-2494.

Xia, Y. and Larock, R. C. 2010. Vegetable oil-based polymeric materials: synthesis, properties, and applications. Green Chemistry 12:1893-1909.

Xu, J. Y., Liu, Z. S. and Erhan, S. Z. 2008. Viscoelastic properties of a biological hydrogel produced from soybean oil. Journal of the American Oil Chemists Society 85:285-290.

Zhong, B., Shaw, C., Rahim, M. and Massingill, J. 2001. Novel coatings from soybean oil phosphate ester polyols. Journal of Coatings Technology 73:53-57.

Chapter 4 - Phosphate esters functionalized dihydroxyl soybean oil tackifier of pressure-sensitive adhesives

[This work has been accepted: Ahn, B. K., Sung, J. G., Sun, X. S., (2011). *Journal of American Oil Chemists' Society.* 2011. DOI: 10.1007/s 111746-011-1978-6]

4.1. Abstract

Dihydroxyl soybean oil (DSO) has shown potential as a tackifier for pressure-sensitive adhesive (PSA) applications, and perchloric acid was used as a catalyst to open the oxirane rings of epoxidized soybean oils (ESO) to prepared DSO and PSA in our previous reports. Phosphoric acid is a more eco-friendly catalyst than perchloric acid; therefore, the objective of this work was to prepare DSO using phosphoric acid as a catalyst and thereby create DSO-contained phosphate esters, or PDSO. The chemical scaffolds of PDSO were elucidated with ^{1}H, ^{1}H-^{1}H COSY, ^{31}P NMR, FTIR, MALDI-TOF MS, and GPC. ESO PSAs were prepared from a mixture of ESO/PDSO. The ESO PSA prepared with PDSO had peel strength on a plastic carrier comparable to commercial PSA, and while on an aluminum carrier, the ESO PSA had stronger peel strength. ESO PSA prepared with phosphoric acid was also stronger than the peel strength of the ESO PSA prepared with DSO using perchloric acid.

4.2. Introduction

Limited petroleum resources and environmental regulations have urged scientists and engineers to develop sustainable materials from renewable resources (Belgacem and Gandini 2008; Lligadas et al. 2010; Meier et al. 2007; Metzger and Bornscheuer 2006). Plant oils are one renewable resource with promise to replace petroleum chemicals, and such oils have environmental advantages including low toxicity and inherent biodegradability (Helling and Russell 2009; Lligadas et al. 2010; Meier et al. 2007; Metzger and Bornscheuer 2006). Epoxidized soybean oil (ESO) is a well known commercially available renewable resource (Andjelkovic and Larock 2006; Helling and Russell 2009; Lu et al. 2010). Phosphate ester-containing soy polyols have been synthesized (Guo et al. 2007; Zhong et al. 2001) and blended

with melamine/formaldehyde resins for coating applications (Zhong et al. 2001); however, phosphate esters are very vulnerable to moisture (M.E. Okazaki 1993; Zhong et al. 2001). Guo et al (2007) reported the only phosphate ester links using FTIR analysis, and Zhong et al (2001) essayed mono-branched α-hydroxy-phosphate ester and diol, but without analytical chemical structural study. Nyk et al (1991) reported on both ether and phosphate esters derived from diepoxide and phosphoric acid (H_3PO_4) through ^{1}H and ^{31}P NMR analysis. In our previous report (Ahn et al. 2011a), we elucidated that this chemistry bias of epoxidized (mid-chain) oleo-chemicals with phosphoric acid yields multiple phosphate esters, including cyclic phosphate ester, diols, and ethers. More interestingly, controlling the concentration of phosphoric acid and nucleophiles rendered enough functional groups (phosphate ester/ether/diol) to affect end-use properties (Ahn et al. 2011a; Ahn et al. 2011b).

Pressure-sensitive adhesive (PSA) is one major end use of ESO, and represents a huge market (i.e, transparent tapes and bandages) currently dominated by petroleum feedstocks. In our previous study, we prepared PSA successfully by mixing ESO and dihydroxyl soybean oils (DSO) (Ahn et al. 2011a; Ahn et al. 2011b), and the DSO acted as a tackifier of the PSA; however, the DSO was prepared through vicinal diolysis of ESO using perchloric acid, which is a strong acid that may cause health problems and environmental pollution (Zhao et al. 2008).

DSO can be obtained directly by converting unsaturated allyl groups using potassium permanganate, osmium tetraoxide, tungstic acid, or rhenium catalysts (Behr et al. 2008; Herrmann 1990), but alcoholysis of epoxide is commonly practiced in industry (Meier et al. 2007) due to its safer and easier process. Formic acid (Harry-O'kuru et al. 2002) and acetic acid (Sharmin et al. 2007) could be important examples for a greener DSO synthesis from ESO, but energy consumption of those syntheses (high temperature for overnight duration) can be problematic in terms of greenhouse gas emission. Environmentally friendly enzymatic diolysis of epoxy fatty acid also has been introduced, but its long reaction time (90 d) is still a challenge (Tulloch 1963). Phosphoric acid is not only much less toxic than perchloric acid (Zhao et al. 2008), but also is amenable to alcoholysis/hydrolysis at room temperature (Ahn et al. 2011a). In addition, the phosphate metal attraction (Iliescu et al. 1996) allows production of tackier PSAs using metal-based materials (i.e., aluminum) as carriers (Ahn et al. 2011b). Lubguban (2009) reported highly viscous, and a low-acid soy phosphate having high average functionality for polyurethane application via solvent free condition 1.5% phosphoric acid in situ.

In this study, we synthesized phosphate esters containing dihydroxyl soybean oils (PDSO) using phosphoric acid (H_3PO_4) in H_2O/tetrahydrofuran (THF) and characterized their chemical scaffolds with aid of ^1H NMR, ^1H-^1H COSY, and ^{31}P NMR; Fourier Transform Infrared Spectroscopy (FTIR); matrix-assisted laser desorption ionisation time-of-flight mass (MALDI-TOF MS); and gel permeation chromatography (GPC). In addition, we prepared the ESO PSAs (**Figure 4.1**) using PDSO and conducted a 90° peel test to compare our product with commercial PSAs.

4.3. Experimental

Materials

ESO was purchased from Scientific Polymer Products, Inc. (Ontario, NY). Phosphoric acid (85 w/w % in water), ethyl acetate, and tetrahydrofuran (THF) were purchased from Fisher Scientific, Inc. (Waltham, MA).

Synthesis and chemical characterization

PDSOs were synthesized from ESO (20 g, 20 mmol) in 1 w/w % (0.2 g, 2 mmol), 10 w/w % (2 g, 20 mmol), and 25 w/w % (5 g, 51 mmol), respectively, of phosphoric acid (H_3PO_4) in H_2O/THF (300/200 mL) at room temperature for 42 h. Subsequently, the PDSOs were extracted with ethyl acetate, then dried with magnesium sulfate; solvent was removed by rotary evaporator. ESO PSAs were prepared according to a previously reported method (Ahn et al. 2011b). Briefly, a mixture of ESO/PDSO/H_3PO_4 in methyl acetate was stirred for 5 min at room temperature, then spread on a plastic film or aluminum foil, followed by the hot-air drying (Ahn et al. 2011b) at 110 °C for 60 s. ^1H, ^1H-^1H COSY and ^{31}P NMR (500 MHz) spectra were obtained for all PDSO samples (0.14 g, 0.14 mmol) in deuterated dichloromethane ($CDCl_3$) (0.65 mL) with triphenyl phosphate (0.014 g, 0.04 mmol) as a detection limit. FTIR, MALDI-TOF MS, and GPC results were conducted to characterize the polymerization.

NMR. ^1H and ^{31}P NMR spectra were recorded at room temperature on a 500 MHz Bruker DRX spectrometer with a broadband observe probe. ^1H spectra were acquired using the Bruker pulse program zg30 with 16 scans (2 dummy scans) and a 1-s interscan delay and were processed using an exponential line broadening function with a decay constant of 0.3 Hz, followed by zero-filling, Fourier transform, phasing, and polynomial baseline correction. ^{31}P

spectra were acquired using the Bruker pulse program zg30 with 32 scans (4 dummy scans) and a 2-s interscan delay and were processed using an exponential line broadening function with a decay constant of 1.0 Hz, followed by zero-filling, Fourier transform, phasing, and polynomial baseline correction.

FTIR. FTIR of ESO PSA film and non-cross-linked ESO were obtained using FT-IR/FT-NIR spectrometer (Perkin-Elmer Spectrum 400).

GPC. GPC was performed using Waters Alliance HPLC 2695 Separation Module equipped with Waters 2414 Differential Refractometer and Waters 2996 Photodiode Array Detectors. All molecular weights are relative to polystyrene standards. Polymer samples were dissolved in $CHCl_3$ (approximately 0.1% w/v) and filtered before injection using a 0.45-um teflon filter. The GPC was equipped with four columns: two I-Series Mixed Bed High Molecular Weight Viscotek columns with a separation range of 1000–10 M (30 cm x 7.8 mm i.d.) and two with a separation range of 100–20 K (30 cm x 7.8 mm i.d.). $CHCl_3$ was used as the eluent at a constant flow rate of 1.0 ml/min. Retention times were calibrated against narrow molecular weight polystyrene standards (Fluka, St. Louis, MO). All standards were selected to produce Mw and Mn values well beyond the polymer's expected range. Usually 12 data points were acquired for a calibration curve.

MALDI-TOF MS. MALDI-TOF MS measurements were performed with a Voyager DE-STR mass spectrometer (AB SCIEX, Foster City, CA) equipped with a nitrogen laser delivering 3-ns laser pulses at 337 nm. 2,5-Dihydroxybenzoic acid (DHB) was used as a matrix, and silver trifluoroacetate was used as a dopant. Size exclusion chromatography (SEC) analysis was carried out with a Waters 510 pump system equipped with a Shimadzu RID-6A refractive-index detector. THF was used as an eluent at a flow rate of 1.0 mL/ min. The calibration curves for SEC analysis were obtained with polystyrene standards.

Mechanical characterization. The 90° peel adhesion test was conducted according to previous reports (Ahn et al. 2011a; Ahn et al. 2011b) based on ASTM method D3330/D3330M-04.

4.4. Results and discussion

The synthesis of phosphate ester containing dihydroxyl soybean oil (PDSO) was attempted with various ratios of H_3PO_4 (1, 10, and 25 w/w %) at room temperature for 42 h. We elucidated the chemical scaffolds of the products by ^1H, ^1H-^1H COSY, and ^{31}P NMR. We used triphenyl phosphate as a detection limit for quantitative ^{31}P NMR analysis.

Concentration of phosphoric acid played a key role in chemical composition and structure of the products, which can affect adhesion properties. One percent H_3PO_4 (**Figure 4.2b**) was not enough to initiate the conversion of epoxide based on NMR data shown at δ 2.80-3.20 for epoxide sites of ESO (**Figure 4.2a**). Ten percent H_3PO_4 (**Figure 4.2c**) shows minor conversion of epoxide to hydroxyl groups at δ 3.25–4.25. These experiments had silent phosphate signals on ^{31}P NMR that spiked no phosphate ester formation at H_3PO_4 less than 10%. On the other hand, the product from the reaction with 25% H_3PO_4 (**Figure 4.2d**) presented both phosphate ester [RR'C(*H*)O-phosphate ester at δ 5.08 coupled with RC(*H*)(OH)C(H)(R')O-phosphate ester at δ 4.81] and hydroxyl moieties (δ 3.25–4.25). In addition, ^{31}P NMR showed phosphate signals (**Figure 4.3**). This finding of phosphate esters by ^1H and ^{31}P NMR analyses demonstrated phosphate esters could be formed with only 25% or higher concentration of H_3PO_4 in this room temperature condition. Quantitative ^{31}P NMR (**Figure 4.3**) of the product from 25% H_3PO_4 with a detection limit of triphenyl phosphate signal at δ -17.85 spiked the ^1H NMR results of the phosphate ester groups. The NMR analyses demonstrated that PDSO was successfully synthesized from ESO with 25% H_3PO_4. The quantitative NMR analyses indicated that PDSO contained 0.18 phosphate ester sites per triglyceride unit. Based on the NMR analysis, the functional group composition of PDSO (prevalent dihydroxyl and minor phosphate esters) suggested that excess water molecules had statistically more opportunities (Route A, **Scheme 4.1**) for an S_N2 attack to a cis-epoxide than phosphate anions (Route B, **Scheme 4.1**) in this chemistry (**Scheme 4.1**) (Ahn et al. 2011a). In addition, it is also possible that transesterification of the triglycerides (**Scheme 4.1**) with phosphoric acid took place instead (or in parallel) to the epoxide ring opening. As a result, hydrolysis (carboxylic acid) happened in the condition of excess water which discussed in the FTIR results later in this manuscript.

GPC, MALDI-TOF MS, and FTIR results were compared with NMR results. GPC results (**Figure 4.4**) of the products with 1 and 10% H_3PO_4 showed mainly unreacted ESO signals at 36.5 min of retention time, which was identical to the GPC result of neat ESO. On the other hand,

the PDSO from the reaction with 25% H_3PO_4 presented various products at different retention times. This result (**Figure 4.4**) suggested that the PDSO from ESO with 25% H_3PO_4 generated not only oligomerization (two shoulders on the left), but also acid-catalyzed hydrolysis of triglyceride (three shoulders on the right) that corresponded to MALDI-TOF MS (**Figure 4.5**) and FTIR (**Figure 4.6**). MALDI-TOF MS analysis of PDSO from the reaction of ESO with 25% H_3PO_4 presented various molecular weights under MW≈1000 g/mol (ESO), and FTIR detected a new carboxylic acid (C=O) band around 1720 cm^{-1} besides the carboxylic ester (C=O) of triglycerides around 1740 cm^{-1}. This band confirmed that the hydrolysis of triglycerides occurred in the process of epoxide ring opening. In addition, a phosphate ester band around 1000 cm^{-1} and an alcohol band around 3400 cm^{-1} appeared on PDSO whereas the epoxides band at 824 cm^{-1} of ESO disappeared. The FTIR further confirmed the functional groups composition (-OH at 3400 cm^{-1}, -COOR at 1740 cm^{-1}, -COOH at 1720 cm^{-1}, phosphate ester at 1000 cm^{-1}) of PDSO.

ESO PSAs were prepared from a mixture of ESO/PDSO/H_3PO_4 in methyl acetate, then hot-air coated on plastic or aluminum films. Ninety degree peel strength was measured. The PSA with PDSO derived from ESO using H_3PO_4 as a catalyst at the 25% loading level recorded predominantly stronger peel strength than the products at 1% and 10% loading levels (**Figure 4.7**). Furthermore, the PDSO from 25% H_3PO_4 increased the peel strength of ESO PSA (1.25 N/cm on a plastic carrier, 2.6 N/cm on an aluminum carrier) compared with previously reported DSO (Ahn et al. 2011b) using perchloric acid as a catalyst (0.78 N/cm on a plastic carrier, 2.2 N/cm on an aluminum carrier; see reference Ahn et al. 2011b, Figure 7 and 8). The PSA on the aluminum carrier was stronger than the commercial Scotch Tape (3M, Inc., St. Paul, MN). We believe predominant tack properties on a metal substrate are related to phosphorous polymer adhesion to metal and metal-ion binding characteristics with increased polarity (Ahn et al. 2011b; Iliescu et al. 1996) through the phosphate metal attraction (Iliescu et al. 1996).

4.5. Conclusion

Newly synthesized phosphate esters containing DSO (PDSO) improved the peel strength of ESO PSA compared with previously reported DSO derived with perchloric acid. The ESO PSA on an aluminum carrier showed stronger peel strength than commercial PSAs because of phosphate metal attraction. The chemical structures of the PDSO were elucidated by multi-

dimensional ^{1}H and ^{31}P NMR, GPC, MALD-TOF MS, and FTIR related to their mechanical properties (90° peel strength regarding cohesion strength).

Figure 4.1. Synthetic scheme of the ESO PSA from ESO/PDSO.

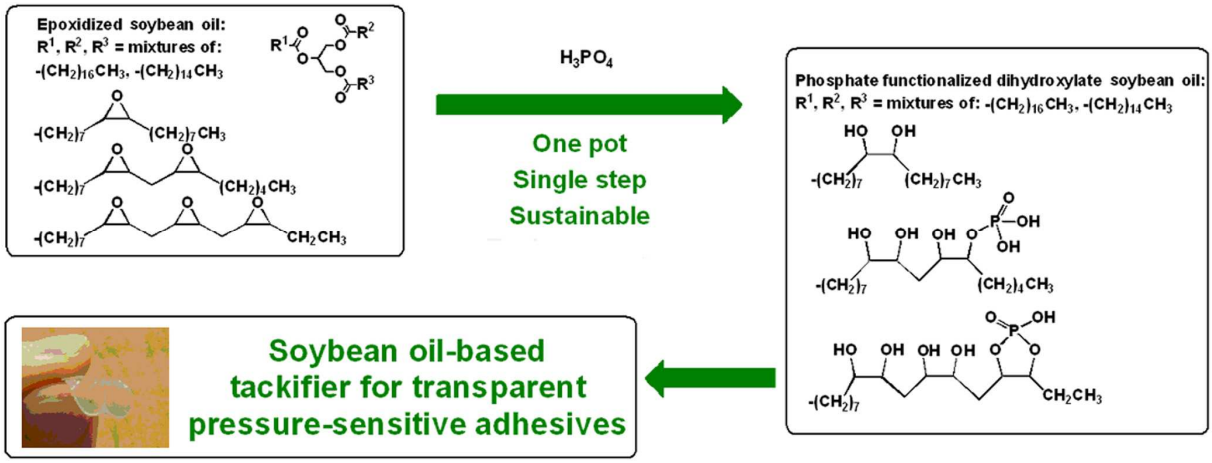

Figure 4.2. ^{1}H NMR spectra of a) ESO, b) PDSO from ESO with 1 w/w % phosphoric acid H_2O/THF (3:2 w/w) solution, c) PDSO from ESO with 10 w/w % phosphoric acid H_2O/THF (3:2 w/w) solution, d) PDSO from ESO with 25 w/w % phosphoric acid H_2O/THF (3:2 w/w) solution.

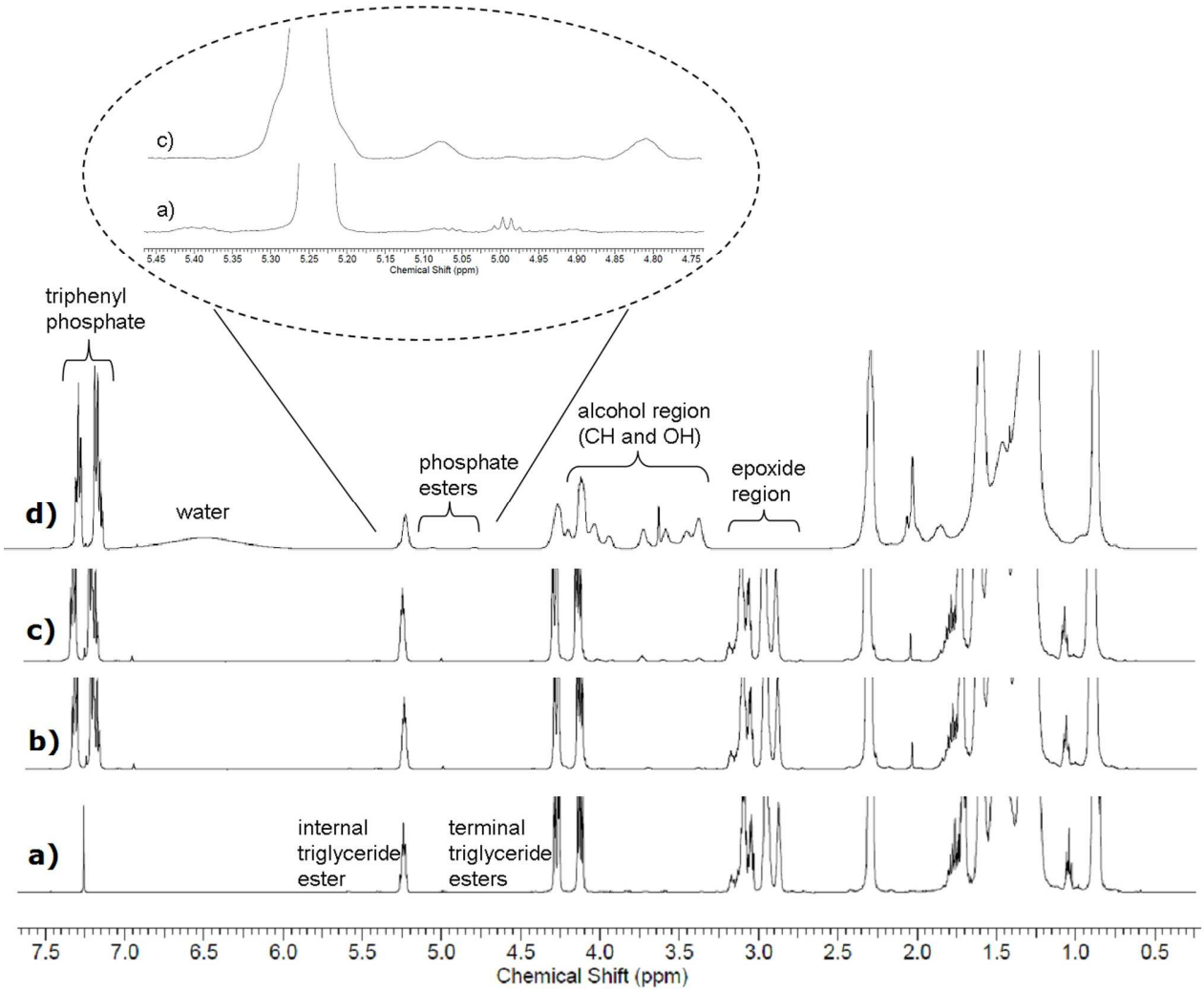

Figure 4.3. ^{31}P NMR spectrum of PDSO from ESO with 25 w/w % phosphoric acid H_2O/THF (3:2 w/w) solution.

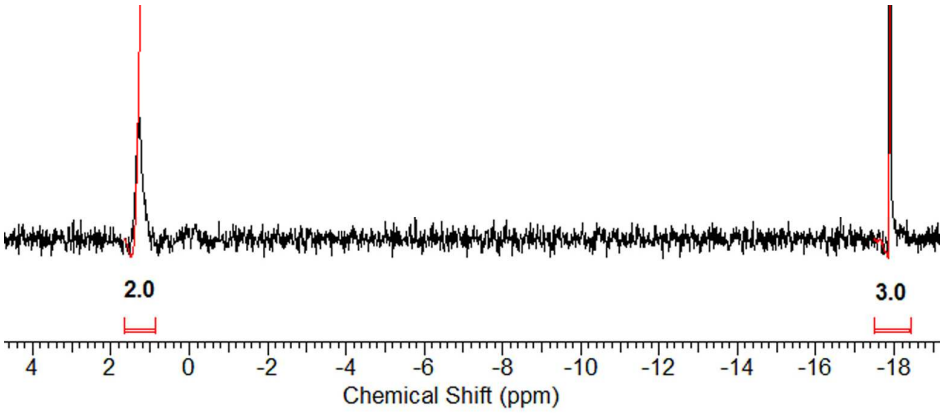

Figure 4.4. GPC chromatograms of PDSO from ESO with (top to bottom) 1, 10, 25 w/w % of H_3PO_4.

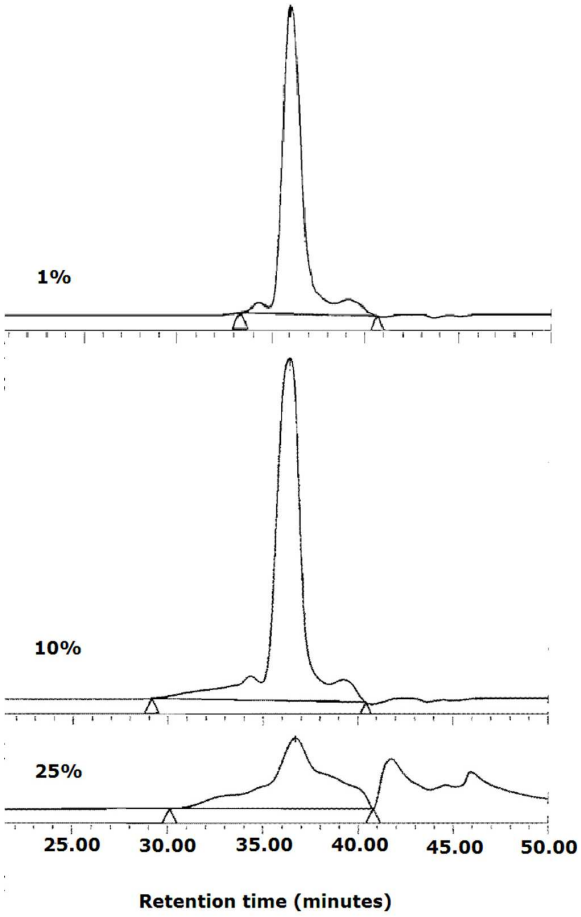

Figure 4.5. MALDI-TOF MS results of PDSO from ESO with (top to bottom) 1, 10, 25 w/w % of H_3PO_4.

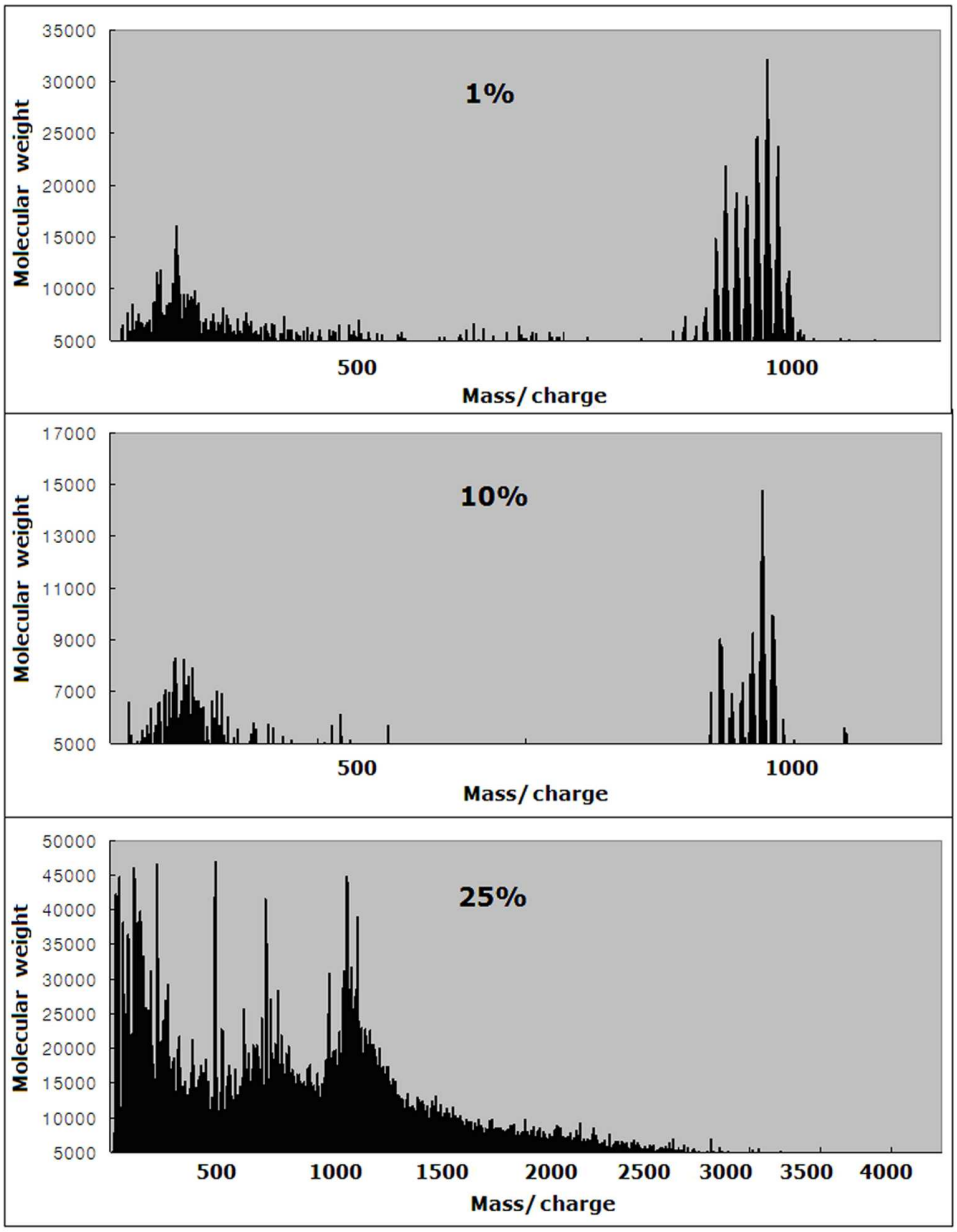

Figure 4.6. FTIR spectra of ESO and PDSO from ESO with 25 w/w % of H_3PO_4.

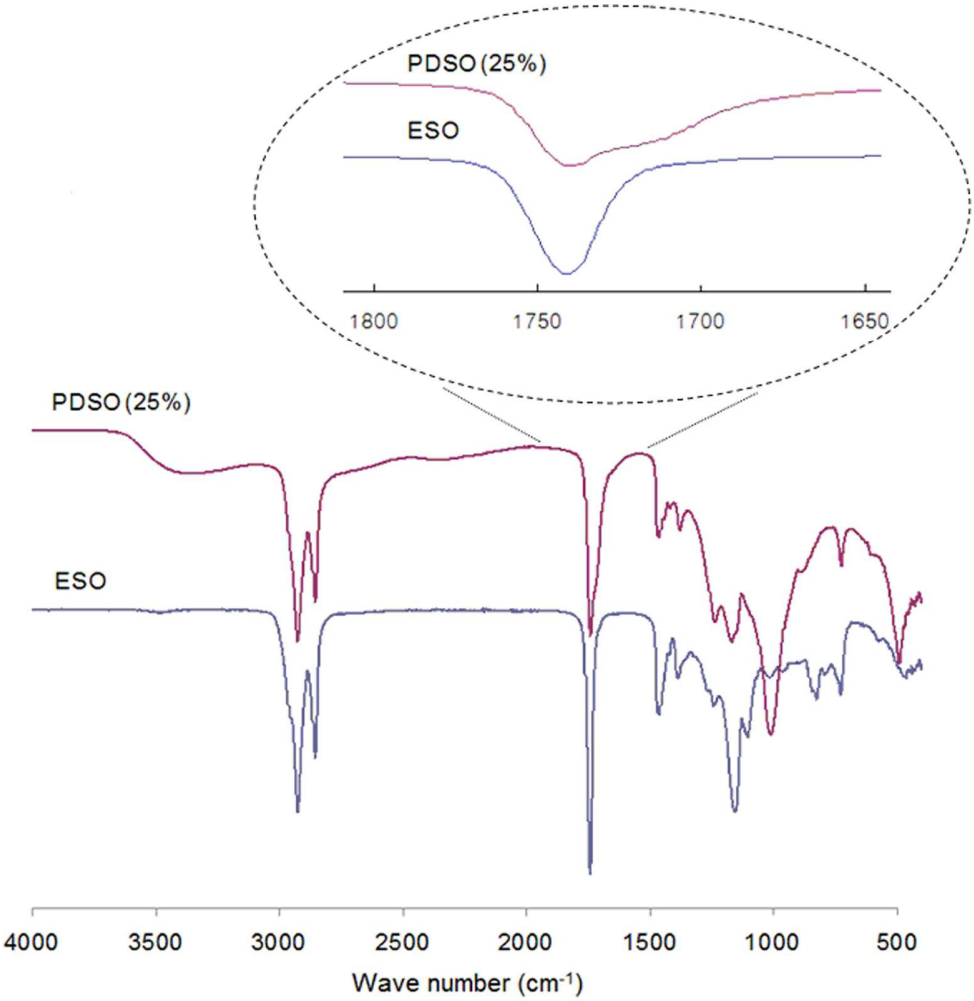

Figure 4.7. 90° peel strength test of PSAs with different ratio of ESO:PDSO (0.5-1.5:1) and 10 or 25 w/w % H_3PO_4 in H_2O/THF (3:2 w/w) solution on plastic and aluminum carriers compared with commercial PSA tapes (Post-it and Scotch Magic Tape, 3M, Inc.).

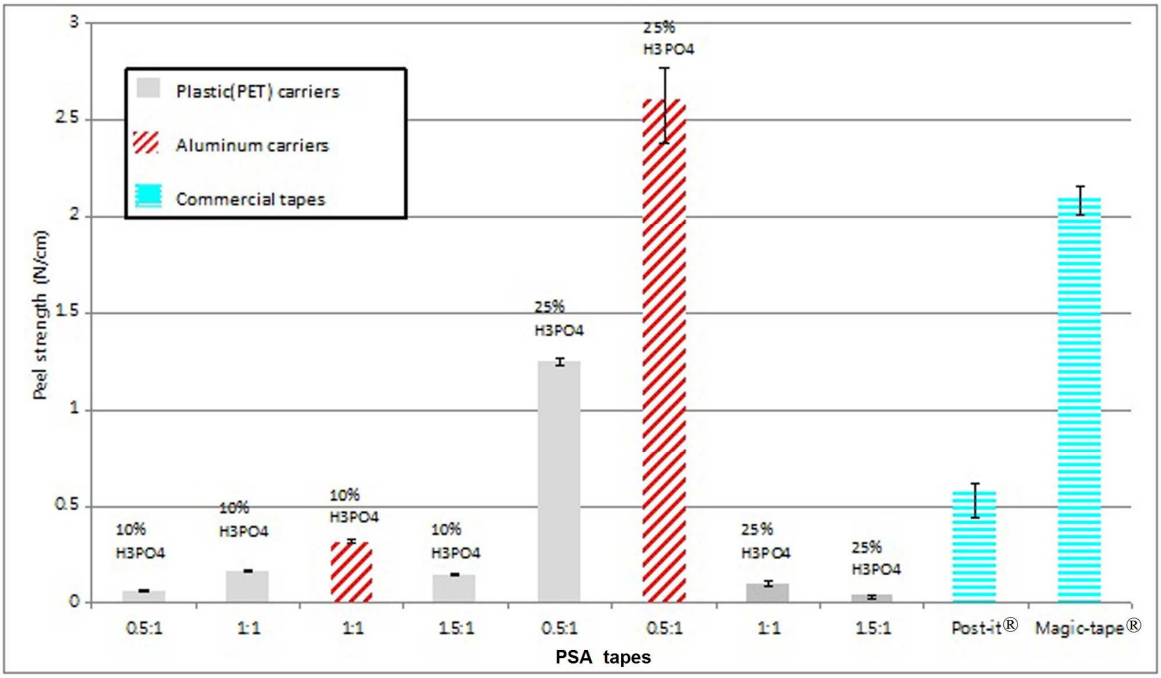

Scheme 4.1. Chemistry of the reaction of ESO/phosphoric acid (25%) in water/THF

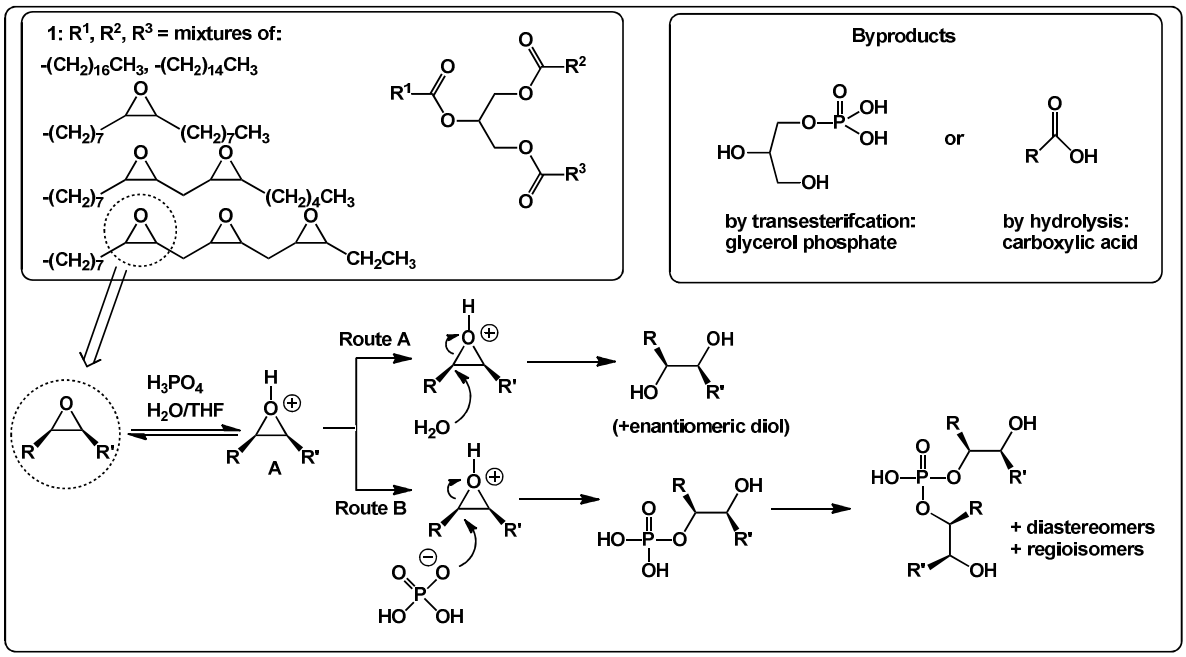

4.6. References

Ahn, B. K., Kraft, S. and Sun, X. S. 2011a. Chemical pathways of epoxidized and hydroxylated fatty acid methyl esters and triglycerides with phosphoric acid. Journal of Materials Chemistry 21:9498-9505.

Ahn, B. K., Kraft, S., Wang, D. and Sun, X. S. 2011b. Thermally Stable, Transparent, Pressure-Sensitive Adhesives from Epoxidized and Dihydroxyl Soybean Oil. Biomacromolecules 12:1839-1843.

Andjelkovic, D. D. and Larock, R. C. 2006. Novel rubbers from cationic copolymerization of soybean oils and dicyclopentadiene. 1. Synthesis and characterization. Biomacromolecules 7:927-936.

Behr, A., Westfechtel, A. and Gomes, J. P. 2008. Catalytic processes for the technical use of natural fats and oils. Chemical Engineering & Technology 31:700-714.

Belgacem, M. N. and Gandini, A. 2008. Monomers, Polymers and Composites from Renewable Resources. Elsevier: Oxford.

Guo, Y. Z., Hardesty, J. H., Mannari, V. M. and Massingill, J. L. 2007. Hydrolysis of epoxidized soybean oil in the presence of phosphoric acid. Journal of the American Oil Chemists Society 84:929-935.

Harry-O'kuru, R. E., Holser, R. A., Abbott, T. P. and Weisleder, D. 2002. Synthesis and characteristics of polyhydroxy triglycerides from milkweed oil. Industrial Crops and Products 15:51-58.

Helling, R. K. and Russell, D. A. 2009. Use of life cycle assessment to characterize the environmental impacts of polyol production options. Green Chemistry 11:380-389.

Herrmann, W. A. 1990. Essays on organometallic chemistry. 5. Rhenium chemistry in catalysis - present and future. Journal of Organometallic Chemistry 382:1-18.

Iliescu, S., Manoviciu, L., Ilia, G. and Dehelean, G. 1996. Phosphorus-Containing Polymers. 1 Polyphosphates and polyphosphonates. Roumanian chemical quarterly reviews 5:267-277.

Lligadas, G., Ronda, J. C., Galia, M. and Cadiz, V. 2010. Plant oils as platform chemicals for polyurethane synthesis: current state-of-the-art. Biomacromolecules 11:2825-2835.

Lu, H., Sun, S. D., Bi, Y. L., Yang, G. L., Ma, R. L. and Yang, H. F. 2010. Enzymatic epoxidation of soybean oil methyl esters in the presence of free fatty acids. European Journal of Lipid Science and Technology 112:1101-1105.

Lubguban, A. A. 2009. Synthesis and testing of soy-based polyols: phosphate and glycerolysis oligomers in: Chemical engineering. University of Missouri: Columbia

M.E. Okazaki, S. M. A. 1993. Hydrolysis of phosphate-based aviation hydraulic fluids. Journal of Synthetic Lubrication 10:107-118.

Meier, M. A. R., Metzger, J. O. and Schubert, U. S. 2007. Plant oil renewable resources as green alternatives in polymer science. Chemical Society Reviews 36:1788-1802.

Metzger, J. O. and Bornscheuer, U. 2006. Lipids as renewable resources: current state of chemical and biotechnological conversion and diversification. Applied Microbiology and Biotechnology 71:13-22.

Nyk, A., Klosinski, P. and Penczek, S. 1991. Water-swelling hydrolyzable gels through polyaddition of H3PO4 to diepoxides. Makromolekulare Chemie-Macromolecular Chemistry and Physics 192:833-846.

Sharmin, E., Ashraf, S. M. and Ahmad, S. 2007. Synthesis, characterization, antibacterial and corrosion protective properties of epoxies, epoxy-polyols and epoxy-polyurethane

coatings from linseed and Pongamia glabra seed oils. International Journal of Biological Macromolecules 40:407-422.
Tulloch, A. P. 1963. Enzymatic production of (+) threo-9,10-dihydroxyloctoadeconic acid in spores of plant rusts. Canadian Journal of Biochemistry and Physiology 41:1115-&.
Zhao, H. P., Zhang, J. F., Sun, X. S. and Hua, D. H. 2008. Syntheses and properties of cross-linked polymers from functionalized triglycerides. Journal of Applied Polymer Science 110:647-656.
Zhong, B., Shaw, C., Rahim, M. and Massingill, J. 2001. Novel coatings from soybean oil phosphate ester polyols. Journal of Coatings Technology 73:53-57.

Chapter 5 - UV curable high shear pressure sensitive adhesives derived from acrylated epoxidized soybean oil

5.1. Abstract

Several oleo-based pressure sensitive adhesives (PSA) were studied to substitute current petro-based PSAs. However, the PSAs derived from plant oils have unsolved challenges for commercial uses, such as low bio-based contents (20-90%) and complex processes (i. e., purifying, emulsifying and drying steps). Here we demonstrated the possibility of preparing transparent PSAs from neat acrylated epoxidized soybean oil (AESO) via fast and simple UV free-radical polymerization with 97-100% bio-based contents. In this study, we controlled the degree of free radical polymerization by modulating the amount of UV irradiation to obtain a balanced cohesion and adhesion strength for PSA applications. This AESO PSA tape on a polyester film carrier had better peel and significantly higher shear strength on glass surfaces compared to a commercial reusable tape (Post-it made by 3M, St. Paul, MN). The adhesion of the AESO PSA corresponded to its dynamic rheological properties. In addition, the adhesion/cohesion behavior of the PSAs was characterized using the Johnson-Kendall-Roberts (JKR) technique.

5.2. Introduction

Plant oil is one of the most important renewable feedstocks with its low toxicity and inherent biodegradibility (Ahn et al. 2011a; Ahn et al. 2011b; Meier et al. 2007; Metzger and Bornscheuer 2006; Xia and Larock 2010). Well-known commercially available oleochemicals derived from plant oils are fatty acid ester (biodiesel), fatty alcohols, glycerol, and epoxidized or acrylated triglycerides (or their monoester), and so forth. Several patents (Hyde 2009; Koch 2010) and peer review articles (Bunker et al. 2003; Bunker and Wool 2002; Chen et al. 2011; David et al. 2009; Wu et al. 2011) have been published about acrylated epoxidized triglycerides and acrylated methyl oleate (AMO) for coatings and/or pressure sensitive adhesives. Acrylated epoxidized soybean oil (AESO) (Chen et al. 2011; Wu et al. 2011) and acrylated epoxidized palm oil (Cheong et al. 2009) were breifly reported as UV curable coatings. Emulsified acrylated

epoxidized triglyceride (David et al. 2009; Koch 2010) and AMO (Bunker et al. 2003; Bunker and Wool 2002; Hyde 2009; Klapperich et al. 2009) were presented with potential for pressure sensitive adhesives. However, there have been challenges to achieve reasonable end-use properties without the aid of petrochemicals, such as methyl acrylate (MMA) or buthyl methacrylate, which have shortage and toxicity issues. Also, the long curing time (~1h) of the AMO emulsified PSAs can not be applied to practical processes. In addition, obtaining methyl oleate (one unsaturated site in one fatty acid chain) for AMO production requires additional trans-esterification and purification processes from plant oils, or producing high oleic plant oil require extra cost processing compared to using commercially available AESO. Toward this end, we polymerized AESO rather than AMO using UV radiation to eliminate purification steps and minimize curing time. Viscoelastic properties (Chang 1997) of UV cured AESO

In this study, we presented the possibility of preparation of solvent-free and biobased PSA from AESO using only UV radiation without any other petrochemicals as additives (photoinitiator, hardener and tackifier) to demonstrate PSA properties of the genuine polymer. The tack of the PSA means the instantaneous wetting of PSA on a substrate with a little pressure followed by measureable adhesion to applied surface (Pocius 1997). If adhesives are too stiff (or soft), adhesion (or cohesion) failure occurs. Therefore, appropriate viscoelasticity must be achieved to optimize both cohesion and adhesion strength for PSA application (Chang 1997). We, therefore, characterized the viscoelastic properties of the UV cured AESO polymer for PSA applications. The most important advantage of free radical polymerization is to conveniently control chain length by modulating the radiation source (Boey et al. 2002) so as to achieve desirable viscoelasticity of the polymer.

The free-radical polymerization was monitored by Fourier transform infrared spectroscopy (FTIR). Viscoelasticity was measured by dynamic rheometer, and mechanical properties (loop tack, peel, and shear strength) were demonstrated according to the American Standard Testing Method (ASTM). In addition, thermal properties of the polymer were examined by differential scanning calorimetry (DSC) and thermogravimetric analysis (TGA).

In general, the the Johnson-Kendall-Roberts (JKR) experiment consists of a loading and an unloading portion. The raw data obtained from the JKR test are the load (P) and the contact radius (a). Using an energy balance approach, Johnson, Kendall, and Roberts developed a relationship between the contact area and the applied load as (Johnson et al. 1971):

$$a^3 = \frac{R}{K}\left[P + 3\pi RW + \sqrt{(3\pi RW)^2 + (6\pi RPW)}\right] \quad \textbf{(1)}$$

where R is the radius of the curvature of the probe, K is the reduced bulk modulus given by equation (2), and W is the thermodynamic work of adhesion.

$$\frac{1}{K} = \frac{3}{4}\left(\frac{1-\nu_1^2}{E_1} + \frac{1-\nu_2^2}{E_2}\right) \quad \textbf{(2)}$$

where E_i and ν_i are the Young's modulus and the Poisson's ratio of the probe and substrate. Typically K and W are obtained by fitting the raw data to the JKR relationship given in equation (1). In the case where the hemispherical probe and the substrate are made of the same material (self-adhesion or cohesion), $W=2\gamma$ where γ is the surface free energy of the material.

Originally, the JKR theory was developed for reversible systems showing similar loading and unloading behavior. For many polymeric systems, however, the loading and unloading behavior observed during the contact is dissimilar. This discrepancy is referred to as the adhesion hysteresis. For non-hysteretic systems the energy that is required to detach two surfaces in unloading is equal to the energy that brings these surfaces into contact in loading (W). For hysteretic systems, however, the pull-off energy exceeds the thermodynamic work of adhesion. Using the analogy between a circumferential crack in fracture mechanics and receding contact area in the unloading portion of the JKR experiments, Maugis (Johnson et al. 1971) was able to formulate the relationship for the energy release rate (G) in terms of the applied load and contact radius as:

$$G = \frac{\left(\frac{Ka^3}{R} - P\right)^2}{6\pi a^3 K} \quad \textbf{(3)}$$

The adhesion hysteresis is defined as the difference between G in unloading and W in loading. The adhesion hysteresis is indicative of bulk viscoelasticity, chemical changes in the interface of the materials, or surface roughness (Johnson et al. 1971). The adhesion hysteresis may also reveal additional information regarding the rearrangement of the molecules at the interface or the ability of two surfaces to develop specific/non-specific bonds at their interface (Johnson et al. 1971).

In this study, the JKR technique (Johnson et al. 1971) was used as a quantitative and qualitative method to evaluate the surface energy (or solid-solid wetting) of these AESO PSA

polymers as well as the interactions that are developed at the interface of AESO with itself or another polymer. The JKR information was used to study the adhesion/cohesion behavior of the PSAs derived from AESO.

5.3. Experimental

Materials and Methods

UV system. The Fusion UV system (Gaithersburg, MD) consisted of a 300 watt/inch H-mercury lamp and LC6B benchtop conveyor belt. The lamp distance from the conveyor belt was 10 cm. This UV system recorded UVA Band (320-390nm) and 615-660 mJ/cm^2 of UV radiation dose with EIT Power Puck 1 Radiometer (Sterling, VA) at a belt speed of 20 feet/min at focus.

AESO PSA. Acrylated epoxidized soybean oil (AESO) was purchased from Sigma-Aldrich (St. Louis, MO). The PSAs were prepared via free radical polymerization of AESO under UV radiation. AESO (0.1g) was spread in the marked area (4.5×16 cm) on a polyester (PET) carrier, and then the prepared films were scanned through the Fusion UV system (Gaithersburg, MD). The belt speed was set up at 7 feet/min (UV radiation dose: 215-231 mJ/cm^2) and repeated UV scans from 3 to 9 times until the polymer of AESO lost its tackiness almost completely.

The radiation dose, we prepared the polymers with a photointiator (DAROCUR 1173), which was kindly provided from BASF resins (Wyandotte, MI), Three w/w % of DAROCUR 1173 (3 mg) was added to neat AESO (1g). The belt speed was controlled from 7 ft/min (UV radiation dose: 215-231 mJ/cm^2) to 45 ft/min (UV radiation dose: 35-38 mJ/cm^2).

Fourier transform infrared spectroscopy (FTIR). FTIR spectra of the samples were obtained using FT-IR/FT-NIR spectrometer (Perkin Elmer Spectrum 400). To prepare FTIR specimens, AESO was filled in a round mold (1 mm thin, 1 cm diameter), and passed through UV system from 3 to 9 times at 7 ft/min of the belt speed (UV radiation dose: 215-231 mJ/cm^2), then the UV cured AESO polymer was removed from the mold.

Viscoelasticity. The viscoelasticity of the UV cured AESO PSA polymers was measured by a Bohlin CVOR 150 rheometer (Malvern Instruments, Southborough, MA) with a PP 8 parallel plate at room temperature. Frequency sweep of the specimen was measured from 0.01 to 100 rad/s, and single frequency as a function of time was tested at a constant shear rate of 1 Hz.

Tack, peel, and shear strength of AESO PSAs. The AESO PSA tapes were prepared on PET film via UV initiated polymerization. 90° peel, loop tack, and shear adhesion were tested according to ASTM D6195-03, D3330/D3330M-04, and D3654/D3654M-06, respectively. A strip of tape was applied to a glass panel for all tests using 2 passes of a 2 kg steel roller. The glass specimen was placed on a fixture clamped to the moving steel panel of the peel adhesion tester (Vertical Motorized Test Stand, MV-110-S). The non-adhesive-coated end of each strip was doubled back at a 90 °angle and clamped into the moving jaw to ensure a peel angle of 90 ° during peel testing. The speed of the moving jaw for the peel test was 5.0 ± 0.2 mm/s. Loop tack and static shear test specimens were adhered to a 2.54 cm by 2.54 cm portion. For the shear strength, a 1 kg weight was hung at end of the tape and the failure time in minutes was recorded.

JKR tests. The JKR tests were performed using a flat substrate and a hemispherical lens probe. AESO samples cured under UV radiation of 6, 7, 8 and 9 times passed at times at 7 ft/min of the belt speed (UV radiation dose: 215-231 mJ/cm^2) were evaluated using the JKR technique. For self-adhesion study, the flat substrate and the hemispherical lens were prepared from the UV cured AESO polymers. The AESO substrate was formed by means of a mold on an aluminum plate and then UV cured following the same UV condition described above. The AESO lens was formed by placing small drops of AESO on a fluorinated glass slide and curing the lenses for the indicated UV cycles. The radius of curvature of the hemispherical lens is calculated from the side image of the lens on the glass slide taken with a microscope. The radii of the curvature of AESO lenses used are typically in the range of 0.9-1.5 mm. For adhesion, a polydimethylsiloxane (PDMS) lens was used to probe the AESO substrate. PDMS samples were prepared from 2-part Sylgard 184. In Sylgard 184, the base mixture was dimethylvinyl-terminated dimethyl siloxane, and the curing agent was dimethyl methylhydrogen siloxane. PDMS was prepared by mixing the base and the curing agent at a ratio of 10:1 by mass. The PDMS hemispherical lenses were formed using the same technique described above for the AESO material. The radii of the curvature of PDMS lenses used were typically in the range of 0.9-1.1 mm

Thermal properties of AESO PSA. Thermal transitions (T_g and T_m) were obtained with a TA DSC Q200 (New Castle, DE) instrument. About 5 mg of AESO PSA film sample was sealed in an hermetic pan. The sample was heated from -80 to 250 °C at a rate of 10 °C/min, isothermally conditioned at -80 °C for 5 min. Decomposition characteristics were determined

with a Perkin-Elmer Pyris1 TGA (Norwalk, CT). About 5 mg of each sample was placed in the pan and heated from 25 to 850 °C at a heating rate of 20 °C/min under nitrogen atmosphere.

5.4. Results and discussion

Pure AESO was used to prepare PSAs via free radical polymerization with the use of UV radiation (Figure 5.1). Theoretically, faster UV curing (less energy) and tackier properties on demand can be achieved with the addition of petrochemicals such as a photoinitiator, crosslinking agent, and/or hardener. In this study, we focused on free-radical polymerization of pure AEMO under UV radiation though we prepared AESO with a photoinitiator as comparison.

The kinetic profiles of the UV radical polymerization of AESO can be monitored by FTIR absorbance bands at 1600 cm^{-1} (C=C) as a function of increasing UV dose[22] in proportion to the number of UV scans (Figure 5.1f). This FTIR kinetic study showed C=C of the acrylates decreased related to an increasing number of UV scans. Interestingly, the AESO PSA cured under 7-9 UV scans attracted only polished surfaces such as glass or plastic coating but not rough surfaces such as textile fibers, hairs, fibers, minerals, and skins. Therefore, there would be non-residue of removal lines on the applied surface and non-hand print on adhesive coated surface on the tape. This PSA can possibly replace petrochemical-based, removable, surface-protective, transparent tapes which are broadly applied on highly polished surfaces such as electronic displays to protect from scratching (Figure 5.1e), glass bottle labeling, or reusable tapes for office supplies with low tack but high chemical and temperature resistance. Interestingly, we found that the AESO with 6 scans (UV radiation dose: 1290-1386 mJ/cm^2) had a comparable tackiness to commercial band aids on our fingers (or skin) without cohesion failure, even though it showed low cohesion and adhesion strength on a glass substrate. Therefore, it could be a great candidate for biological applications (David et al. 2009).

Although the AESO PSA had excellent PSA properties without UV initiator, the high amount of UV radiation dose could hinder its practical application. Thereby, we used 3 w/w % of UV radical initiator (DAROCUR 1173) (Pelletier et al. 2006) to reduce the UV radiation dose with 43-46 mJ/cm^2. The PSA with 3 w/w % of DAROCUR 1173 showed relatively low peel, tack strength than that without UV initiator with UV radiation dose at 1720-1848 mJ/cm^2, yet presented similar peel, tack strength to the commercial reusable PSA (Post-it made by 3M, St.

Paul, MN). This study showed that low UV energy consumption can be achieved by using 3 w/w % of petroleum-based initiator which would be practical when faster process and lower energy consumption are required.

In visoelastic windows of PSAs (Chang 1997), the viscoelastic properties of the AESO PSAs presented a transition-plateau region (high modulus and high dissipation) for high shear PSA (Fig. 5.2a). Comparison between AESO PSAs with 4-9 UV sans showed the PSA with 7 UV scans had relatively higher loss modulus (G") and storage modulus (G') as a function of time (Fig. 5.2b) and frequency (Fig. 5.2c). Different polymerization degrees from UV radiation which affected mechanical peel, tack, and shear strength of the PSA tapes which highly corresponded to FTIR analysis. AESO PSA with 7 UV scans (UV radiation dose: 1505-1617 mJ/cm^2) had the most balanced cohesion/adhesion strength as shown in Figure 5.2d. The tape had relatively low peel and tack strength of around 1 N/cm^2 and 0.98 N/cm^2 comparable to general purpose PSA tapes (located in the middle window at Fig. 5.2a), yet stronger peel and tack strength than low tack reusable PSA tape such as Post-it (3M, St. Paul, MN) with a strength at around 0.5 N/cm^2. In addition, the shear hang time of PSA tapes with 6-8 scans (sample 6-8) recorded excellent shear strength (+30000 min) on a glass plate compared to sample 9 (45 min) with 9 UV scans. It was hung until the end of the test (30000 min) and was much stronger than the post-it (less than 1 min). This result also corresponded to the viscoleastic window analysis (Fig. 5.2a, Transition-plateau region) that AESO polymer can be defined as a high shear PSA. Therefore, this AESO PSA tape has potential for a high shear reusable tape application for polished surfaces such as a glass, but it did not adhere at all to unpolished surfaces such as paper and skin. However, the AESO PSAs with 5-6 UV scans adhered well to human skin, but showed cohesion failure on glass.

The JKR experiments were performed to evaluate the self-adhesion (or cohesion) behavior of AESO PSA samples as well as the adhesion of these samples with PDMS in a qualitative and quantitative manner. Qualitative results were used to compare the shape or the trend of the contact area during the loading and unloading, and quantitative results were used to determine the reduced bulk modulus (K), work of adhesion (W), and the fracture energy (G). Typical images of the contact area developed during the self-adhesion study of AESO polymers are depicted in Figure 5.3a for loading (L) and unloading (UL), respectively. The radius (a) of the contact area was approximately between 0.04 mm and 0.1 mm. During unloading, a circular

edge was observed around the contact area (see the outer ring in Figure 5.3b). The radius of this circular edge is close to the radius of the maximum contact area in the loading portion. In self-adhesion of glucose, the outer ring was defined as the boundary of the initial contact area, and the inner ring was defined as the peeling front (Zhao et al. 2006). Similarly, the viscoelastic behavior of AESO PSA samples caused this peeling effect observed as a circular region around the contact zone in our case. The self-adhesion experiments of samples with 7, 8, and 9 UV scans showed the loading and unloading contact areas similar to those depicted in Figure 5.3a. The contact areas observed during the self-adhesion of sample 6 was, however, markedly different, as shown in Figure 5.3b. During both loading (L) and unloading (UL), the contact areas showed a "fingering effect" around the edge of the contact region. This fingering effect in unloading has been observed earlier in viscoelastic materials, such as self-adhesion of uncross-linked PSAs (Falsafi and Tirrell 2000) and the peeling of PSA tape from glass (Frankel and Whitesides 1997). The fingering effect observed in unloading has been associated with viscoelastic dissipation in adhesion of PSAs (Creton et al. 1997; Falsafi and Tirrell 2000). The fingering effect in loading, however, has not been previously reported. We believe this was associated with the less-cured (or tackiness) behavior of sample 6, because the contact area was circular without fingering effect after 7 or more of UV scans.

In loading portion of the JKR test, the quantitative results include the calculation of reduced bulk modulus (K) and the work of adhesion (W), using equation (1) in introduction. In unloading portion, the quantitative results consist of the calculation of the energy release rate (G), using equation (3), but only if adhesion hysteresis is observed, while G=W if hysteresis is not observed. Figure 3c (a) shows a^3 (a = the contact radius) vs P (P = the applied load) and G vs P plots for self-adhesion of AESO PSAs. Noticeable adhesion hysteresis was shown in Figure 3c (b), which implied that G was significantly larger than W (Figure 5.3c (b)). Table 1 shows the quantitative results for the self-adhesion of AESO PSAs with 7, 8, and 9 UV scans. For the self-adhesion of the AESO PSA with 6 UV scans, JKR results cannot be used due to the fingering effect observed during loading. Other than a slightly lower K value for sample 7, there is very little difference between the calculated W and K values for the three samples. Based on the values of W, the surface energy of the AESO PSAs range was approximately 61-65 mJ/m^2, which was significantly higher than that of PDMS (ca. 45-51 mJ/m^2). The noticeable adhesion hysteresis observed from AESO PSAs demonstrated that specific bonds occurred between

surfaces. The trend in unloading behavior also confirms that there is a hydrogen-bonding formed between the molecules of AESO polymer (Choi et al. 1997). In addition AESO PSA with 7 UV scans showed a slightly higher adhesion hysteresis (G-W) within the data scatter as compared to other AESO PSAs' self-adhesion, which corresponded to the mechanical and rheological properties

To demonstrate adhesion of AESO PSAs with different polymer's surface, PDMS was used. Prior to AESO-PDMS adhesion experiments, self-adhesion of PDMS samples was carried out to determine its K, W, and G values. K, W, and G valuses of PDSM were 1.43±0.15 MPa, 43.7±0.8 mJ/m^2, and 54±2.1 mJ/m^2, respectively. In Figure 5.3d, insignificant adhesion hysteresis was shown between AESO PSAs and PDMS, which implied that G should be fairly close to W [Figure 5.3d (b)]. The quantitative results for the self adhesion of AESO PSAs and adhesion between AESO PSAs and PDMS are listed in Table 1. The JKR results of adhesion between AESO PSAs and PDMS showed similar K, W, and G values for all AESO PSAs. The values of W for adhesion between AESO PSAs and PDMS were also close to the values of PDMS self-adhesion. This results demonstrated that the adhesion behavior of AESO PSAs mostly dominated by an applied surface.

We selected AESO PSA with 7 UV scans for thermal analyses using DSC and TGA, since this sample showed the most promising physical properties for PSA applications. DSC recorded its low glass transition temperature (T_g) at -24 °C, which is desirable for PSA applications (Figure 5.4a). The melting temperature (T_m) was shown at 120 °C. Meanwhile, the discrete endotherm at around 0 °C seems to be entrapped water molecules which often occurs in oleopolymers (Ahn et al. 2011b). The TGA result of the AEMO PSA (Figure 5.4b) indicated a major weight loss (thermal degradation) at around 430 °C with an onset at around 200 °C that was completed at 700 °C (Figure 5.4b).

5.5. Conclusion

Solvent-free AESO PSA was prepared via UV free-radical polymerization. The UV cured AESO had excellent mechanical properties in reusable high shear PSA applications, especially on glass. The UV cured AESO polymer with UV radiation dose of 1505-1617 mJ/cm^2 showed comparable peel and loop tack strength but superior shear strength to Post-it. In addition, the UV

radiation dose was able to be reduced to 43-46 mJ/cm^2 with 3 w/w % of a photoinitiator: DAROCUR 1173, and showed similar mechanical properties to Post-it. Further viscoleastic behavior analysis revealed that the UV cure AESO PSAs is a high shear PSA. These PSA tests with rheology and JKR techniques showed corresponding results to the mechanical properties. The AESO PSA also showed T_g at -24 °C, T_m at 120 °C, and thermal degradation at around 430 °C. In addition, its inherently low toxicity and high biodegradability promise great potential for possible biological applications.

Figure 5.1. Chemical pathway of AESO synthesis, and its free radical polymerization: a, Chemical structures of soybean oil. b, Structures of ESO. c, Structures of AESO. d, General mechanism for the free-radical-process of acrylates of AESO under UV. e, Image of transparent PSA derived from AESO via UV curing. f, FTIR spectra of UV scanned AESO from 4 to 9 times (bottom to top).

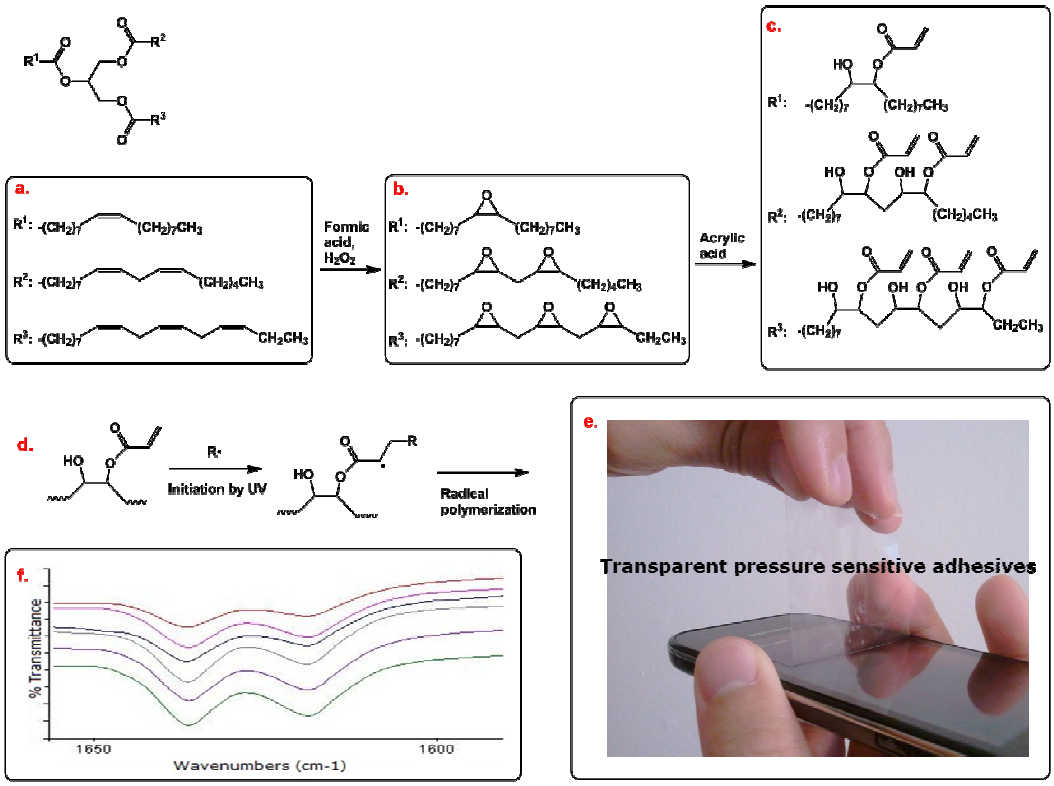

Figure 5.2. a, Viscoelastic windows of PSAs as related to different regions based on their rheological bevavior. b, Loss modulus (elastic modulus, G') and storage modulus (viscous modulus, G") as a function of time at constant shear rate (1 Hz). c, G' and G" as a function of frequency (rad/s). d, Peel and loop tack strength with cohesion/adhesion balance.

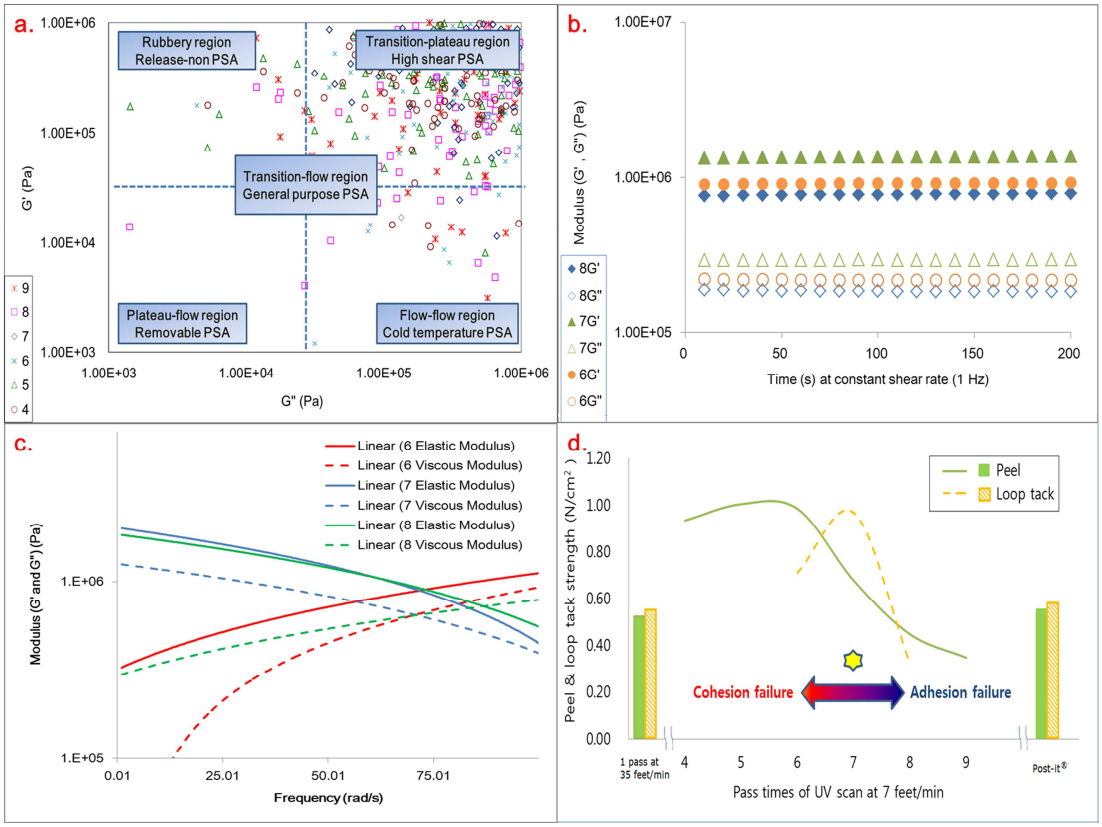

Figure 5.3. a, The contact area viewed in loading (L) and unloading (UL) of AESO PSA self-adhesion (image of AESO PSA sample 7). b, The contact area viewed in loading (L) and unloading (UL) of AESO PSA sample 6. c, Typical JKR data for AESO PSA self-adhesion. (a) a^3 vs P and (b) G vs P for AESO PSA sample 7. The blue line in loading shows the average value of W. d, Typical JKR data for adhesion between PDMS and AESO PSA sample 9 (a) a^3 vs P and (b) G vs P. The blue line in loading is the average value of W

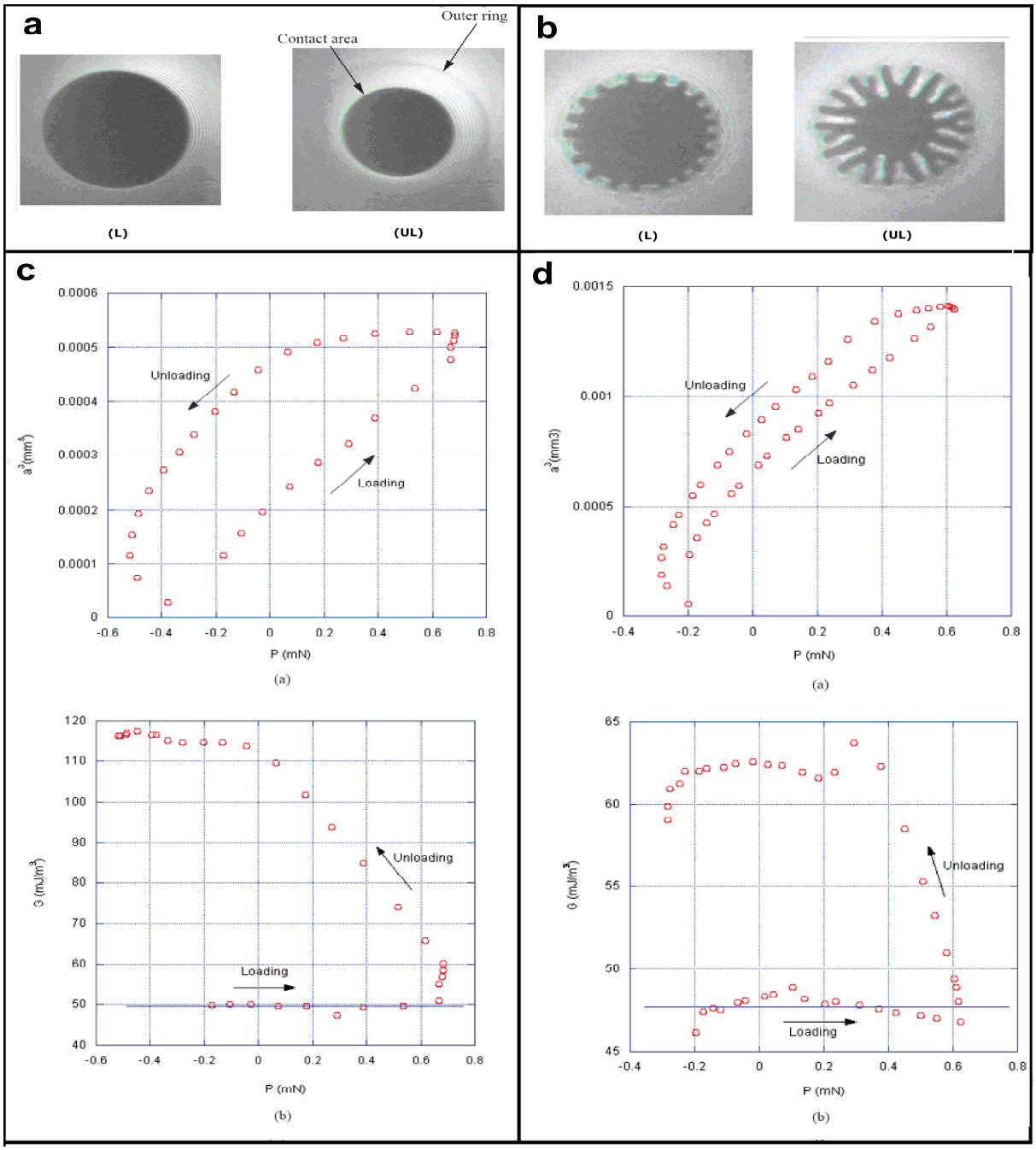

Figure 5.4. a, DSC of AESO sample 7. b, TGA of AESO sample 7.

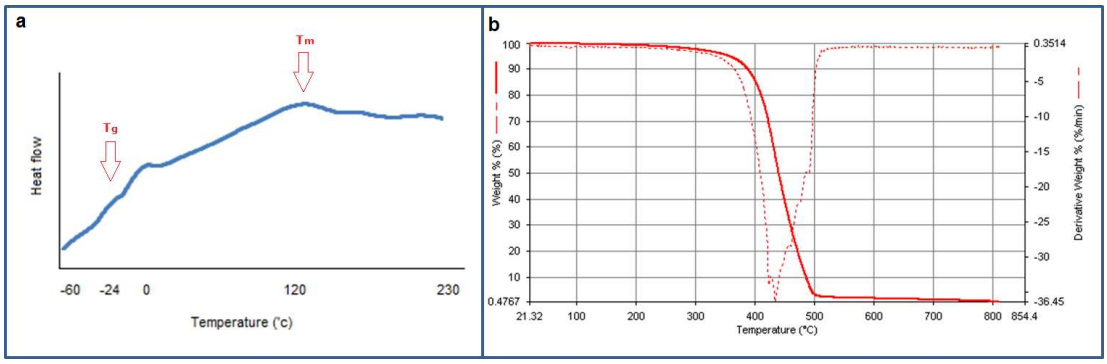

Table 5.1. JKR results of AESO PSAs' self-adhesion and AESO PSAs-PDMS adhesion with various UV irradiation cycles

AESO PSAs with UV scan times	Self Adhesion			PDMS-Adhesion		
	Loading		Unloading	Loading		Unloading
	K (MPa)	W (mJ/m^2)	G (mJ/m^2)	K (MPa)	W (mJ/m^2)	G (mJ/m^2)
9 (UV dose ≈1935 mJ/cm^2)	4.13±0.28	61.91±6.09	104.3±9.8	1.6048±0.02	46.07±0.81	59.3±1.15
8 (UV dose ≈1720 mJ/cm^2)	4.15±0.21	64.95±3.70	108±6.93	1.58±0.03	48.38±0.95	60.5±2.12
7 (UV dose ≈1505 mJ/cm^2)	3.85±0.01	63.28±2.14	114±2.83	1.58±0.03	45.20±0.66	60.67±0.58
6 (UV dose ≈1290 mJ/cm^2)	NA	NA	NA	1.68±0.01	51.70±1.20	63.70±0.58

5.6. References

Ahn, B. K., Kraft, S. and Sun, X. S. 2011a. Chemical pathways of epoxidized and hydroxylated fatty acid methyl esters and triglycerides with phosphoric acid. Journal of Materials Chemistry 21:9498-9505.

Ahn, B. K., Kraft, S., Wang, D. and Sun, X. S. 2011b. Thermally Stable, Transparent, Pressure-Sensitive Adhesives from Epoxidized and Dihydroxyl Soybean Oil. Biomacromolecules 12:1839-1843.

Boey, F., Rath, S. K., Ng, A. K. and Abadie, M. J. M. 2002. Cationic UV cure kinetics for multifunctional epoxies. Journal of Applied Polymer Science 86:518-525.

Bunker, S., Staller, C., Willenbacher, N. and Wool, R. 2003. Miniemulsion polymerization of acrylated methyl oleate for pressure sensitive adhesives. International Journal of Adhesion and Adhesives 23:29-38.

Bunker, S. P. and Wool, R. P. 2002. Synthesis and characterization of monomers and polymers for adhesives from methyl oleate. Journal of Polymer Science Part a-Polymer Chemistry 40:451-458.

Chang, E. P. 1997. Viscoelastic properties of pressure-sensitive adhesives. Journal of Adhesion 60:233-248.

Chen, Z. G., Wu, J. F., Fernando, S. and Jagodzinski, K. 2011. Soy-based, high biorenewable content UV curable coatings. Progress in Organic Coatings 71:98-109.

Cheong, M. Y., Ooi, T. L., Ahmad, S., Yunus, W. and Kuang, D. 2009. Synthesis and Characterization of Palm-Based Resin for UV Coating. Journal of Applied Polymer Science 111:2353-2361.

Choi, G. Y., Kim, S. and Ulman, A. 1997. Adhesion hysteresis studies of extracted Poly(dimethylsiloxane) using contact mechanics. Langmuir 13:6333-6338.

Creton, C., Cahn, R. W., Haasen, P. and Kramer, E. J., eds. 1997. Materials Science And Technology: A Comprehensive. Treatment. VCH: Weinheim.

David, S. B., Sathiyalekshmi, K. and Raj, G. A. G. 2009. Studies on acrylated epoxydised triglyceride resin-co-butyl methacrylate towards the development of biodegradable pressure sensitive adhesives. Journal of Materials Science-Materials in Medicine 20:61-70.

Falsafi, A. and Tirrell, M. 2000. Compositional effects on the adhesion of acrylic pressure sensitive adhesive. Langmuir 16:1619-24.

Frankel, F. and Whitesides, G. M. 1997. On the surface of things. Chronicle Books.

Hyde, P., D. 2009. Ultraviolet radiation - polymerizable compositions: EP 2 021 386 B1.

Johnson, K. L., Kendall, K. and Roberts, D. 1971. Surface energy and the contact of elastic solids. Proceedings of the Royal Society of London. Series A 324:301-313.

Klapperich, C. M., Noack, C. L., Kaufman, J. D., Zhu, L., Bonnaillie, L. and Wool, R. P. 2009. A novel biocompatible adhesive incorporating plant-derived monomers. Journal of Biomedical Materials Research Part A 91A:378-384.

Koch, C. A. 2010. Pressure Sensitive Adhesives Made From Renewable Resources and Related Methods: US 2010/0261806 A1.

Meier, M. A. R., Metzger, J. O. and Schubert, U. S. 2007. Plant oil renewable resources as green alternatives in polymer science. Chemical Society Reviews 36:1788-1802.

Metzger, J. O. and Bornscheuer, U. 2006. Lipids as renewable resources: current state of chemical and biotechnological conversion and diversification. Applied Microbiology and Biotechnology 71:13-22.
Pelletier, K., Belgacem, N. and Gandini, A. 2006. Acrylated vegetable oils as photocrosslinkable materials. Journal of Applied Polymer Science 99:3218-3221.
Pocius, A. V. 1997. The chemistry and physical properties of elastomer-based adhesives. Adhesion and adhesives technology:216-245.
Wu, J. F., Fernando, S., Jagodzinski, K., Weerasinghe, D. and Chen, Z. G. 2011. Effect of hyperbranched acrylates on UV-curable soy-based biorenewable coatings. Polymer International 60:571-577.
Xia, Y. and Larock, R. C. 2010. Vegetable oil-based polymeric materials: synthesis, properties, and applications. Green Chemistry 12:1893-1909.
Zhao, B., Zeng, H., Tian, Y. and Israelachvili, J. 2006. Adhesion and detachment mechanisms of sugar surfaces from the solid (glassy) to liquid (viscous) state. Proceedings of the National Academy of Sciences 103:19624-19629.

Chapter 6 - Solvent-free acid-catalyzed ring opening of epoxidized oleochemicals using stearates/stearic acid, and its applications

[This manuscript has been submitted to Journal of Agricultural and Food Chemistry]

6.1. Abstract

Toxic solvent and strong acid-catalysts causing environmental issues have been mainly used for ring opening of the epoxidized oleochemicals. Here, we demonstrated that magnesium stearate (Mg-stearate) was a high efficient catalyst for solvent-free ring opening of epoxidized methyl oleate, a model compound of mid-chain epoxide. Mg-stearate resulted in the highest yield (95%) and conversion rate (99%) toward mid-chain alkoxyesters at the same condition (160˚C, 12 h) superior to other fatty acid derivatives such as a Lewis acid (lithium and sodium stearate) and Brønsted acid (stearic acid). Based on this chemical study, we synthesized biogrease and thermoplastic using epoxidized soybean oil (ESO) and Mg-stearate via one-pot, solvent-free, and purification-free process. Mg-stearate played a significant role as a reactant for epoxide ring-opening and as a thickener when excess loading rate was used; viscosity increased from 1800 to 4500 Pa·s at 25 °C when ESO:Mg-stearate increased from 1:1 equiv to 1:2, then behaved like thermoplastics (T_g= -27 °C, T_m =90 °C) with 1:4.

6.2. Introduction

New renewable materials derived from soybean oil and other oleochemicals are continuously increasing their market share over traditional petroleum-based products due to stricter government regulations, economic pressures, and international mandates (Behr and Gomes ; Bozell 2008; Carlsson 2009; Eissen et al. 2002; Meier et al. 2007; Metzger 2009; Metzger and Bornscheuer 2006; Salimon et al. 2010a). Approximately 50% of most lubricants are ultimately released into the environment (Hörner 2002); therefore, environmentally harmless lubricants such as oleochemicals (Bondioli 2001) are needed. Unfortunately, plant oils often exhibit poor thermal and oxidative stability due to their propensity for *E/Z*-isomerizations (cis/trans isomerizations) and allylic autoxidation (Erhan and Asadauskas 2000). To alleviate these problems, chemical modification of internal double bonds (Behr et al. 2008; Xia and

Larock 2010) is often undertaken to produce materials with more favorable characteristics; for example, the conversion of soybean oil into epoxidized soybean oil (ESO) dramatically improved oxidative stability as a high-temperature lubricant (Adhvaryu and Erhan 2002; Campanella et al. 2010). ESO is an attractive "green" oleochemical raw material (Andjelkovic and Larock 2006; Helling and Russell 2009; Lu et al. 2010) because of its low toxicity and inherent biodegrabability (Burgos et al. 2009). Most importantly, subsequent chemical modifications of ESO can give rise to mid-chain branched oleochemicals that have desirable rheological properties (i.e., low pour points, good lubricity, and low volatility) (Aluyor et al. 2009; Campanella et al. 2010; Erhan and Asadauskas 2000; Erhan et al. 2008; Hörner 2002; Lathi and Mattiasson 2007; Legisa et al. 1997; Salimon and Salih ; 2009a; b; c; Salimon et al. 2010a; Salimon et al. 2010b). Fine-tuning of these modifications can be achieved through the size and morphology of the newly introduced branch. A particularly attractive mid-chain functionalization is the result of conversion of an internal epoxide into a vicinal hydroxy-carboxylate (**Scheme 6.1**); such a reaction provides an entry for superior lubricants with high oxidative stability as documented by Salimon and Salih (2009b), who showed that the introduction of mid-group branching points can alter low-temperature characteristics of plant oil-based lubricants by disrupting crystallization.

Based on lifecycle assessments as well as toxicological and ecological data for various cases, products based on renewable resources are commonly assumed to be more ecologically compatible when compared with petrochemical-based substances (Aluyor et al. 2009; Helling and Russell 2009; Salimon et al. 2010b). In the specific case of mid-chain esters in plant oils, good biodegradability was experimentally recorded (Lathi and Mattiasson 2007), which may be due in part to easily hydrolyzable ester moieties at the branching point; in contrast, simple alkyl branched fatty acids can be impervious to biological breakdown (Sin and Chua 2000).

A common problem in the synthesis of α-hydroxy-carboxylates from epoxidized oleochemicals is the need for strong Brønsted acids to activate the epoxide ring toward the attack of weakly nucleophilic carboxylic acids (**Scheme 6.1**). This can be accomplished through the addition of heterogeneous sulfonic acids and in the presence of a biphasic solvent mixture (Campanella and Baltanas 2004; 2006; 2007; Schuster et al. 2008) or through the action of strong homogeneous acids such as H_2SO_4 (Salimon and Salih 2009a; b; c) or *p*-toluenesulfonic acid (Salimon and Salih ; 2009b; Salimon et al. 2010a). In all cases, the removal of acid and solvent

requires a purification step. Ring-opening esterification has been accomplished in the absence of catalysts and solvents simply by heating, but the extra carboxylic acid reaction component must be removed after the reaction (Moser et al. 2007). Similar problems occur in the synthesis of estolides (fatty acid polyesters) (Pelaez et al. 2003; Plattner et al. 1979) via a formal hydroxy-carboxylation of a fatty acid to internal double bonds; the latter require toxic and highly acidic $HClO_4$ as a catalyst for such reaction from oleic acid (Harry-O'kuru et al. 2001).

In this research, we were encouraged by the fundamental work conducted by Chini *et al.*, which demonstrated that attack of epoxides by weak *O*-, and *N*-nucleophiles can be catalyzed by Lewis-acidic alkaline and alkaline earth metals (Chini et al. 1992b; Chini et al. 1992c; Chini et al. 1990b; 1991). We reacted epoxidized methyl oleate (EMO) with Mg^{2+}- Li^{+}-, Na^{+}- salts (soaps), and stearic acids in the absence of solvents, and their nucleophilic competition in terms of atom economy and environmental factor was elucidated. Reaction products were identified by ^{1}H NMR and electrospray ionization mass spectrometry (ESI-MS). Cation-dependent conversions/yields in the case of EMO were also determined by ^{1}H NMR spectroscopy. Based on this fundamental chemistry, we synthesized soybean oil derivatives in the addition of alkaline and alkaline earth metal carboxylates (soaps) to internal epoxides of ESO. The role of the soap was conceived to be three-fold in providing a) a carboxylate nucleophile, b) a cation acting as a Lewis-acid catalyst (Chini et al. 1992b; Parker and Isaacs 1959; Paterson and Berrisford 1992), and c) miscibility with the product to act as a potential thickener additive. The reaction of ESO with magnesium stearate resulted in attractive thermal, mechanical, and rhelogical properties that can be modulated by the loading level of Mg-soap. Thermal dynamic and mechanical properties of the resulting grease and thermoplastic-like materials were investigated by differential scanning calorimetry (DSC), thermogravity analysis (TGA), dynamic mechanical analysis (DMA), and dynamic rheometers.

6.3. Experimental Section

General

Methyl oleate was purchased from Fisher Scientific (Pittsburgh, PA). ESO was purchased from Scientific Polymer Products.

^{1}H NMR. 1D ^{1}H NMR and 2D ^{1}H-^{1}H COSY NMR spectra for our samples were recorded quantitatively using a Varian S spectrometer (Varian Inc, Palo Alto, CA) at observing frequency of 500 MHz for ^{1}H on a 5 mm triple resonance probe. The sample solutions were prepared in $CDCl_3$. ^{1}H NMR spectra were obtained with 32 scans at a delay time of 1 s between scans. 2D ^{1}H-^{1}H COSY spectra were obtained with 128 increments and 4 scans for each increment. A sine bell function was used during processing for both dimensions

ESI-MS. Electrospray Ionization spectra were acquired on a LCT Premier (Waters Corp., Milford MA) time of flight mass spectrometer. The instrument was operated at 10,000 resolution (W mode) with dynamic range enhancement that attenuates large intensity signals. The cone voltage was 60eV. Spectra were acquired at 16666 Hz pusher frequency covering the mass range 100–1200 u and accumulating data for 2 s per cycle. Mass correction for exact mass determinations was made automatically with the lock mass feature in the MassLynx data system. A reference compound in an auxiliary sprayer was sampled every third cycle by toggling a shutter between the analysis and reference needles. The reference mass was used for a linear mass correction of the analytical cycles. Samples were presented in acetonitrile as a 20ul loop injection using an autoinjector (LC PAL, CTC Analytics AG, Zwingen, Switzerland).

FTIR. FT-IR spectra were recorded using a PerkinElmer Spectrum 400 FT-IR/FT-NIR spectrometer (PerkinElmer, Waltham, MA).

X-ray diffraction (XRD). Powder X-ray diffraction was used to characterize the composition of the thermoplastic-like material. Cu Kα radiation was used with a curved crystal graphite monochromator. The operating range for X-ray target was 35 kV and 25 mA. The X-ray scans were in range of 2>2Ø>75°.

DSC. Thermal transitions (T_g and T_m) were obtained with a TA DSC Q200 instrument. About 5.8 mg of the developed thermoplastic samp was sealed in a hermetic pan. The sample was heated from -70 to 250 °C at a rate of 10 °C/min, then cooled to -70 °C and reheated to 250 °C at same rate, and isothermally conditioned at -70 °C and 250 °C for 10 min. A second scan was collected.

TGA. Decomposition characteristics were determined with a PerkinElmer Pyris1 TGA (Norwalk, CT). About 5 mg of each sample was placed in the pan and heated from 40 to 800 °C at a heating rate of 20 °C/min under nitrogen atmosphere.

DMA. Dynamic mechanical analysis was carried out using a DMA-7e dynamic mechanical analyzer (PerkinElmer, Norwalk, CT) with the compressive method following ASTM D5024. The rate was 3 °C/min.

Rheology. Apparent viscosity measurements of blends were performed using a Bohlin CVOR 150 rheometer (Malvern Instruments, Southborough, MA) with a PP 20 parallel plate. Shear rate dependence was measured from 1–50 rpm and time dependence was collected at a fixed speed of 1 rpm. Temperature dependence was measured from 25–150 °C with 20 °C increment at fixed speed of 1 rpm.

Synthesis and Reaction Monitoring

9,10-Epoxidized methyl oleate (1). Methyl oleate was epoxidized with mCPBA using the method of Holland et al (2003). Briefly, methyl oleate (4.5 g, 15 mmol) in 100 mL dichloromethane was stirred at 0 °C, and a solution of mCPBA (7.9 g, 46 mmol) in 50 mL dichloromethane was added gently. After completion, the temperature was raised to room temperature, and the mixture was stirred for another 18 h. After purification, 1 was obtained as clear oil in 87% yield after drying under high vacuum.

^{1}H NMR ($CDCl_3$, 500Mhz): δ 3.61 (s, 3H), 2.84 (m, 2H), 2.25 (t, J = 7.5 Hz, 2H), 1.57 (m, 2H), 1.50-1.17 (m, 24H), 0.83 (t, J = 7.6 Hz, 3H).

9-(or 10-)stearic ester-10-(or 9-)ol methyl stearate (2^{Mg}, 2, 2^{Li}, 2^{Na}). 1 (0.450 g, 1.44 mmol) was mixed with magnesium stearate (0.425 g, 0.72 mmol), stearic acid (0.409 g, 1.44 mmol), lithium stearate (0.418 g, 1.44 mmol), and sodium stearate (0.441 g, 1.44 mmol), respectively, at 160 °C for 12 h. Aliquots were taken after 10 min and 12 h, dissolved in $CDCl_3$, and ^{1}H NMR spectra were acquired.

An identical experiment was conducted with **1** (0.450 g, 1.44 mmol) and magnesium stearate (0.425 g, 0.72 mmol).

Semi-solid biolubricant (grease). A semi-solid biolubricant (grease) was obtained at the molar ratio of 1:2 and 1:1 (**Fig. 6.4a**) from the reaction of ESO (20 g, 20 mmol) with a molar ratio of 1:2 (23.6 g, 40 mmol) and 1:1 (11.8 g, 20 mmol), respectively, at 160 °C for 12 h. A yellow transparent thermoplastic-like material was obtained (**Fig. 6.4b**) from the reaction of ESO (1.8 g, 1.8 mmol) and magnesium stearate in a molar ratio of 1:4 (4.2 g, 7.2 mmol) at 160 °C for 12 h.

6.4. Results and Discussion

Chemical pathways of EMO with stearates/stearic acid

In studying the reactions of internal epoxides of fatty acids with carboxylic acids and carboxylates, we initially used epoxidized methyl oleate (**1-EMO**) as a model compound representing epoxidized oleochemiclas including ESO. Although the functional groups (internal epoxide and terminal ester) are identical in both ESO and model **1**, the use of the latter has two key advantages in data analysis. First, **1** is a discreet compound with a distinct molecular weight whereas ESO consists of a mixture of triglycerides, so **1** allows for a more straightforward mass-spectroscopy analysis. Second, the ^{1}H NMR analysis of ESO and its derivatives is complex above δ 4.0 due to three multiplets from one internal and two terminal diastereotopic ester hydrogens that would obscure the formation of new esters from an epoxide attack. Furthermore, **1** displays a single epoxide multiplet at δ 2.84 whereas ESO has a set of at least six multiplets (in the range of δ 3.21–2.85) whose disappearance can be difficult to quantify in its reaction over time.

Heating mixtures of **1** and stearic acid (1 equiv) or magnesium stearate (1 equiv) for 12 h at 160 °C in the absence of solvents resulted in a 96% disappearance of the ^{1}H NMR ($CDCl_3$) epoxide signal of **1** relative to the methyl ester signal at δ 3.65 (CO_2CH_3) that we used as an internal standard (**Fig. 6.1a** from stearic acid and **Fig 6.2a** from magnesium stearate).The ester peak at 3.65 ppm was a composite signal from products and from starting material **1**. In both cases, multiplets at δ 4.83 revealed the formation of an ester of a secondary alcohol ($R^1R^2C(\mathit{H})OOCR^3$). In support of the ring-opening event, a new signal at δ 3.57 was consistent with the CH-proton of an alcohol functionality [$R^4R^5C(\mathit{H})OH$] next to the ester. Both signals have integrals that are approximately 1/3 the intensity of the methyl ester signal. Two-dimensional ^{1}H-^{1}H COSY NMR (**Fig. 1b** and **Fig. 2b**) of the products presented a cross peak between $R^1R^2C(\mathit{H})OOCR^3$ and $R^4R^5C(\mathit{H})OH$ signals that unequivocally established their vicinal relationship within one product. Mass spectroscopy for both products further confirmed the covalent connection of the two fatty acid fragments of 9(10)-hydroxy-10(9)-octadecanoyloxy stearic acid methyl ester (**2**) (ESI-MS, m/z = 635.5 [$M+K^+$]).

Under identical reaction conditions (160 °C, neat 1:1 mixture of reactants), the reaction between **1** and stearic acid, the conversion rate of **1** was 96% after 12 h (**Table 6.1**, entry 1) with a yield of 47% for **2**. As a by-product, a second ester of a secondary alcohol was formed in 20%

yield with a signal for $R^1R^2C(H)OOCR^3$ at δ 5.00 (**Fig. 6.1a** and **Fig 6.3**). The ^1H-^1H COSY NMR spectrum (**Fig. 6.1b**) revealed a cross peak with a signal at δ 3.41 well within the range of a vicinal ether proton [$R^4R^5C(H)OCR^6$]. This is complemented by another set of signals at δ 3.33 and δ 3.27 that can be attributed to the presence of alcohols and/or ethers. The mass spectrum (ESI-MS) revealed a peak at m/z = 948.8 for [**3**+K^+]. In combination, both ^1H NMR- and MS-spectroscopic results point out the formation of ether-adduct (**3**) (in the form of 9,10- and 9',10'-regioisomers). We proposed that **3** (ESI-MS, m/z = 635.5 [M+K^+]) was formed from the acid-catalyzed alcoholysis of epoxide in **1** with alcohol in **2** (Chini et al. 1992a; Chini et al. 1990a; Chini et al. 1992b; Jones and Rapoport 1990; Ley and Redgrave 1990; McBee et al. 1956; Parker and Isaacs 1959; Ramachandran et al. 1995; Thompson et al. 1994). Although such reactions typically require stronger acids, we have recently discovered that the relatively weak acid H_3PO_4 can catalyze alcoholyses of epoxidized methyl oleate (Ahn et al. 2011).

The use of lithium and sodium stearate (1 equiv) produced lower conversions of **1** (24% and 67%) (**Table 6.1**, entries 2,3) under otherwise identical reaction conditions. The two sterate salts not only exhibited lower reactivity, but also were unable to improve selectivities for **2** over **3,** and the product ratios **2**:**3** of 1.9:1 and 5.4:1 (entries 2,3 in **Table 6.1**) were not significantly different from the 2.4:1 value for stearic acid (entry 1).In the absence of moisture, the initially formed adducts from **1** and Li-, Na-, and Mg-stearate are the alkoxides $\mathbf{2^{Li}}$, $\mathbf{2^{Na}}$, and $\mathbf{2^{Mg}}$. Similarly, the alkoxides $\mathbf{3^{Li}}$, $\mathbf{3^{Na}}$, and $\mathbf{3^{Mg}}$ were formed from $\mathbf{2^{Li}}$, $\mathbf{2^{Na}}$, and $\mathbf{2^{Mg}}$ and **1**. Upon hydrolysis alcohol **2** is formed (step 2a, **Scheme 6.2**). ^1H NMR samples were prepared in air and the solvent $CDCl_3$ was not pre-dried; the formation of alcohols **2** and **3** is therefore likely to be a consequence of hydrolysis during sample peparation. On the other hand, magnesium stearate opened the epoxide ring of **1** efficiently (99% conversion after 12 h at 160 ^oC) (entry 4); moreover, the product selectivity **2**:**3** was improved to 24:1 (presumably both adducts were initially formed as magnesium alkoxides $\mathbf{2^{Mg}}$ and $\mathbf{3^{Mg}}$). We attributed the higher conversion primarily to the relatively low melting point of magnesium stearate (88 °C) allowing complete miscibility of liquid **1** and the liquid Mg-salt at 160 °C. In contrast, lithium stearate (mp = 220 °C) and sodium stearate (mp = 245-255 ^oC) are solids at 160 °C, and form only heterogeneous mixtures with **1** during the reaction despite constant stirring of the suspension. Low efficient mass transfer due to low solubility of the Li-soaps and Na-soaps may therefore be partially responsible for the sluggish conversion. Furthermore, the relatively mild Lewis acidity

of alkaline metals (in conjunction with relatively strongly coordinating carboxylates) may provide only limited electrophilic activation through oxygen coordination prior to nucleophilic attack, whereas the dicationic and more electrophilic magnesium ion is likely to interact with the oxirane ring more strongly.

The reaction of **1** and metal stearates produced metal alkoxides $\mathbf{2}^{\mathbf{Li}}$, $\mathbf{2}^{\mathbf{Na}}$, and $\mathbf{2}^{\mathbf{Mg}}$ (**Scheme 6.2**). The formation of $\mathbf{3}^{\mathbf{Li}}$, $\mathbf{3}^{\mathbf{Na}}$, and $\mathbf{3}^{\mathbf{Mg}}$ from $\mathbf{2}^{\mathbf{Li}}$, $\mathbf{2}^{\mathbf{Na}}$, **and** $\mathbf{2}^{\mathbf{Mg}}$ is likely to occur through similar mechanisms involving Lewis acid activation (**Scheme 6.2**) (Chini et al. 1992b; Chini et al. 1992c; Parker and Isaacs 1959; Paterson and Berrisford 1992).

Data in **Table 6.1** showed excellent atomeconomy (predominant selectivity) of magnesium stearate. Only entry 4 presented that the conversion rate matched to product (**2** and **3**) yields while stearic acid and other salts resulted in unidentified multiple byproducts. In entries 2–4 (**Table 6.1**)**,** the formed products are metal alkoxides that in turn acted as reagents and attacked a second epoxide molecule. In fact, sodium alkoxides previously have been found to attack secondary epoxide centers (Lemieux et al. 1958; McRae et al. 1952; Reeve and Christoffel 1950). At the beginning of reaction, the stearate anion concentrations in entries 2-4 are higher than the concentrations of $\mathbf{2}^{\mathbf{Li}}$, $\mathbf{2}^{\mathbf{Na}}$, and $\mathbf{2}^{\mathbf{Mg}}$; at this point, the conversion rates in *step 2* are statistically advantageous over conversion rates in step 3 (**Scheme 6.2**). This contributed to the reaction's yield of more product **2** than **3** (the neutral species **2** and **3** were formed during hydrolyses in *steps 2a* and *3a* during NMR sample preparation); in the case of magnesium stearate, a 99% conversion (of both **1** and stearate anions) was found (entry 4). As conversions approached 50%, the alkoxide nucleophiles of $\mathbf{2}^{\mathbf{Li}}$, $\mathbf{2}^{\mathbf{Na}}$, $\mathbf{2}^{\mathbf{Mg}}$ are more abundant than stearate anions, which would make *step 3* a statistical advantage over *step 2*; in this case, the reaction would yield more product **3** than **2**, effectively nullifying the initial statistical bias favoring the formation of **2**. In the presence of magnesium salts in entry 4, however, with an experimentally determined **2**:**3** ratio of 24:1, we concluded that the ether-forming *step 3* must be intrinsically slower than the epoxide-opening *step 2*. Therefore, magnesium alkoxide $\mathbf{2}^{\mathbf{Mg}}$ must be less reactive toward epoxide **1** than magnesium stearate despite the fact that alkoxides are generally stronger nucleophiles than carboxylates (Pearson et al. 1968; Phan and Mayr 2005). We proposed that a tight ion pair association in $\mathbf{2}^{\mathbf{Mg}}$ is strong enough to mutually attenuate Lewis acidity of the metal and Lewis basicity of the oxy-anion of the alkoxide. A related course of action was previously found in the reaction of MgI_2 with secondary benzylic and secondary aliphatic epoxides in which

in situ formed alkoxides (of iodohydrins) did not engage in further attacks on epoxide starting materials (Bonini and Righi 1992; Bonini et al. 1991; Federici et al. 1994; Golumbic and Cottle 1939).

Chemical properties of products derived from ESO and magnesium stearate

The clean conversions and high yields in the reaction of **1** and magnesium stearate prompted us to investigate reactions of the Mg-soap with epoxidized soybean oil (ESO, 3.9 epoxides per triglyceride). Heating a 1:1 mixture of magnesium stearate and ESO (stearate anions per epoxide = 0.51:1) at 160 ^{o}C for 12 h caused partial epoxide ring opening (conversion 51% relative to ESO) and formation of alkoxyesters (yield of hydroxyesters after hydrolysis: 51% relative to ESO) (**Fig. 6.4a**). Although no distinct ^{1}H NMR signals (**Fig. 6.5b**) are suitable for tracking the fate of magnesium stearate directly, the yield and conversion of ESO indicate the quantitative uptake of the soap. The obtained material has grease-like properties (Grease I). Heating a 1:2 mixture of ESO with magnesium stearate (ratio of carboxylate anions to epoxide = 1.1:1) at 160 ^{o}C for 12 h also produced a grease (Grease II). The ^{1}H NMR spectra of the hydrolyzed materials (**Fig. 6.5b–d**) underscore the virtual consumption of epoxides (δ 3.21–2.84) of the starting material ESO (**Fig. 6.5a**). New signals in the range δ 5.37–4.80 (secondary esters, R'R"*H*CO_2CR) and δ 4.25–3.35 (CH and OH alcohol signals, R'R"*H*COH and R'R"HCO*H*) were consistent with the formation of mid-chain hydroxyesters. The ratio of ester and alcohol integrals in Grease II (**Fig. 6.5c**) was 1:2 as expected for the presence of CH and OH signals (integral 2H) in the range δ 4.25–3.35. Relative to the terminal glyceride ester signals at δ 4.25 (integral 2H), the integral for newly formed esters was 3.7 H and the integral for newly formed alcohols (CH and OH) was 7.4 H, which is consistent with a quantitative product yield. Then, we further increased the content of the soap in the starting mixture and heated a 1:4 mixture of ESO and magnesium stearate (ratio of carboxylate anions to epoxide: 2.2:1) for 12 h at 160 ^{o}C (**Fig. 6.5d**). This reaction produced a transparent thermoplastic-like material after cooling (**Fig. 6.4b**). For the product analysis, the composite was subsequently extracted with chloroform in which the excess magnesium stearate was poorly soluble. The Mg-soap was identified by FT-IR through its antisymmetrical and symmetrical C=O stretches at 1549.2 cm^{-1} and 1455.4 cm^{-1} (**Fig. 6.6a**). In contrast, the filtrate did not contain these carboxylate bands (**Fig. 6.6b**), but revealed ester C=O bands (ν = 1732.9 cm^{-1}) and a broad alcohol OH band (ν ≈ 3500 cm^{-1}) consistent with the presence of an organic hydroxy-ester scaffold.

The ^{1}H NMR spectrum of the $CDCl_3$-extract of the thermoplastic-like material (**Fig. 6.4b**) is shown in **Fig. 6.5d**. Although a slightly lower spectral quality, a good match with **Fig. 6.5c** ("grease") is apparent, which suggests that the basic organic constituents in Greases I and II are identical with the thermoplastic-like material. The main difference between both materials is due to the presence of excess magnesium stearate within the thermoplastic-like material (about 4.3 equiv of unreacted carboxylate anions per triglyceride after complete epoxide conversion). The magnesium stearate is apparently capable of thickening the organic base material to the extent of becoming a solid. We tested this hypothesis by melting a sample of Grease II with 2 equiv of additional magnesium stearate (4 equiv of stearate anions) until complete mixing was achieved (within 5 minutes); subsequent cooling of the mixture did, in fact, produce a thermoplastic material similar to that in **Fig. 6.4b**. Previously, *in situ* generated magnesium soaps were used as thickeners in petrochemical-based magnesium greases (Forsberg 1980). In addition, the X-ray diffraction (XRD) was performed to determine whether the thermoplastic-like material is totally amorphous or partially crystalline. The XRD (**Fig. 6.7**) provided a typical XRD pattern of magnesium stearate (wide peak around 22°) (Koivisto et al. 2004) which explained it was partially crystalline. This XRD result also supported our hypothesis that magnesium stearate can be a thickener at extra higher concentration.

In a separate experiment, we found that the chemical conversion of epoxides in ESO to alkoxyesters were crucial for the establishment of both grease and thermoplastic properties as simple (physical) melting of ESO and magnesium stearate for 5 min (with very few epoxides chemically converting during that time) created only opaque and soft putty-like materials upon cooling.

Thermal and mechanical properties of ESO with magnesium stearate

Thermal properties of the bio-grease (**Fig. 6.4a**) and thermoplastic-like material (**Fig. 6.4b**) were investigated with the aid of differential scanning calorimetry (DSC) and thermogravimetric analysis (TGA). Dynamic mechanical thermal analysis (DMTA) was used to study the viscoelastic behavior of the thermoplastic-like material. DSC results showed that the magnesium stearate had two discrete endotherms at around 90 °C (T_m) (Koivisto et al. 2004) and 110 °C (**Fig. 6.8, top**), possibly due to the loss of hydrated or entrapped water. The second scan of thermoplastic-like material displayed the same "double endotherm," but it was less pronounced (**Fig. 6.8, bottom)**; this is expected due to the presence of unreacted magnesium

stearate in the blended material. The glass transition temperature was found at T_g= -27 °C (Chuang and Han 1984; Upadhyay et al. 2011).

In contrast, Grease I did not show the double endotherm at higher temperatures due to the absence of excess magnesium stearate. Its glass transition temperature (T_g= -25 °C) was slightly different from the thermoplastic-like material.

The TGA-plot of the thermoplastic-like material indicated a small weight loss at around 160 °C followed by a major weight loss (thermal degradation) at around 420 °C with an onset at around 260 °C that was completed at 530 °C (**Fig. 6.9**). The TGA curve of the Grease I presented a similar thermal degradation profile with major weight loss at around 390 °C.

DMTA results showed that storage modulus (E') and loss modulus (E'') were independent of frequency (**Fig. 6.10**) but decreased as temperature increased (**Fig. 6.11**). This transparent thermoplastic-like material has unique thermal and mechanical properties; it is sensitive to temperature changes with a long rubbery region.

In rheological studies, Greases I and II were compared to commercial silicone grease (Dow Corning high-vacuum grease, Midland, MI) as a function of shear rate, time, and temperature (Bohlin CVOR 150 rheometer). Grease I displayed a shear thinning behavior similar to commercial silicone grease (**Fig. 6.12**) whereas Grease II had continuously higher viscosities at the same shear rates. The decrease in viscosity with increasing shear rates is typical of greases in general. All samples showed fairly time-independent flow (**Fig. 6.13**).

When temperature increased, Grease I experienced a gradual decline of viscosity from 1800 Pa·s at 25 °C to about 1000 Pa·s at 120 °C, which closely matched the behavior of the commercial silicone grease (**Fig. 6.14**). In contrast, Grease II, which is more viscous at 25 °C (4500 Pa·s compared to 1800 Pa·s for Grease I), rapidly declines in viscosity when temperature increases, measuring < 100 Pa·s at 120 °C. Clearly, the viscosity in greases derived from ESO and magnesium stearate depends on various factors. At lower temperatures, the higher viscosity of Grease II compared to Grease I can be correlated with the higher average molecular weight of its components due to exhaustive conversion of epoxides to alkoxyesters (**Fig. 6.5**) or the effect of partial crystallization (**Fig. 6.7**) in the magnesium stearate-rich domains in Grease II. At elevated temperatures a separate factor must come into play to lower the viscosity of the "heavier" Grease II below the values of the "lighter" Grease I.

6.5. Conclusion

The acid-catlyzed ring opening of epoxidized methyl oleate (**1-EMO**) with magnesium stearates produced a mid-chain alkoxyester in near quantitative conversion and yield in 12 h at 160 °C with traces of ether formation (oligomerization) detected as a result from alcoholysis of the product alkoxide with **1**. This reaction was significantly cleaner as measured by ether-forming oligomerizations than analogous reactions with stearic acid, lithium, and sodium stearate. Based on this chemistry, we obtained grease I by reacting epoxidized soybean oil (ESO) with magnesium stearate via a green process (solvent free, one pot, purification free). Grease I has great potential for industrial uses in the temperature tested in this work. We were able to manipulate the properties of the reacted materials by controlling the ratio of ESO and magnesium stearate. Greases, for example, were obtained at ratios of 1:1 to 1:2 equiv of ESO:Mg-stearate, and a transparent thermoplastic-like material was the result of higher loading of Mg-soap (i.e., 1:4 of ESO:Mg-Stearate). Magnesium stearate played two roles depending on its loading level: it functionalized either partially or completely the epoxides in ESO, and it also acted as a thickener in excess loading. These biobased materials were formed in solvent-free processes that did not require further workup or purification steps. In the absence of waste generation, these reactions attain 100% atom economy and environmental factor.

Figure 6.1. a: ^{1}H NMR of 9(10)-hydroxy-10(9)-octadecanoyloxy stearic acid methyl ester (2) from ring-opening of epoxidized methyl oleate (1) with stearic acid, b: ^{1}H-^{1}H COSY of the identical 2 sample from Fig. 1a. In circles are a cross peak between ester protons $R^1R^2C(H)OOCR^3$ at δ 4.83 and the C-H proton of a secondary alcohol [$R^1R^2C(H)OOCR^3$] at δ 3.57 of 2 as well as a another cross peak between the ester proton of 3 at δ 5.00 and an ether C-H proton [$R^4R^5C(H)OCR^6$] at δ 3.41.

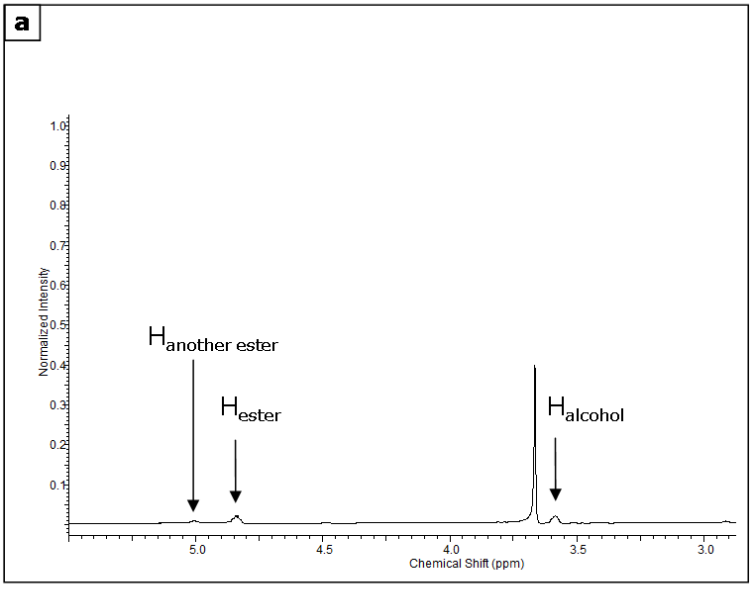

Figure 6.2. a: ^{1}H NMR of 2 from ring-opening of 1 with magnesium stearate; product signals are identical with those in Fig. 1a as initially formed 2^{Mg} that is hydrolyzed to 2 during NMR sample preparation. b: ^{1}H-^{1}H COSY of the sample in Fig. 2a. In circles are a cross peak between ester protons $R^{1}R^{2}C(\mathit{H})OOCR^{3}$ at δ 4.83 and the C-H proton of a secondary alcohol [$R^{1}R^{2}C(\mathit{H})OOCR^{3}$] at δ 3.57 of 2.

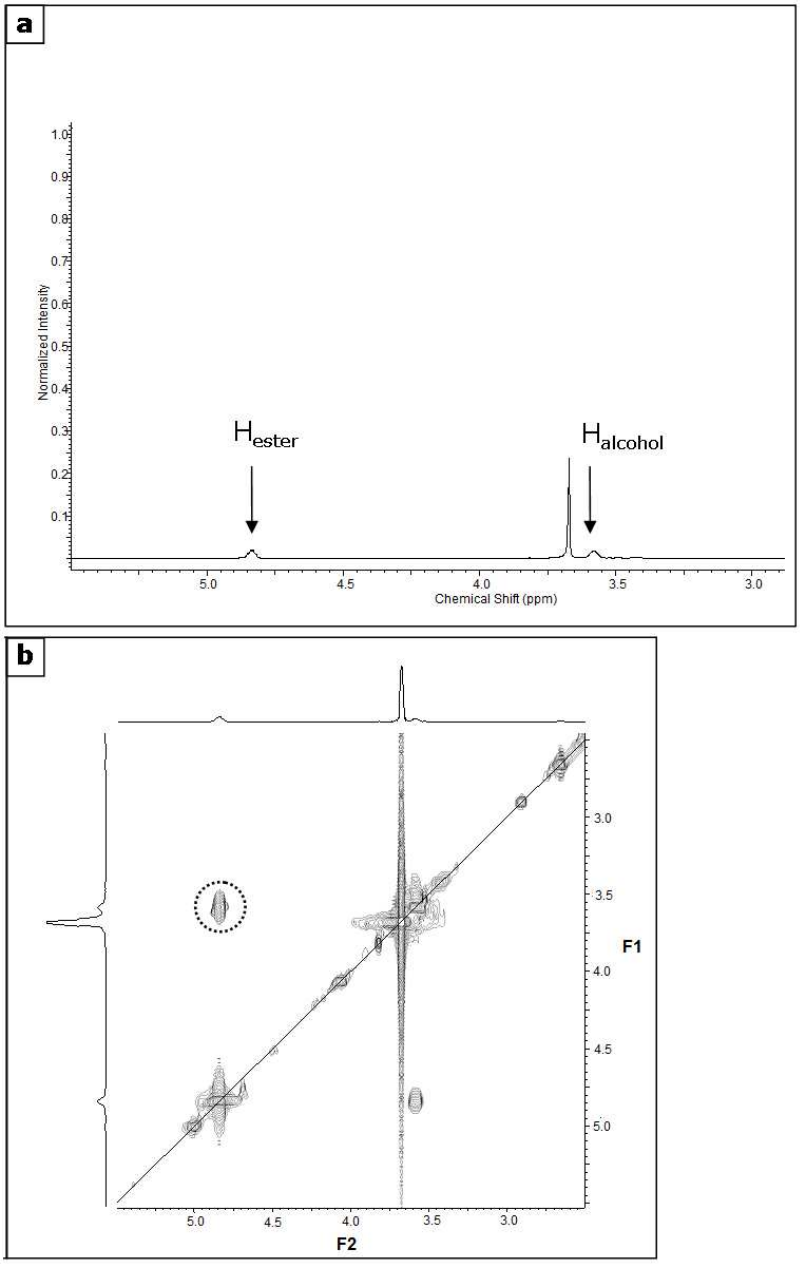

Figure 6.3. ^{1}H NMR of reaction products of 1 and magnesium, sodium, and lithium stearate and stearic acid (bottom to top) a) **product mixture obtained from the reaction of** 1 **and stearic acid,** b) **product mixture obtained from the reaction of** 1 **and lithium stearate (the initially formed** 2^{Li} **and** 3^{Li} **were hydrolyzed to** 2 **and** 3 **during sample preparation),** c) **product mixture obtained from the reaction of 1 and sodium stearate (the initially formed** 2^{Na} **and** 3^{Na} **were hydrolyzed to** 2 **and** 3 **during sample preparation),** d) **product mixture obtained from the reaction of** 1 **and magnesium stearate (the initially formed** 2^{Mg} **and** 3^{Mg} **were hydrolyzed to** 2 **and** 3 **during sample preparation).**

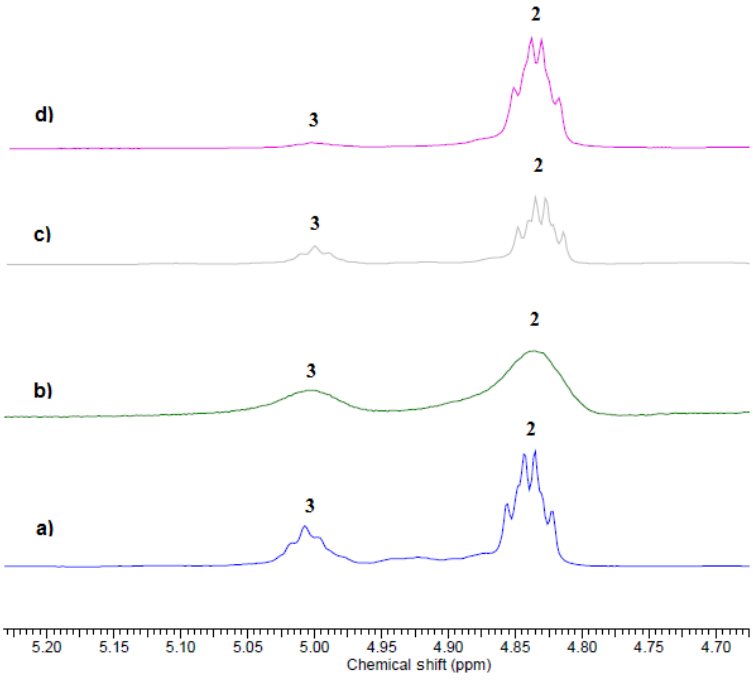

Figure 6.4. a: Semi-solid biolubricant ('Grease I') compared to commercial silicon-based grease (Dow Corning high-vacuum grease), b: Transparent thermoplastic-like material.

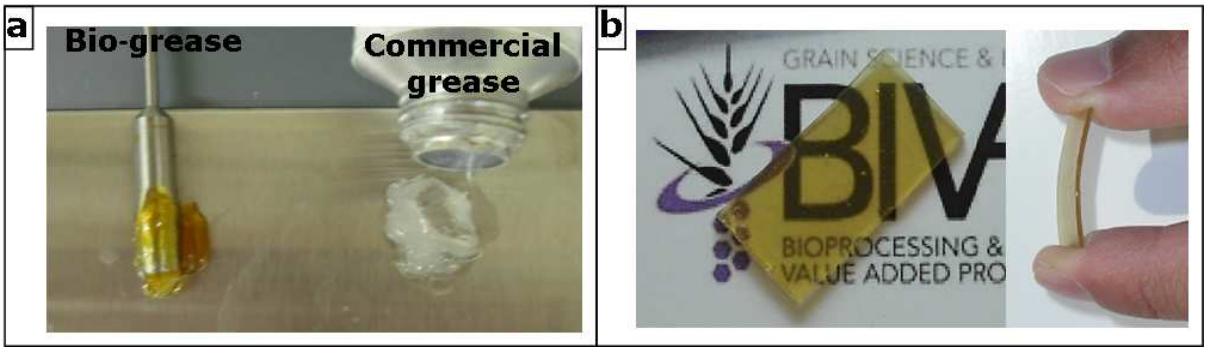

Figure 6.5. Expansions of ^{1}H NMR spectra of the region δ 6.00-2.50. a) Spectrum of starting material ESO featuring triglyceride esters (δ 5.25, 4.27, 4.13) and epoxides (region at δ 3.21–2.84) (ratio of integrals = 1H:2H:2H:7.8H amounting to an average ratio of 3.9 epoxides per triglyceride). b) Spectrum of Grease I obtained from the reaction of ESO with magnesium stearate (1 equiv) (amounting to 2 equiv of stearate anions; ratio of stearate anions per epoxide = 0.51:1) for 12 h at 160 ^{o}C. The ratio of integrals of the terminal trigyceride signal at δ 4.27 (asterisk; integral 2H) to the epoxide region to was 2H:3.8H, which amounts to an average of 1.9 residual epoxide units per triglyceride [loss of approximately two epoxide units from ESO in a)]. New signals for mid-chain esters (R'R"*H*CO_2CR) appeared in the range δ 5.37–4.80 (overlapping with the signal for the internal triglyceride ester) (new signals integrate for 2 H). Resonances at δ 4.25–3.35 were caused from CH and OH protons of newly formed secondary alcohols (R'R"*H*COH and R'R"HCO*H*) [integral 4 H relative to δ 4.27 (2H, terminal glyceride ester, asterisk)] from a total of two alcohol units). c) Spectrum of Grease II obtained from the reaction of ESO with magnesium stearate (2 equiv) for 12 h at 160 ^{o}C (ratio of stearate per epoxide = 1.1:1). Virtually complete disappearance of ESO epoxide signals was accompanied by the appearance of signals in the range δ 5.37–4.80 [secondary esters, R'R"*H*CO_2CR; adjusted integral = 3.7H relative to an integral of 2H for the terminal glyceride ester (relative to δ 4.27, integral 2H, asterisk)] and δ 4.25–3.35 (secondary alcohols, R'R"*H*COH and R'R"HCO*H*; adjusted integral = 7.4 H). d) Spectrum of the thermoplastic material from the reaction of ESO with 4 equiv magnesium stearate (ratio of stearate per epoxide: 2.2:1) for 12 h at 160 ^{o}C. The spectral expansion is nearly identical to that in c).

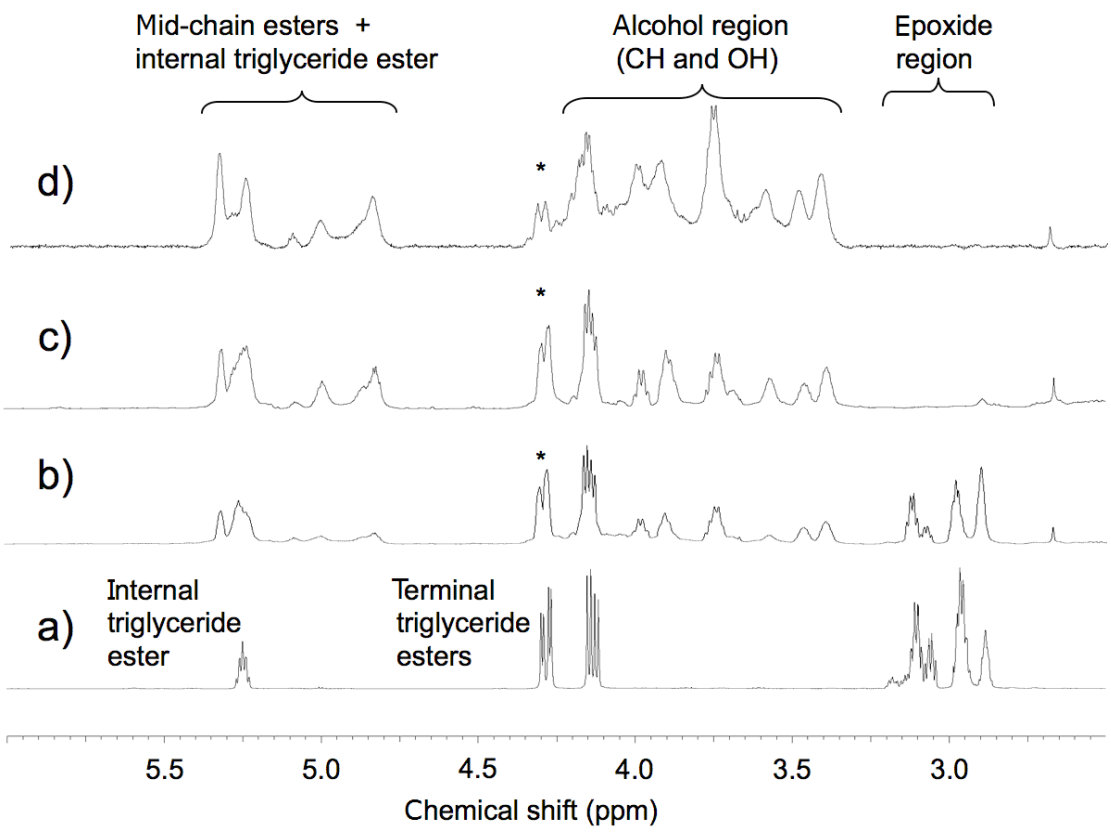
Mid-chain esters +
internal triglyceride ester
Alcohol region
(CH and OH)
Epoxide
region
d)
c)
b)
a)
*
Internal
triglyceride
ester
Terminal
triglyceride
esters
5.5
5.0
4.5
4.0
3.5
3.0
Chemical shift (ppm)

Figure 6.6. FT-IR spectra of the thermoplastic-like material derived from ESO and magnesium stearate after adding $CHCl_3$ and separating a soluble and an insoluble component a: FT-IR of the insoluble material (magnesium stearate = 1549.2 cm-1 and 1455.4 cm-1), b: The filtrate containing hydroxy esters of 2 (ester = 1732.9 cm-1; alcohol ≈ 3500 cm-1).

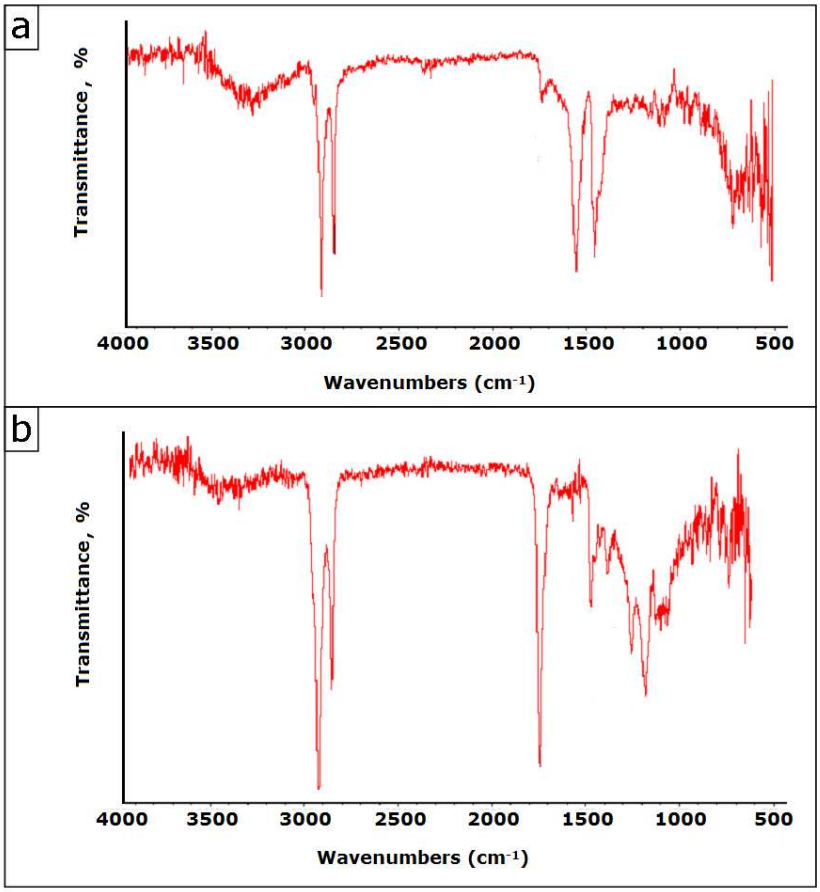

Figure 6.7. XRD of the magnesium stearate-rich theromplastic-like material

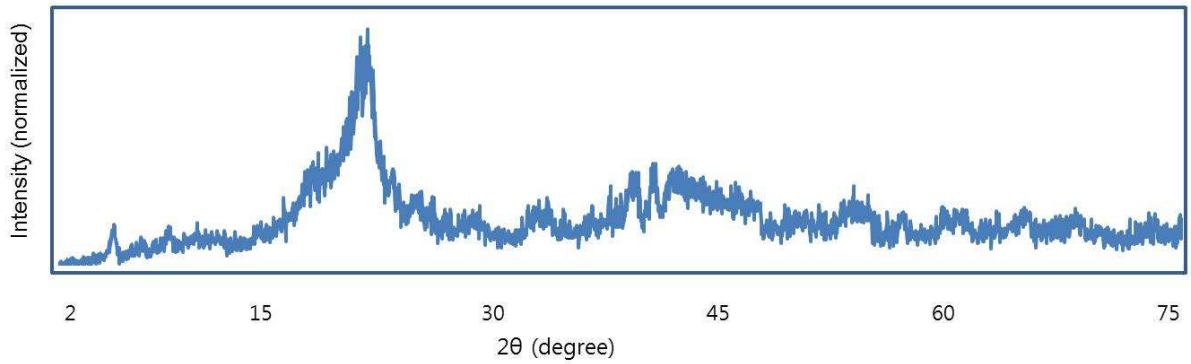

Figure 6.8. (Bottom to top) DSC of the first and second scan of the thermoplastic-like material from ESO/magnesium stearate (1:4 equiv), bio-grease [Grease I from ESO/magnesium stearate (1:1 equiv)], and magnesium stearate.

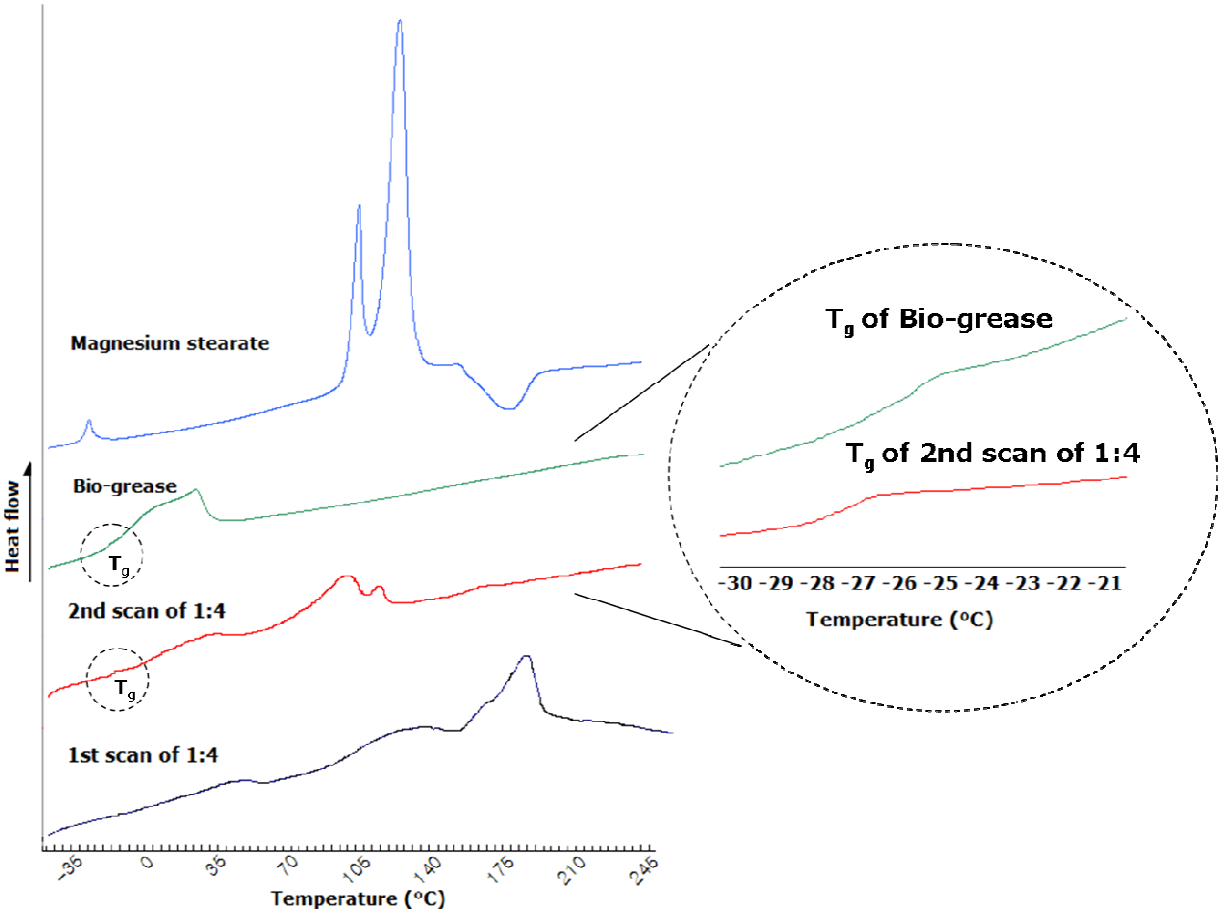

Figure 6.9. TGA of the thermoplastic-like material derived from ESO/magnesium stearate (1:4 equiv).

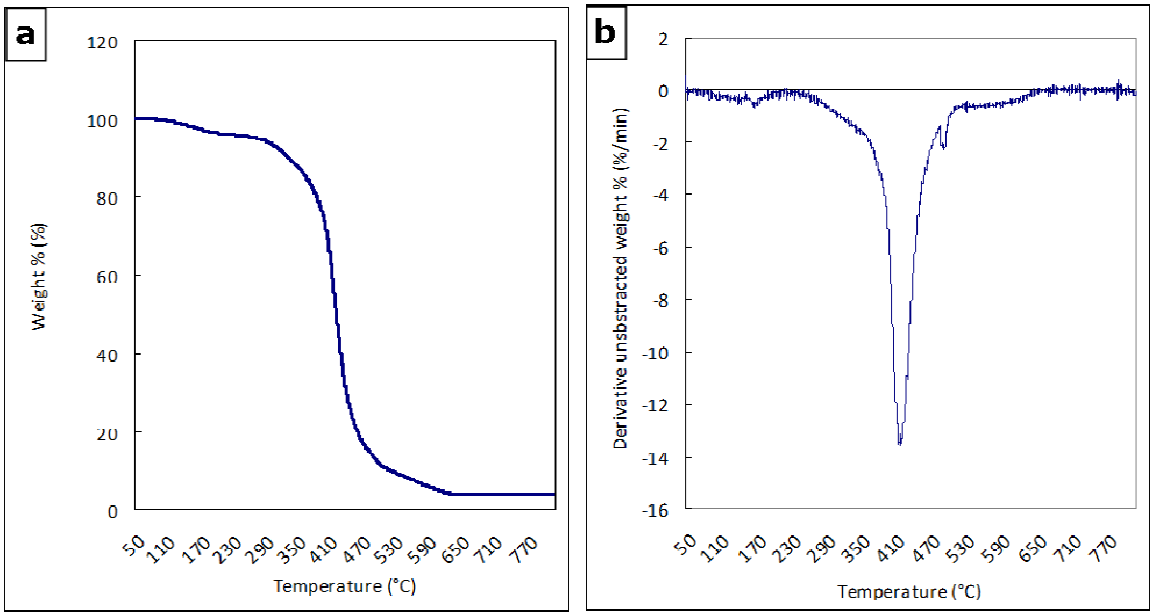

Figure 6.10. Dynamic mechanical properties of the thermoplastic-like material from ESO/magnesium stearate (1:4 equiv) by frequency: storage modulus E' (a) and loss modulus E" (b).

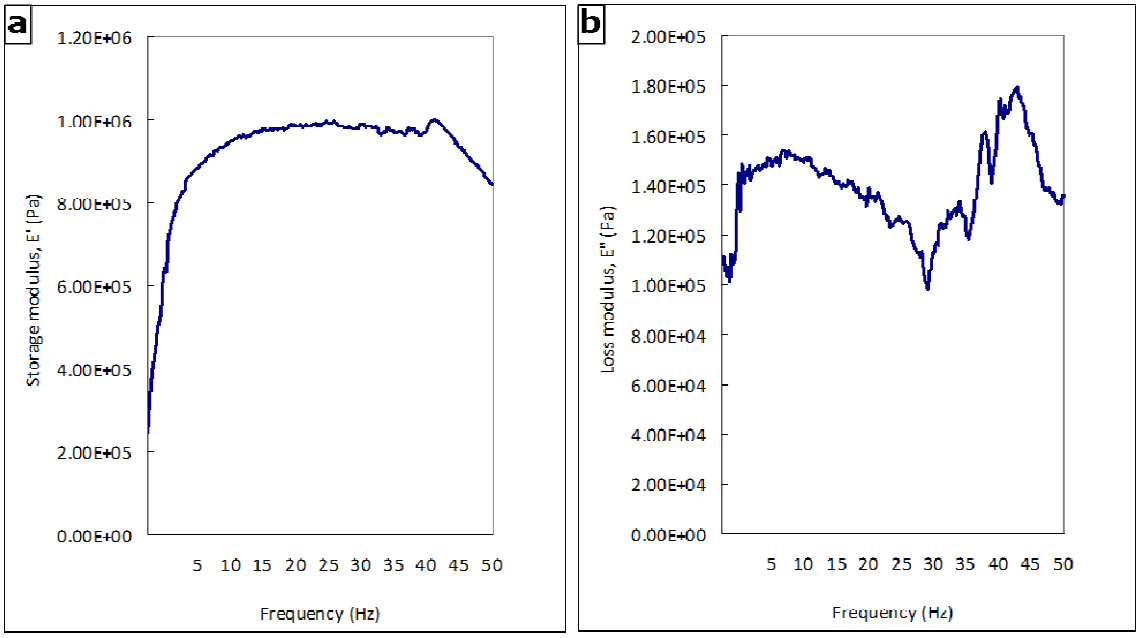

Figure 6.11. Dynamic mechanical properties of the composite by temperature: storage modulus E' (a) and loss modulus E" (b).

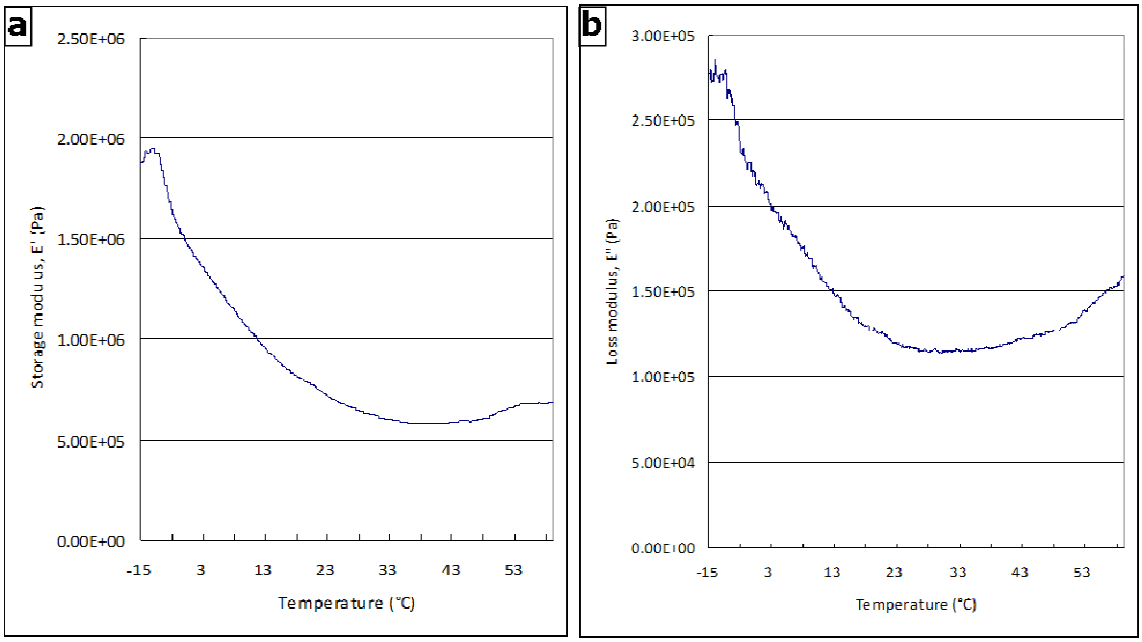

Figure 6.12. Viscosity vs. shear rate of Grease I (derived from ESO/magnesium stearate, 1:1 ratio), and Grease II (derived from ESO/magnesium stearate, 1:2 ratio); commercial silicon grease was measured as a reference.

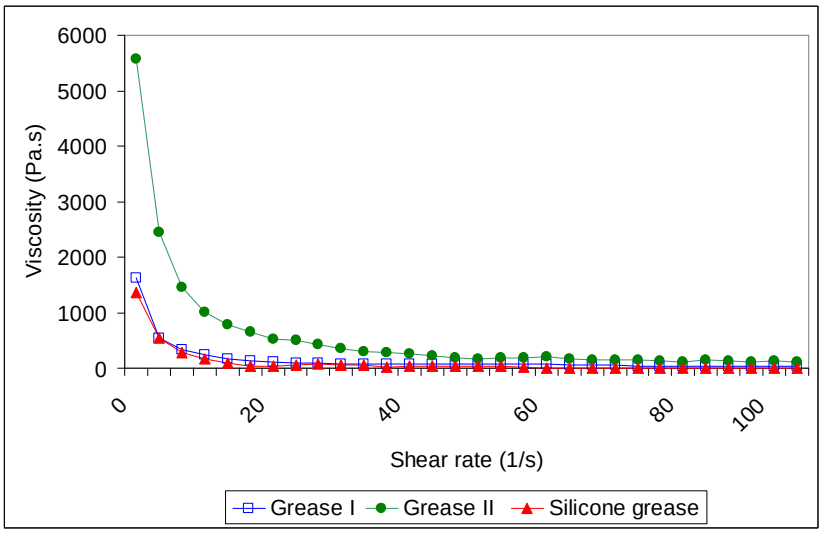

Figure 6.13. Viscosity vs. time of Grease I (from ESO/magnesium stearate, 1:1 ratio), Grease II (from ESO/magnesium stearate, 1:2 ratio), and commercial silicone grease.

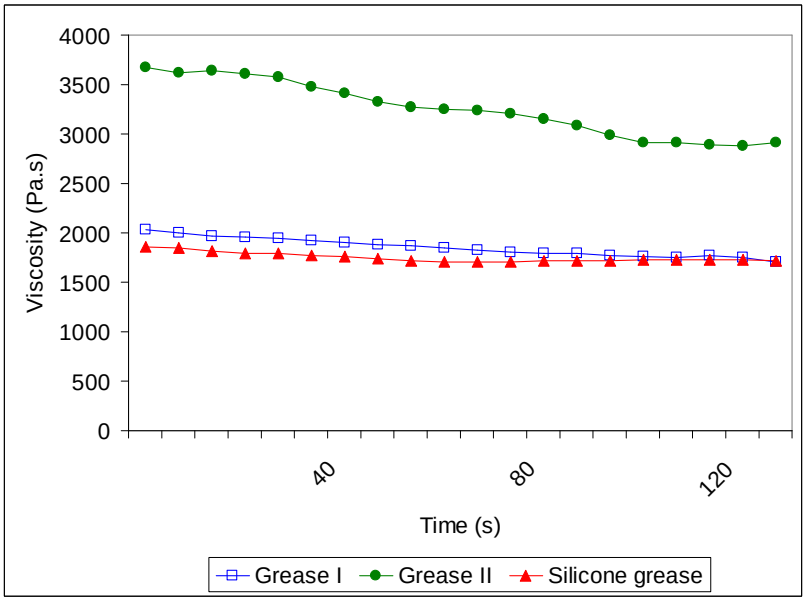

Figure 6.14. Viscosity vs. temperature plot for Grease I (from ESO/magnesium stearate, 1:1 ratio), Grease II (from ESO/magnesium stearate, 1:2 ratio), and commercial silicone grease.

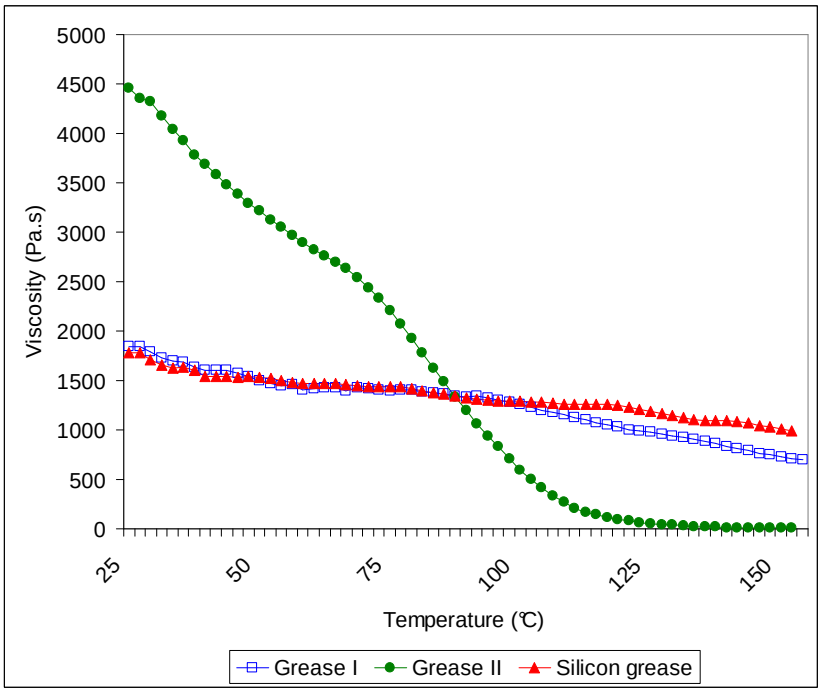

Scheme 6.1. Mid-chain α-hydroxy-carboxylation of ESO or other epoxidized oleochemicals.

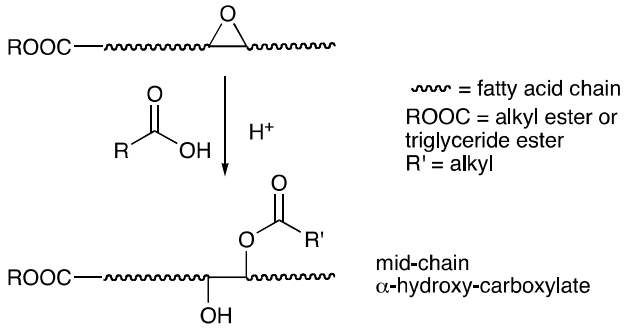

Scheme 6.2. Proposed reaction pathways for the reaction of 1 with magnesium, sodium, and lithium stearate and stearic acid. Diastereomer: the products can be 9 ester (ether) 10 alcohol (ether) or 9 alcohol (ether) 10 ester (ether).

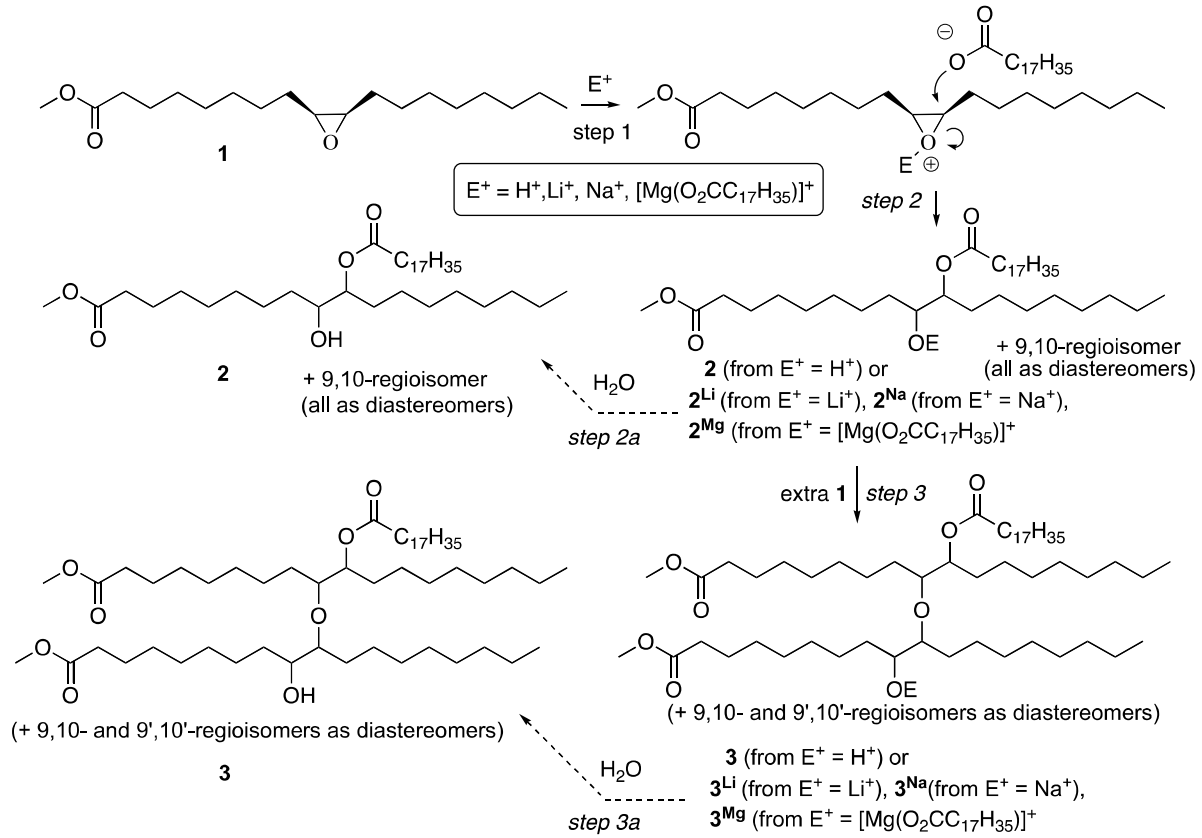

Table 6.1. Yields and conversion of the reaction of 1 with a stearate source to form 2.

Entry	Stearate source[a]	Conversion of **1**	Yield[b,c] % **2** (% **3**)	Ratio **2**:**3**
1	Stearic Acid	96 %	47 % (20 %)	2.4:1
2	Li-stearate	24 %	15 % (8 %)	1.9:1
3	Na-stearate	67 %	27 % (5 %)	5.4:1
4	Mg-stearate	99 %	95 % (4 %)	24:1

[a]Mixed with **1** in a 1:1 ratio and heated at 160 ^{o}C for 12 h. [b]Determined by ^{1}H NMR integration using the CO_2CH_3 singlet at δ 3.65 (composite signal from **1** and all ring-opened products derived from **1**).[c] Initially formed $\mathbf{2^{Li}}$, $\mathbf{2^{Na}}$, and $\mathbf{2^{Mg}}$ were hydrolyzed to **2** under conditions of NMR sample preparation. Equally, $\mathbf{3^{Li}}$, $\mathbf{3^{Na}}$, and $\mathbf{3^{Mg}}$ were hydrolyzed to **3** (see Scheme 6.2).

6.6. References

Adhvaryu, A. and Erhan, S. Z. 2002. Epoxidized soybean oil as a potential source of high-temperature lubricants. Industrial Crops and Products 15:247-254.

Ahn, B. K., Kraft, S. and Sun, X. S. 2011. Chemical pathways of epoxidized and hydroxylated fatty acid methyl esters and triglycerides with phosphoric acid. Journal of Materials Chemistry 21:9498-9505.

Aluyor, E. O., Obahiagbon, K. O. and Ori-jesu, M. 2009. Biodegradation of vegetable oils: A review. Scientific Research and Essays 4:543-548.

Andjelkovic, D. D. and Larock, R. C. 2006. Novel rubbers from cationic copolymerization of soybean oils and dicyclopentadiene. 1. Synthesis and characterization. Biomacromolecules 7:927-936.

Behr, A. and Gomes, J. P. The refinement of renewable resources: New important derivatives of fatty acids and glycerol. European Journal of Lipid Science and Technology 112:31-50.

Behr, A., Westfechtel, A. and Gomes, J. P. 2008. Catalytic processes for the technical use of natural fats and oils. Chemical Engineering & Technology 31:700-714.

Bondioli, P. 2001. Lubricants and hydraulic fluids. Pages 74-105 in: Oleochemical Manufacture and Applications. F. D. Gunstone and R. J. Hamilton, eds. Sheffield Academic Press.

Bonini, C. and Righi, G. 1992. Diols obtained via chemoselective and regioselective ring-opening of epoxy alcohols-a straightforward synthesis of 2S,3S-octanediol. Tetrahedron 48:1531-1538.

Bonini, C., Righi, G. and Sotgiu, G. 1991. Regioselctive opening of epoxy alcohols - mild chemoselective and stereoselective preparation of iodohydrins and 1,2-diols. Journal of Organic Chemistry 56:6206-6209.

Bozell, J. J. 2008. Feedstocks for the future - Biorefinery production of chemicals from renewable carbon. Clean-Soil Air Water 36:641-647.

Burgos, N., Fiori, S. and Jiménez, A. 2009. Recent advances in research on biodegradable polymers and sustainable composites. Nova Science Publisher: Hauppauge, NY.

Campanella, A. and Baltanas, M. A. 2004. Degradation of the oxirane ring of epoxidized vegetable oils with solvated acetic acid using cation-exchange resins. European Journal of Lipid Science and Technology 106:524-530.

Campanella, A. and Baltanas, M. A. 2006. Degradation of the oxirane ring of epoxidized vegetable oils in liquid-liquid heterogeneous reaction systems. Chemical Engineering Journal 118:141-152.

Campanella, A. and Baltanas, M. A. 2007. Degradation of the oxirane ring of epoxidized vegetable oils in a liquid-liquid-solid heterogeneous reaction system. Chemical Engineering and Processing 46:210-221.

Campanella, A., Rustoy, E., Baldessari, A. and Baltanás, M. A. 2010. Lubricants from chemically modified vegetable oils. Bioresource Technology 101:245-254.

Carlsson, A. S. 2009. Plant oils as feedstock alternatives to petroleum - A short survey of potential oil crop platforms. Biochimie 91:665-670.

Chini, M., Crotti, P., Flippin, L. A., Gardelli, C. and Macchia, F. 1992a. Regiochemical control of the ring opening of 1,2-epoxides by means of chelating processes. 4. Synthesis and reactions of the cis- and trans-oxides derived from 3-[(benzyloxy)methyl]cyclohexene. The Journal of Organic Chemistry 57:1713-1718.

Chini, M., Crotti, P., Flippin, L. A. and Macchia, F. 1990a. Regiochemical control of the ring-opening of 1,2-epoxides by means of chelating processes. Synthesis and reactions of the

cis- and trans-oxides derived from 4-(benzyloxy)cyclohexene. The Journal of Organic Chemistry 55:4265-4272.
Chini, M., Crotti, P., Flippin, L. A., Macchia, F. and Pineschi, M. 1992b. Regiochemical control of the ring-opening of 1,2-epoxides by means of chelating processes. 2. Synthesis and reactions of the cis- and trans-oxides of 4-[(benzyloxy)methyl]cyclohexene, 3-cyclohexenemethanol, and methyl 3-cyclohexenecarboxylate. The Journal of Organic Chemistry 57:1405-1412.
Chini, M., Crotti, P., Gardelli, C. and Macchia, F. 1992c. Metal salt-promoted alcoholysis of 1,2-epoxides. Synlett:673-676.
Chini, M., Crotti, P. and Macchia, F. 1990b. Metal-salts as new catalysts for mild and effecient aminolysis of oxiranes. Tetrahedron Letters 31:4661-4664.
Chini, M., Crotti, P. and Macchia, F. 1991. Regioal ternating selectivity in the metal salt catalyzed aminolysis of styrene oxide. Journal of Organic Chemistry 56:5939-5942.
Chuang, H. K. and Han, C. D. 1984. Rheological behavior of blends of nylon with a chemically modified polyolefin. Advances in Chemistry Series:171-183.
Eissen, M., Metzger, J. O., Schmidt, E. and Schneidewind, U. 2002. 10 years after Rio - Concepts on the contribution of chemistry to a sustainable development. Angewandte Chemie-International Edition 41:414-436.
Erhan, S. Z. and Asadauskas, S. 2000. Lubricant basestocks from vegetable oils. Industrial Crops and Products 11:277-282.
Erhan, S. Z., Sharma, B. K., Liu, Z. and Adhvaryu, A. 2008. Lubricant Base Stock Potential of Chemically Modified Vegetable Oils. Journal of Agricultural and Food Chemistry 56:8919-8925.
Federici, C., Righi, G., Rossi, L., Bonini, C., Chiummiento, L. and Funicello, M. 1994. Ring opening of 2,3-epoxy 1-tosylates to halohydrins and subsequent elaboration to asymmetrical alcohols. Tetrahedron Letters 35:797-800.
Forsberg, J. W. 1980. Magnesium-containing greases and method for their preparation. The Lubrizol Corporation (Wickliffe, OH): United States.
Golumbic, C. and Cottle, D. L. 1939. The Reaction of styrene oxide with methylmagnesium iodide. Journal of the American Chemical Society 61:996-1000.
Hörner, D. 2002. Recent trends in environmentally friendly lubricants. Journal of Synthetic Lubrication 18:327-347.
Harry-O'kuru, R. E., Isbell, T. A. and Weisleder, D. 2001. Synthesis of estolide esters from cis-9-octadecenoic acid estolides. Journal of the American Oil Chemists Society 78:219-222.
Helling, R. K. and Russell, D. A. 2009. Use of life cycle assessment to characterize the environmental impacts of polyol production options. Green Chemistry 11:380-389.
Holland, J. M., Lewis, M. and Nelson, A. 2003. Desymmetrization of a centrosymmetric diepoxide: Efficient synthesis of a key intermediate in a total synthesis of hemibrevetoxin B. Journal of Organic Chemistry 68:747-753.
Jones, R. J. and Rapoport, H. 1990. Enantiospecific synthesis of an aziridinobenzazocinone, an advanced intermediate containing the core nucleus of FR900482 and FK973. The Journal of Organic Chemistry 55:1144-1146.
Koivisto, M., Jalonen, H. and Lehto, V. P. 2004. Effect of temperature and humidity on vegetable grade magnesium stearate. Powder Technology 147:79-85.
Lathi, P. S. and Mattiasson, B. 2007. - 69:- 212.

Legisa, I., Picek, M. and Nahal, K. 1997. Some experience with biodegradable lubricants. Journal of Synthetic Lubrication 13:347-360.
Lemieux, R. U., Kullnig, R. K. and Moir, R. Y. 1958. The configurations of the 3-methoxycyclohexene oxides. A novel application of proton magnetic resonance spectroscopy to the determination of structure and configuration1. Journal of the American Chemical Society 80:2237-2242.
Ley, S. V. and Redgrave, A. J. 1990. Microbial oxidation in synthesis: concise preparation of (+)-conduritol F from benzene. Synlett 1990:393,394.
Lu, H., Sun, S. D., Bi, Y. L., Yang, G. L., Ma, R. L. and Yang, H. F. 2010. Enzymatic epoxidation of soybean oil methyl esters in the presence of free fatty acids. European Journal of Lipid Science and Technology 112:1101-1105.
McBee, E. T., Hathaway, C. E. and Roberts, C. W. 1956. The Ring-cleavage reactions of 1,1,1-trifluoro-2,3-epoxypropane. Journal of the American Chemical Society 78:3851-3854.
McRae, J. A., Moir, R. Y., Haynes, J. W. and Ripley, L. G. 1952. Methanolysis of stereoisomeric oxides of 3-methoxycyclohexene. The Journal of Organic Chemistry 17:1621-1629.
Meier, M. A. R., Metzger, J. O. and Schubert, U. S. 2007. Plant oil renewable resources as green alternatives in polymer science. Chemical Society Reviews 36:1788-1802.
Metzger, J. O. 2009. Fats and oils as renewable feedstock for chemistry. European Journal of Lipid Science and Technology 111:865-876.
Metzger, J. O. and Bornscheuer, U. 2006. Lipids as renewable resources: current state of chemical and biotechnological conversion and diversification. Applied Microbiology and Biotechnology 71:13-22.
Moser, B. R., Sharma, B. K., Doll, K. M. and Erhan, S. Z. 2007. Diesters from oleic acid: Synthesis, low temperature properties, and oxidation stability. Journal of the American Oil Chemists Society 84:675-680.
Parker, R. E. and Isaacs, N. S. 1959. Mechanisms Of epoxide reactions. Chemical Reviews 59:737-799.
Paterson, I. and Berrisford, D. J. 1992. meso Epoxides in asymmetric synthesis: Enantioselective Opening by Nucleophiles in the Presence of Chiral Lewis Acids. Angewandte Chemie International Edition in English 31:1179-1180.
Pearson, R. G., Sobel, H. R. and Songstad, J. 1968. 90:319- 326.
Pelaez, M., Orellana, C., Marques, A., Busquets, M., Guerrero, A. and Manresa, A. 2003. Natural estolides produced by Pseudomonas sp 42A2 grown on oleic acid: Production and characterization. Journal of the American Oil Chemists Society 80:859-866.
Phan, T. B. and Mayr, H. 2005. Comparison of the nucleophilicities of alcohols and alkoxides. Cadian Journal of Chemistry-Revue Canadienne de Chimie 83:1554-1560.
Plattner, R. D., Paynewahl, K., Tjarks, L. W. and Kleiman, R. 1979. Hydroxy-acids and estolide triglycerides of Heliophila-amplexicaulis LF seed oil. Lipids 14:576-579.
Ramachandran, P. V., Gong, B. and Brown, H. C. 1995. Chiral synthesis via organoboranes. The Journal of Organic Chemistry 60:41-46.
Reeve, W. and Christoffel, I. 1950. The Reaction of styrene oxide with methanol. Journal of the American Chemical Society 72:1480-1483.
Salimon, J. and Salih, N. Modification of Epoxidized Ricinoleic Acid for Biolubricant Base Oil With Improved Flash and Pour Points. Asian Journal of Chemistry 22:5468-5476.
Salimon, J. and Salih, N. 2009a. Improved low temperature properties

of 2-ethylhexyl 9(10)-hydroxy-10(9)-acyloxystreate derivatives. European Journal of Scientific Research 31:583-591.
Salimon, J. and Salih, N. 2009b. Preparation and Characteristic of 9,10-Epoxyoleic Acid α-Hydroxy Ester Derivatives as Biolubricant Base Oil. European Journal of Scientific Research 31:265–272.
Salimon, J. and Salih, N. 2009c. Substituted Esters of Octadecanoic Acid as Potential Biolubricants. European Journal of Scientific Research 31:273-279.
Salimon, J., Salih, N. and Yousif, E. 2010a. Biolubricants: Raw materials, chemical modifications and environmental benefits. European Journal of Lipid Science and Technology 112:519-530.
Salimon, J., Salih, N. and Yousif, E. 2010b. Industrial development and applications of plant oils and their biobased oleochemicals. Arabian Journal of Chemistry In Press, Corrected Proof.
Schuster, H., Rios, L. A., Weckes, P. P. and Hoelderich, W. F. 2008. Heterogeneous catalysts for the production of new lubricants with unique properties. Applied Catalysis a-General 348:266-270.
Sin, S. N. and Chua, H. 2000. Degradation pathway of persistent branched fatty acids in natural anaerobic ecosystem. Chemosphere 41:149-153.
Thompson, D. H., Svendsen, C. B., Di Meglio, C. and Anderson, V. C. 1994. Synthesis of chiral diether and tetraether phospholipids: regiospecific ring opening of epoxy alcohol intermediates derived from asymmetric epoxidation. The Journal of Organic Chemistry 59:2945-2955.
Upadhyay, D., Mohanty, S., Nayak, S. K., Parvaiz, M. R. and Panda, B. P. 2011. Impact Modification of Poly(trimethylene terephthalate)/Polypropylene Blend Nanocomposites: Fabrication and Characterization. Journal of Applied Polymer Science 120:932-943.
Xia, Y. and Larock, R. C. 2010. Vegetable oil-based polymeric materials: synthesis, properties, and applications. Green Chemistry 12:1893-1909.

Chapter 7 - Greener ring opening of epoxidized methyl oleate using a novel acid-functionalized iron nanoparticle catalyst

[This work has been published: Ahn, B. K., Wang, H., Robinson, S., Shrestha, T. B., Troyer, D. L., Bossmann, S, Sun, X. S. (2011). *Green Chemistry*. DOI:10.1039/C1GC16043E]

7.1. Abstract

Hydroxyl soybean oils, also called soy polyols, are biobased chemicals designed to replace petroleum-based polyols mainly for polyurethane (PU) applications. Soy polyols are obtained by acid-catalyzed ring opening of expoxidized soybean oils or other epoxidized plant oils by nucleophilic S_N2 attack of methanol. Recyclable heterogeneous catalysts are preferred for the ring-opening reactions over non-recyclable homogeneous catalysts because they minimize environmental impact. The drawbacks of current solid catalysts such as SAC 13 and Amberlite 15 are low production yield and high energy consumption. Here, we demonstrate a greener synthetic pathway of soy polyols with low energy consumption and excellent atom economy and environment (E) factor by using novel sulfamic acid-functionalized iron (iron/iron oxide core shell) nanoparticles (NPs) as a heterogeneous catalyst. The excellent selectivity of the reaction with the recyclable NPs was confirmed by ^{1}H NMR, 2D ^{1}H-^{1}H COSY NMR, and ESI-MS comparable to non-recyclable H_2SO_4. The synthetic route with the NPs resulted in higher product yield (almost 100%) as H_2SO_4 at room temperature for 30 min over the SAC 13 (83% yield at 60 °C for 60 min) and Amberlite 15 (87% yield at 60 °C for 100 min). Life cycle assessment (LCA) revealed that the NP synthetic technology for soy polyol production is superior or equal to the competing routes (H_2SO_4, SAC 13, and Amberlite 15 methods) with respect to 9 environmental impacts (acidification potential, ozone depletion potential, smog formation potential, global warming potential, human toxicity by ingestion, human toxicity by inhalation, persistence, bioaccumulation, and abiotic resource depletion potential).

7.2. Introduction

Epoxidized soybean oil (ESO), a well-known and commercially available functionalized plant oil as a plasticizer in the plastics industry, is amenable to hydrolysis using conventional chemical methodology of ring-opening reaction of oxirane moities (Ahn et al. 2011b; Guo et al. 2000a; Guo et al. 2000b; Lligadas et al. 2010). Hydroxyl soybean oil called soy polyol is produced from ESO *via* α-methoxy-hydroxylation (Scheme 7.1) and is widely used for PU applications, with a potential market of 8 billion pounds (Lligadas et al. 2010; Meier et al. 2007). Plant oil-based polyol showed better environmental benefits than petroleum-based polyols because of the former's significantly lowered greenhouse gas emissions (Helling and Russell 2009). The global market for polyols is forecasted to reach 4 billion pounds by the year 2015. Recently, Recticel (Evere, Belgium), the largest PU manufacturer in Europe, has started to produce foams using BiOH® (Cargill Inc., Minneapolis, MN).

Although soy polyols were derived from biobased feedstocks, synthetic methods for most soy polyol production do not emphasize green chemistry, which has been spotlighted recently because of stricter government regulations regarding sustainability (Bozell 2008; Carlsson 2009; Metzger 2009). The term *green chemistry* was comprehensively defined by Anastas and Warner as "the utilization of a set of principles that reduces or eliminates the use or generation of hazardous substance in the design, manufacture and application of chemical products (Anastas and Warner 1998)" with 12 principles: 1) prevention, 2) atom economy, 3) less hazardous chemical syntheses, 4) safer chemicals, 5) safer solvents and auxiliaries, 6) energy efficiency, 7) use of renewable feedstocks, 8) derivatives reduction, 9) catalysis, 10) design for degradation, 11) real-time analysis for pollution prevention, and 12) inherently safer chemistry for accident prevention (Anastas and Warner 1998). In terms of green chemistry, a common problem in the synthesis of α-methoxy-hydroxylation from epoxidized oleo-chemicals is the need for strong Brønsted acids to activate the epoxide ring toward the attack of weakly nucleophilic alcohols. This has been accomplished through the action of strong homogeneous acids such as HCl, HBr, or *p*-toluenesulfonic acid (Guo et al. 2000a; Lozada et al. 2009). Even formic acid (a milder acid) accomplished one-pot synthesis of soy polyols, although this reaction presented low reaction selectivity (non-homogeneous distribution and oligomerization) and low conversion yield (residual epoxides) (Meier et al. 2007; Monteavaro et al. 2005). All cases require the removal of acid, solvent purification steps (Lligadas et al. 2010), and high temperature, which generates

carbon emissions and undesirable byproducts such as ketones (Rios et al. 2005). Green chemistry researchers have become interested in solid acid catalysts (*e.g.*, zeolites, heteropolyacids, and ion-exchange resins), which, if they replaced the numerous tons of non-recyclable homogeneous acid catalysts consumed annually in current industrial processes, would minimize environmental defects including waste generation (Dhepe et al. 2005; Hara et al. 2004). Heterogeneous catalysts have shown potential as replacements for traditional homogeneous acid-catalyzed processes, including biodiesel production (Melero et al. 2009; Melero et al. 2010; Mo et al. 2008). Rios et al (2005) presented ring opening of epoxidized methyl oleate using commercial heterogeneous acid resin catalysts such as SAC 13 and Amberlite 15; however, the commercial heterogeneous solid catalysts recorded lower product yield and higher energy consumption than homogeneous sulfuric acid in the ring opening of epoxidized methyl oleate (EMO). Although Melero et al (2010) showed increased activity and stability using the sulfonic acid-functionalized mesostructured silica, the technique carries the inconvenience of the resin swelling (Lopez et al. 2007). Therefore, more studies on ring opening of epoxidized plant oils using a solid acid catalyst are needed with respect to selectivity and product yield.

To this end, in this work we synthesized 3-aminopropyl triethoxysilane (APTES) coated Fe/Fe_3O_4 nanoparticles; the NPs circumvent resin swelling (Lopez et al. 2007) and are efficiently removed with a magnetic field. We achieved a greener synthesis of mid-chain α-methoxy-hydroxylation of EMO for soy polyol production applications by using the new sulfamic acid-functionalized APTES coated Fe/Fe_3O_4 nanoparticles (NPs). NMR, ESI-MS analyses, and a life cycle assessment (LCA) on synthetic methods demonstrated that our NP technology has excellent atom economy, E factor, low energy consumption, and predominant environmental advantages compared with previously reported syntheses using sulfuric acid and other solid catalysts; the LCA comparison was carried out with respect to 9 environmental impacts and thoroughly quantifies the greenness of our NP method (Jessop 2011a), including acidification potential, ozone depletion potential, smog formation potential, global warming potential, human toxicity by ingestion, human toxicity by inhalation, persistence, bioaccumulation, and abiotic resource depletion potential.

7.3. Experimental

Synthesis of acid-functionalized iron nanoparticles.

All starting materials were purchased from Sigma-Aldrich, and all solvents were purchased from Fisher. All chemicals were ACS-grade.

Preparation of monodisperse Fe nanoparticles

Iron nanoparticles were prepared by extensive modification of a procedure described by Peng et al (2006). 20 mL octadecene and 0.3 mL oleylamine were added to a 100 mL Schlenk flask and heated to 120 ^{o}C under Argon (Ar) for 30 min. After raising the temperature to 180 ^{o}C, 0.7 mL Fe $(CO)_5$ was added under Ar. The solution turned black within 3 min. and was kept at 180 ^{o}C for 20 min before cooling to room temperature. Under Ar, the supernatant was transferred to a centrifuge tube. Iron nanoparticles accumulated on the stir bar were washed with degassed hexane (3×10 mL) and combined with the supernatant. Next, 50 mL of degassed absolute ethanol was added and mixed thoroughly. Nanoparticles were collected by centrifugation (8000 rmp for 30 min). After decanting the clear solvent, the nanoparticles were re-dispersed into 15 mL degassed hexane and precipitated out by adding 20 mL of absolute ethanol. The product was dried under vacuum and stored under Ar for further use.

Preparation of superparamagnetic core/shell Fe/Fe_3O_4 nanoparicles

15 mL octadecene and 6 mg $(CH_3)_2NO$ were added into a 50 mL Schlenk flask, and after degassing by three Freeze-Pump-Thaw cycles, the reaction container was refilled with Ar. The reaction mixture was kept at 130 ^{o}C for 30 min, then 80 mg iron nanoparticles in 2 mL of hexane were added *via* a syringe. After stirring at 130 ^{o}C for 2 hours, the mixture was heated to 250 ^{o}C and stirred at this temperature for another 30 min. Upon cooling to room temperature, the reaction mixture was transferred to a centrifuge tube and 25 mL isopropanol was added. The nanoparticles were collected by centrifugation (8000 rpm, 20 min). The obtained nanoparticles were re-dispersed into 5 mL hexane and precipitated out by adding 10 mL absolute ethanol. The product was dried under vacuum and stored under Ar for further use.

Preparation of APTES (3-aminopropyl triethoxysilane)-coated Fe/Fe_3O_4 nanoparticles

40 mg Fe/Fe_3O_4 nanoparticles were dispersed in 80 mL hexane. 0.40 mL (3-aminopropyltriethoxysilane [APTES]) and 8 μl acetic acid (HOAc) were added and the reaction mixture was shaken at room temperature for 72 hours (De Palma et al. 2007). The black-brown

precipitate was collected by centrifugation (8000 rpm, 5 min). The obtained product was further washed with 5 mL of hexane 3 times. After drying under vacuum, 38 mg APTES-functionalized nanoparticles were obtained.

Preparation of sulfamic acid-functionalized Fe/Fe_3O_4 nanoparticles

30 mg APTES-coated Fe/Fe_3O_4 nanoparticles were dispersed in 15 mL dry methylene chloride in an ultrasonic bath (10 min. of sonication) (Kassaee et al. 2011). With a gentle stream of Ar, a solution of 0.1 mL chlorosulfuric acid in 1 mL of dry methylene chloride was added dropwise in 10 min. Nanoparticles were collected by centrifugation (8000 rpm, 5min), and further washed consecutively with dry methylene chloride (3 × 5 mL) and Tetrahydrofuran (THF) (3× 5 mL). After drying under vacuum, 31 mg of nanoparticles were obtained.

Transmission electron microscopy (TEM). TEM images were recorded by using a Philips CM100 microscope 100 kV.

Dynamic light scattering (DLS) and the zeta-potential (ZP). DLS and ZP measurements were carried out in distilled water by a Brookhaven Zeta-PALS with Bi-Mas particle sizing option.

X-ray diffraction (XRD). Powder X-ray diffraction was used to characterize the composition of the core/shell nanoparticles.. Cu Kα radiation was used with a curved crystal graphite monochromator. The operating range for the X-ray target was 45 kV and 45 mA. The X-ray scans were in range of $20>2Ø>70^\circ$.

Ring opening of EMO. Epoxidized fatty acid methyl ester (EFAME) was kindly provided by FuJian ZhiShang Biomass Material Co., Ltd (Fujian, China). After purifying EFAME (yellow) through column chromatography (hexane/ethyl acetate gradient 99/1 to 90/10), we obtained EMO (clear). The synthesized sulfamic acid-functionalized iron NPs and H_2SO_4 were used for ring opening of EMO as a comparison to the commercial resin catalysts (SAC 13 and Amberlyst 15) reported by Rios et al (2005) and the reaction condition was methanol/epoxide=10 (molar) and epoxide/catalyst=10 (mass) accordingly.

1) Mixture of EMO (starting material) 0.2g (0.64 mmol), the NPs 0.02g, methanol 0.2g (6.40 mmol) was agitated for 30 min at 40 °C.

2) Mixture of EMO 0.2g (0.64 mmol), H_2SO_4 0.02g, methanol 0.2g (6.40 mmol) was agitated for 30 min at room temperature.

3) EMO 0.2g (0.64 mmol), SAC 13 0.02g, methanol 0.2g (6.40 mmol) for 60 min at 60 °C.

4) EMO 0.2g (0.64 mmol), Amberlyst 15 0.02g, methanol 0.2g (6.40 mmol) for 100 min at 60 °C.

Quantities/routes were compared in LCA, and they were scaled up in the LCA.

Atom economy and waste generation. We evaluated atom economy and E factor with the aid of quantitative NMR, 2D COSY, and ESI-MS analysis.

NMR. ^{1}H NMR spectra for our samples were recorded quantitatively using a Varian Unity 400 MHz spectrometer (Varian Inc, Palo Alto, CA). For ^{1}H NMR experiments, sample solutions were prepared in $CDCl_3$.

ESI-MS. Spectra were acquired on an API4000 (Applied Biosystems, Foster City, CA) triple quadrupole mass spectrometer with electrospray ionization (ESI). An aliquot of 2-10 ul in 1.0 ml methanol was presented to the ESI needle at 30 ul/min. The mass analyzers were adjusted to a resolution of 0.7 u full width at half height. Twenty continuum scans were averaged in multiple channel analyzer (MCA) mode. The scan speed was 100 u per sec. The source temperature (heated nebulizer) was 100 °C, the interface heater was on, -4.5 kV were applied to the electrospray capillary, the curtain gas was set at 20 (arbitrary units), and the two ion source gases were set at 45 (arbitrary units). The declustering potential was -90 V, and the entrance potential was -12.

7.4. Results and discussion

Synthesis and characterization of sulfamic acid-functionalized core/shell Fe/Fe_3O_4 nanoparticles

Although several successful syntheses of magnetite NPs have been reported (Mohapatra et al. 2007; Theppaleak et al. 2009), they have not been applied as recyclable catalysts in soy polyol synthesis. Nanoparticles featuring an iron(0)-core have not been reported. Iron(0) is a superior magnetic material compared with magnetite (Bossmann 2009). Strong acid catalysts such as sulfuric acid can be replaced with acid-functionalized magnetite NPs. The NPs allow not only a reduced amount of catalyst with higher surface area that can lower activation energy, but also a more convenient process in agitating and recycling (using a magnetic field) than other

heterogeneous catalysts. The usage of magnetic property to achieve simple magnetic separation of catalysts had been reported in water treatments (Costa et al. 2003; Oliveira et al. 2004; Oliveira et al. 2002; Oliveira et al. 2003).

To achieve convenient reaction and catalyst recycling in soy polyol production, we developed acid-functionalized iron/iron oxide core/shell NPs. We first synthesized superparamagnetic core/shell Fe/Fe_3O_4 nanoparicles (Peng et al. 2006), then coated the NPs with APTES (3-aminopropyl triethoxysilane) (De Palma et al. 2007), and the NPs were subsequently functionalized with sulfamic acid (Kassaee et al. 2011) (Scheme 7.2). TEM imaging clearly showed spherical core/shell structure of the acid-functionalized nanoparticles (Figure 7.1). The average core diameter was 3+/-1 nm and the thickness of the shell is around 2 nm, respectively.

The sulfamic acid-functionalized Fe/Fe_3O_4 NPs were highly monodisperse (polydispersity = 0.229) based on the dynamic light scattering (DLS) measurement. The effective diameter was around 58 nm. The different diameters between TEM and DLS measurements can be explained by clustering of the acid-functionalized NPs in water used in DLS measurement. Zeta potential measurement clearly indicated that the sulfamic acid-functionalized Fe/Fe_3O_4 nanoparticles carry negative charges on their surface. The zeta potential value was -30 +/- 2 mV, indicating the nanoparticles prepared by this method are stable in water. Because the terminal amine groups present after APTES functionalization carry positive charges, the recording of a stable negative potential is an indication for a high conversion ratio of the terminal amino to sulfamic acid groups. The acid functionalized nanoparticles are amorphous as indicated by the absence of specific diffraction peaks in their X-ray diffraction (XRD) pattern (Figure 7.2A) (Peng et al. 2006). Typical Fe_3O_4 diffraction peaks are observed after annealing the nanoparticles at 300 ^{o}C under argon for 2 hours (Figure 7.2B), and further annealing of the nanoparticles at 400 ^{o}C under argon for 1 hour led to the appearance of a sharp bcc-Fe diffraction peak (Peng et al. 2006). The XRD characterization give more supportive data for the existence of Fe/Fe_3O_4 core/shell structure as indicated by the TEM image. Acid loading of the nanoparticle (0.36 mmol/g) was determined by acid-base titration according to a literature reported method (Peng et al. 2006).

α-Methoxy-hydroxylation of EMO using APTES-coated Fe/Fe_3O_4 nanoparticles

EMO was used as a model for ESO to avoid the complexity of macromolecules in NMR and ESI-MS analysis (Ahn et al. 2011a; Ahn et al. 2011b). The ring opening of EMO was

conducted using the sulfamic acid-functionalized Fe/Fe_3O_4 NPs. EMO was agitated in methanol (10 mass equivalents) with 10 w/w % of the NPs and H_2SO_4, respectively. We evaluated atom economy (the mass percentage of atoms from reactants that appear in the desired product of a balanced reaction equation) (Trost 1991) and E factor (the ratio of mass of waste over mass of product) (Sheldon 2000) using quantitative NMR (Figure 7.3) analysis. ^{1}H-^{1}H COSY NMR and ESI-MS revealed the scaffold of α-methoxy-hydroxylation of EMO. H_2SO_4 was also used under the same reaction conditions for comparison.

As a result, the reaction efficiency of sulfamic acid-functionalized Fe/Fe_3O_4 NPs was comparable to that of sulfuric acid; the NPs produced identically clean product to H_2SO_4 with reduced reaction time (30 min) at lower temperature (40 °C) than published data using solid catalysts of SAC 13 (60 min at 60 °C) and Amberlite 15 (100 min at 60 °C) (Rios et al. 2005). The NPs also showed excellent atom economy with, as for H_2SO_4, 100% yield compared with SAC 13 (yield: 83%) and Amberlite 15 (yield: 87%) from NMR integration using a methyl group (3H) at δ3.67 and 0.89 as a quantitative internal standard (Figure 7.3). The oxirane ring (0.8H) was completely converted to α-methoxy (0.4H) [RC(H)(OH)C(*H*)(R')O-CH_3] signal at δ3.49 coupled with vicinity hydroxyl (0.4H) [RC(*H*)(OH)C(H)(R')O-CH_3] signal at δ3.00 (Figure 7.3). Methyl site (1.2H) of α-methoxy was also shown at δ3.42. ^{1}H-^{1}H COSY NMR and showed a clear cross peak between α-methoxy and its vicinal hydroxyl. ESI-MS revealed the only presence of α-Methoxy-hydroxylation (m/z = 367.2) without ketone byproduct (Rios et al. 2005) (m/z = 335.5).

In terms of recycling efficiency, the NPs were observed to precipitate in 5 min on a supermagnet (Figure 7.4), and the recycled NPs have shown a steady 100% epoxy ring-opening conversion and 100% selectivity of α-methoxy-hydroxylation in 5 consecutive uses. In this study, we confirmed that the NPs provided not only excellent catalysis, as much as H_2SO_4, but also environmental benefits deriving from their recyclability. These advantages of the NPs will be a green catalysis milestone for soy polyol applications with low energy consumption, excellent atom economy, and waste prevention.

LCA on the syntheses of the soy polyol

Life cycle assessment (LCA, also known as life cycle analysis) is an important tool that allows evaluation of the environmental impacts associated with a chemical process or a material's entire life cycle (Helling and Russell 2009; Luterbacher et al. 2009); however,

research is limited that integrates a comprehensive LCA, and the scope of environmental impacts and unknowns presents a significant challenge (Jessop 2011a; Jessop 2011b; Luterbacher et al. 2009). Using renewable resources is merely one of the 12 principles of green chemistry (Anastas and Warner 1998), so biobased materials scientists and engineers need more comprehensive LCA to designate their processes as properly green (Jessop 2011a; Jessop 2011b). The practical development of greener solutions will become more prevalent awareness of environmental concerns increases. Multivariate metrics used in LCAs to assess environmental impacts are informative to determine overall greenness. In this study, we conducted LCA based on nine environmental impact metrics to select the greenest synthesis from the four different catalysts (the NPs, H_2SO_4, SAC 13, and Amberlite 15). The reaction impact assessment for epoxide ring opening was conducted using a procedure based on the ISO life-cycle assessment method (Allen and Shonnard 2001; Guinee 2002), an approach that includes both the amount of waste as well as the harmfulness of the waste. Our procedure was adapted from a private communication with Sean Mercer and Philip Jessop (Queens Univ., Canada) based on the impact assessment "Choosing the Greenest Synthesis." We compare the four reactions with respect to nine environmental risks: acidification potential (AP), ozone depletion potential (ODP), smog formation potential (SFP), global warming potential (GWP), human toxicity by ingestion (INGTP), human toxicity by inhalation (INHTP), persistence (PER), bioaccumulation (ACCU), and abiotic resource depletion potential (ADP). For most of these risks, the chemical outputs are compared with reference chemicals, which allow addition of all contributors to the risk for comparison within a synthetic route as well as between routes. In our assessment, we built a multimedia compartmental model (MCM) to assess the partitioning behavior of each chemical into four environmental compartments (air, water, soil, and sediment). This was implemented in assessing the human toxicity risk of each procedure.

The ring opening of EMO *via* the four processes (1-NPs, 2-H_2SO_4, 3-SAC13, and 4-Amberlyst-15) poses a relatively small set of environmental concerns, but the low energy requirements and high yield of our NP process set it ahead of the other processes. In addition, recovery and reusability of the iron NPs would likely be less involved than recovery of catalysts for routes 3 and 4 (Table 7.1). The global warming risk is lowest with route 1 and route 2, mainly due to the lower reaction temperature and slight solvent reduction manifested in the distillation contribution. The inhalation risk of all processes is similar, biased mainly by the increased

solvent use in processes 3 and 4 for byproduct purification. The ingestion toxicity risk is very high for route 2 because of the environmental release of sulfuric acid. The risk of releasing environmentally persistent chemicals is similar for all reactions, an average half-life on the order of several weeks. Potential for bioaccumulation by the ketone byproduct (Rios et al. 2005) of route 3 and route 4 is significant; however, when taken in combination with the relatively short half-life and relatively low release levels, this may not be a significant concern. Although no significant resource depletion occurred, sulfur does have documented abiotic resource depletion potential. Overall, the environmental impacts are relatively similar across the board, but route 1 is superior or equal to the competing routes with respect to every risk factor.

7.5. Conclusions

In this study, we synthesized novel sulfamic acid-functionalized APTES coated Fe/Fe_3O_4 nanoparticles and applied the NPs for the ring opening of EMO as a recyclable catalyst for potential soy polyol applications. The NPs yielded 100% selectivity on α-methoxy-hydroxy methyl oleate, an identical yield to non-recyclable strong acid catalyst (H_2SO_4). A greener synthetic route for soy polyol production was proposed *via* NPs with excellent atom economy, E factor, and dominance in nine environmental impacts over H_2SO_4 and commercial recyclable resin catalysts such as SAC 13 and Amberlyst 15. This synthetic strategy using NPs has great potential for replacement of non-recyclable homogeneous acid catalysts with several economic and environmental benefits to the practical industrial applications: 1) the Fe core of the NPs responded strongly to a magnet that can provide more convenient reaction and recycling processes in a magnetic field, 2) APTES coating enabled great stability on the soy polyol process, and 3) high surface area provided very strong catalytic strength in the reaction comparable to H_2SO_4. The sustainability of this chemical reaction pathway to epoxidized soy oil (ESO) for soy polyol production and broader applications of NPs are being explored by our research team.

Acknowledgements. The authors gratefully acknowledge the USB (United Soybean Board) and KSC (Kansas Soybean Commission) for financial support of this work. Contribution no. 12-048-J from the Kansas Agricultural Experiment Station, Manhattan, Kansas 66506. We also acknowledge financial support from the National Science Foundation under Award No.

EPS-0903806 and matching support from the State of Kansas through the Kansas Technology Enterprise Corporation.

Figure 7.1. TEM image of APTES-coated Fe/Fe_3O_4 nanoparticles bearing terminal sulfamic acid groups.

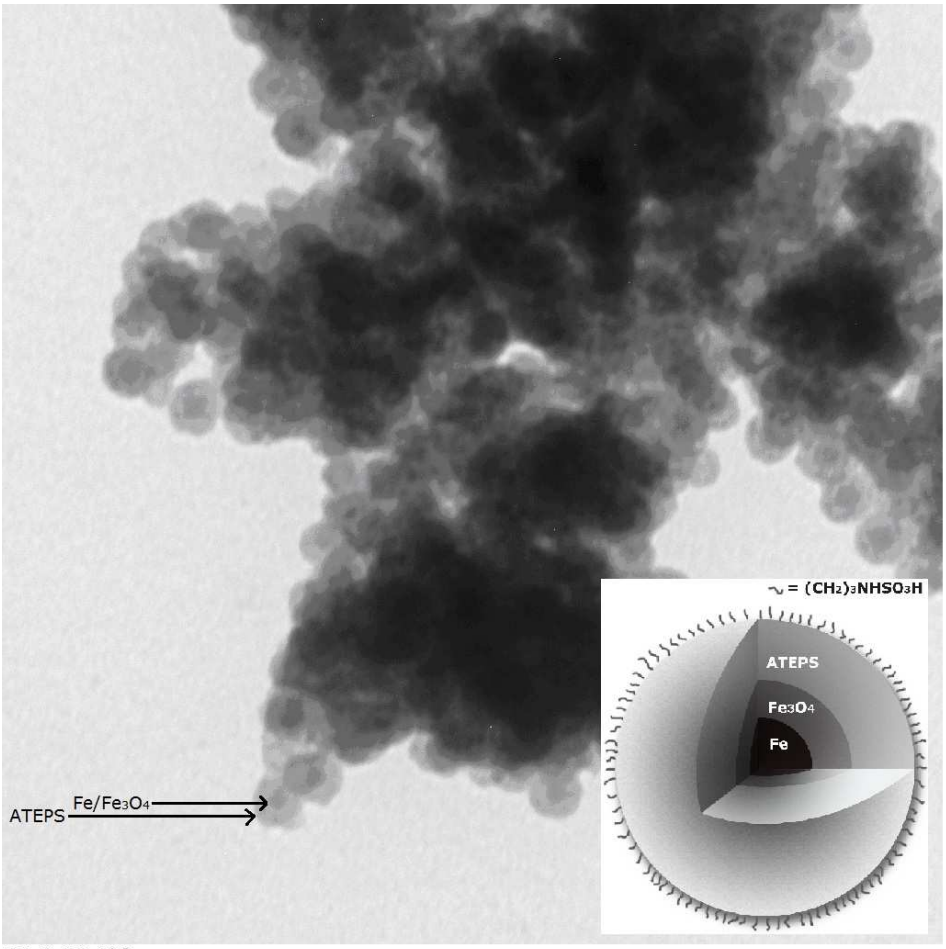

Figure 7.2. XRD patterns of A) APTES-coated Fe/Fe_3O_4 nanoparticles, B) annealed APTES-coated Fe/Fe_3O_4 nanoparticles under Ar at 300°C for 2 h, C) annealed APTES-coated Fe/Fe_3O_4 nanoparticles under Ar at 400°C for 1h.

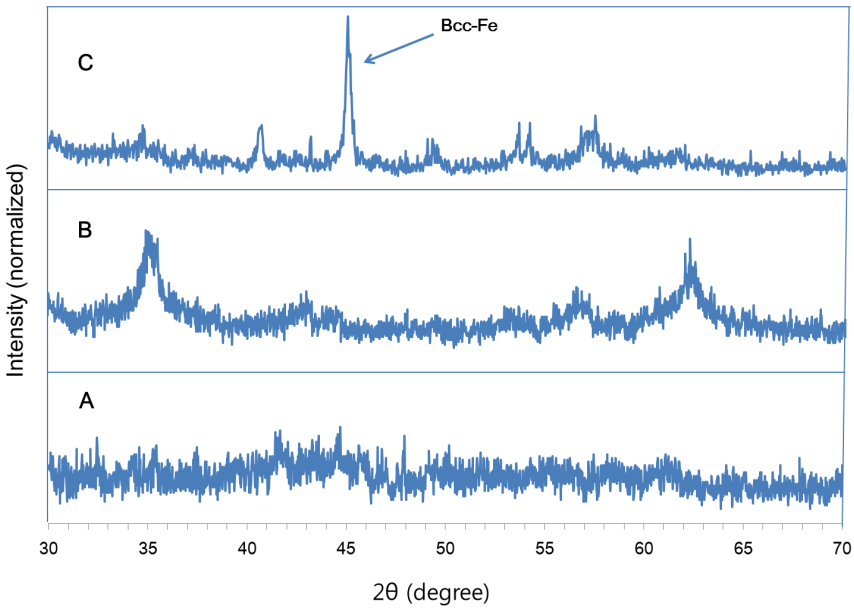

Figure 7.3. ^{1}H NMR of a) EMO, b) α-methoxy-hydroxylation of EMO by the sulfamic acid-functionalized Fe/Fe_3O_4 NPs, and c) α-methoxy-hydroxylation of EMO by H_2SO_4.

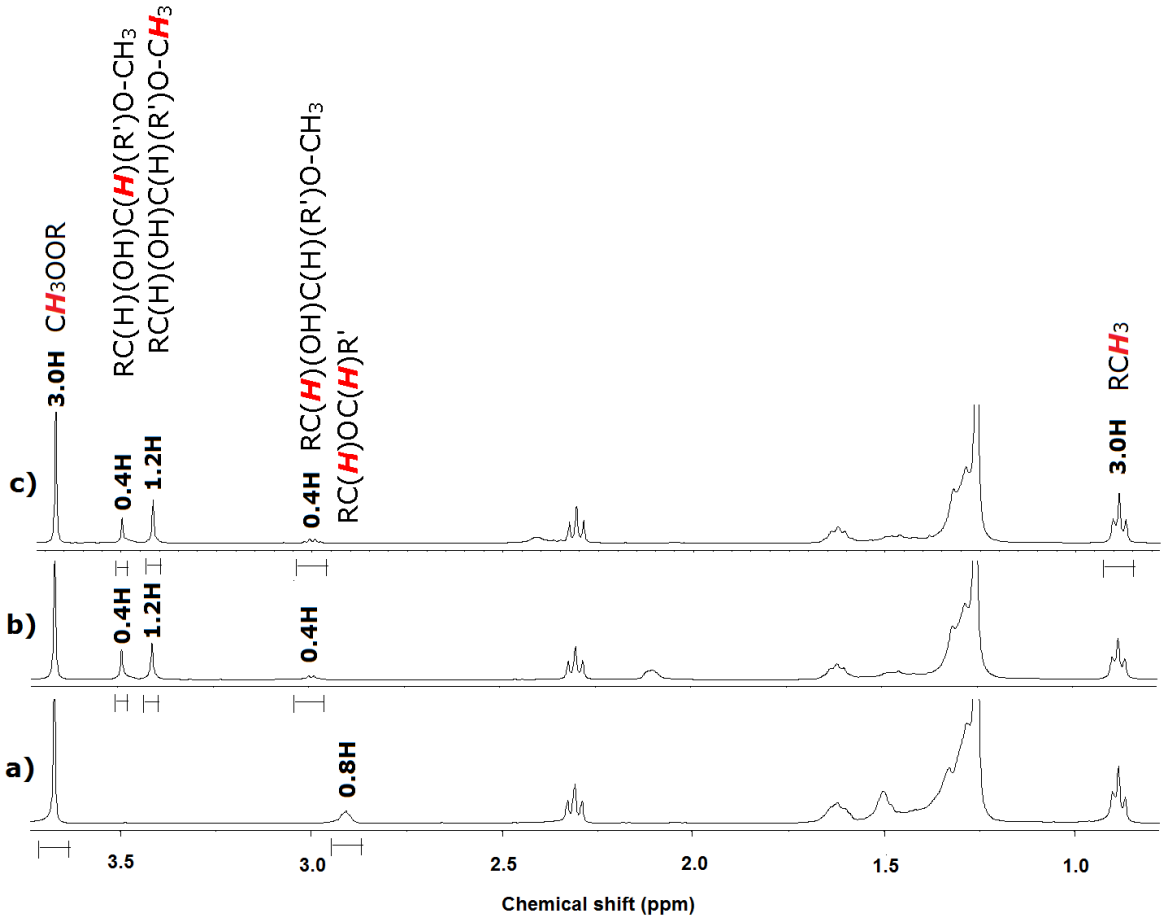

Figure 7.4. Images of a) right after reaction of the NPs in reaction solution, b) 5 min after the solution was placed on the supermagnet.

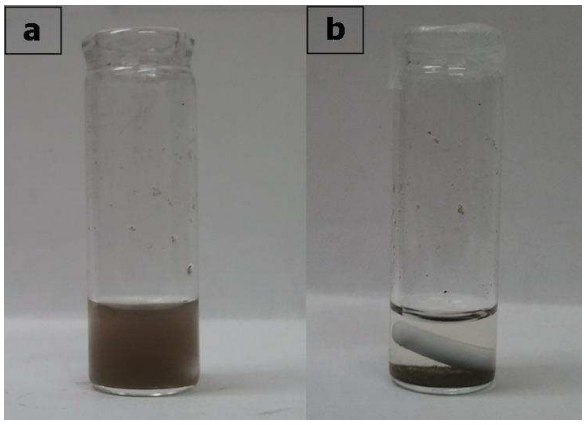

Scheme 7.1. Mid-chain α -methoxy-hydroxylation of ESO or other epoxidized fatty acid esters.

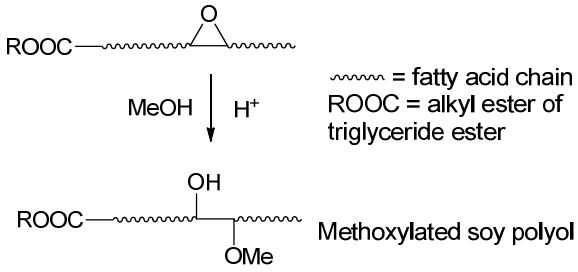

Scheme 7.2. Synthesis of sulfamic acid-functionalized APTES coated core/shell Fe/Fe_3O_4 nanoparticles.

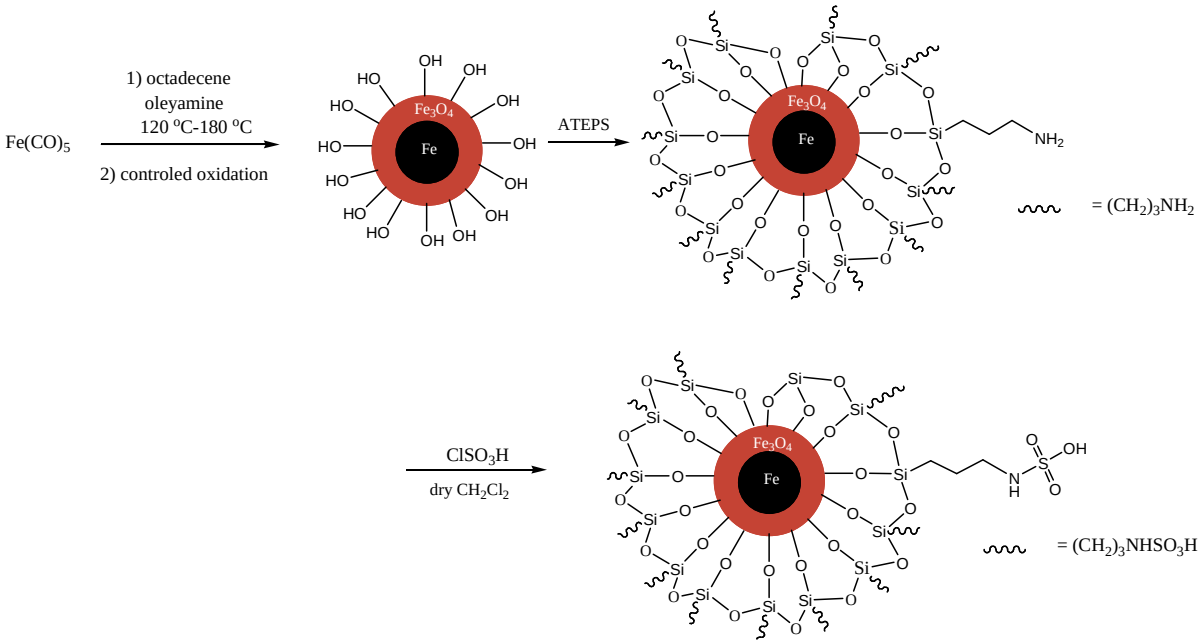

Table 7.1. Comparison of the overall indices (I) for all four routes with respect to the nine factors considered. Values are expressed in kilograms of reference compound (see supplementary material). Persistence (Per) and bioaccumulation (ACCU) refer to the maximum persistence or bioaccumulation of any species in the particular process. Bioaccumulation is expressed in terms of bioconcentration factor.

Route	IAP	IOD	ISF	IGW	IINHT	IINGT	Per, t1/2	ACCU	IAD
1) NPs	0	0	1.49×10^{-4}	5.28×10^{-2}	4.70×10^{-5}	0.824	24 d	1	0
2) H2SO4	0	0	1.49×10^{-4}	4.92×10^{-2}	4.70×10^{-5}	89.3	24 d	1	1.09×10^{-5}
3) SAC13	0	0	1.79×10^{-4}	6.94×10^{-2}	5.70×10^{-5}	0.993	weeks	7.3×105	0
4) Amberlyst	0	0	1.71×10^{-4}	6.58×10^{-2}	5.43×10^{-5}	0.947	weeks	7.3×105	0

7.6. Reference

Ahn, B. K., Kraft, S. and Sun, X. S. 2011a. Chemical pathways of epoxidized and hydroxylated fatty acid methyl esters and triglycerides with phosphoric acid. Journal of Materials Chemistry 21:9498-9505.

Ahn, B. K., Kraft, S., Wang, D. and Sun, X. S. 2011b. Thermally Stable, Transparent, Pressure-Sensitive Adhesives from Epoxidized and Dihydroxyl Soybean Oil. Biomacromolecules 12:1839-1843.

Allen, D. T. and Shonnard, D. R. 2001. Green engineering: Environmentally conscious design of chemical processes and products. Prentice-Hall: Upper Saddle River.

Anastas, P. T. and Warner, J. C. 1998. Green Chemistry: Theory and Practice. Oxford University Press: New York.

Bossmann, S. H. 2009. Nanoparticles for Hyperthermia Treatment of Cancer. Pages 171-206 in: Fabrication and Bio-Application of Functionalized Nanomaterials. X. Wang and E. Katz, eds. Research Signpost: Trivandrum, Kerala, India.

Bozell, J. J. 2008. Feedstocks for the future-biorefinery production of chemicals from renewable carbon. Clean-Soil Air Water 36:641-647.

Carlsson, A. S. 2009. Plant oils as feedstock alternatives to petroleum - A short survey of potential oil crop platforms. Biochimie 91:665-670.

Costa, R. C. C., de Fatima, M., Lelis, F., Oliveira, L. C. A., Fabris, J. D., Ardisson, J. D., Rios, R., Silva, C. N. and Lago, R. M. 2003. Remarkable effect of Co and Mn on the activity of Fe3-xMxO4 promoted oxidation of organic contaminants in aqueous medium with H2O2. Catalysis Communications 4:525-529.

De Palma, R., Peeters, S., Van Bael, M. J., Van den Rul, H., Bonroy, K., Laureyn, W., Mullens, J., Borghs, G. and Maes, G. 2007. Silane ligand exchange to make hydrophobic superparamagnetic nanoparticles water-dispersible. Chemistry of Materials 19:1821-1831.

Dhepe, P. L., Ohashi, M., Inagaki, S., Ichikawa, M. and Fukuoka, A. 2005. Hydrolysis of sugars catalyzed by water-tolerant sulfonated mesoporous silicas. Catalysis Letters 102:163-169.

Guinee, J. 2002. Handbook on life cycle assessment-operational guide to the ISO standards. Kluwer Academic Publishers: Dordrecht.

Guo, A., Cho, Y. J. and Petrovic, Z. S. 2000a. Structure and properties of halogenated and nonhalogenated soy-based polyols. Journal of Polymer Science Part a-Polymer Chemistry 38:3900-3910.

Guo, A., Javni, I. and Petrovic, Z. 2000b. Rigid polyurethane foams based on soybean oil. Journal of Applied Polymer Science 77:467-473.

Hara, M., Yoshida, T., Takagaki, A., Takata, T., Kondo, J. N., Hayashi, S. and Domen, K. 2004. A carbon material as a strong protonic acid. Angewandte Chemie-International Edition 43:2955-2958.

Helling, R. K. and Russell, D. A. 2009. Use of life cycle assessment to characterize the environmental impacts of polyol production options. Green Chemistry 11:380-389.

Jessop, P. G. 2011a. Searching for green solvents. Green Chemistry 13:1391-1398.

Jessop, P. G. 2011b. Searching for green solvents. Green Chemistry.

Kassaee, M. Z., Masrouri, H. and Movahedi, F. 2011. Sulfamic acid-functionalized magnetic Fe3O4 nanoparticles as an efficient and reusable catalyst for one-pot synthesis of alpha-amino nitriles in water. Applied Catalysis a-General 395:28-33.

Lligadas, G., Ronda, J. C., Galia, M. and Cadiz, V. 2010. Plant oils as platform chemicals for polyurethane synthesis: current state-of-the-art. Biomacromolecules 11:2825-2835.

Lopez, D. E., Goodwin, J. G. and Bruce, D. A. 2007. Transesterification of triacetin with methanol on Nafion (R) acid resins. Journal of Catalysis 245:381-391.

Lozada, Z., Suppes, G. J., Tu, Y. C. and Hsieh, F. H. 2009. Soy-based polyols from oxirane ring opening by alcoholysis reaction. Journal of Applied Polymer Science 113:2552-2560.

Luterbacher, J. S., Froling, M., Vogel, F., Marechal, F. and Tester, J. W. 2009. Hydrothermal gasification of waste biomass: process design and life cycle asessment. Environmental Science & Technology 43:1578-1583.

Meier, M. A. R., Metzger, J. O. and Schubert, U. S. 2007. Plant oil renewable resources as green alternatives in polymer science. Chemical Society Reviews 36:1788-1802.

Melero, J. A., Bautista, L. F., Morales, G., Iglesias, J. and Briones, D. 2009. Biodiesel production with heterogeneous sulfonic acid-functionalized mesostructured catalysts. Energy & Fuels 23:539-547.

Melero, J. A., Bautista, L. F., Morales, G., Iglesias, J. and Sanchez-Vazquez, R. 2010. Biodiesel production from crude palm oil using sulfonic acid-modified mesostructured catalysts. Chemical Engineering Journal 161:323-331.

Metzger, J. O. 2009. Fats and oils as renewable feedstock for chemistry. European Journal of Lipid Science and Technology 111:865-876.

Mo, X. H., Lotero, E., Lu, C. Q., Liu, Y. J. and Goodwin, J. G. 2008. A novel sulfonated carbon composite solid acid catalyst for biodiesel synthesis. Catalysis Letters 123:1-6.

Mohapatra, S., Mallick, S. K., Maiti, T. K., Ghosh, S. K. and Pramanik, P. 2007. Synthesis of highly stable folic acid conjugated magnetite nanoparticles for targeting cancer cells. Nanotechnology 18:385102.

Monteavaro, L. L., da Silva, E. O., Costa, A. P. O., Samios, D., Gerbase, A. E. and Petzhold, C. L. 2005. Polyurethane networks from formiated soy polyols: Synthesis and mechanical characterization. Journal of the American Oil Chemists Society 82:365-371.

Oliveira, L. C. A., Petkowicz, D. I., Smaniotto, A. and Pergher, S. B. C. 2004. Magnetic zeolites: a new adsorbent for removal of metallic contaminants from water. Water Research 38:3699-3704.

Oliveira, L. C. A., Rios, R., Fabris, J. D., Garg, V., Sapag, K. and Lago, R. M. 2002. Activated carbon/iron oxide magnetic composites for the adsorption of contaminants in water. Carbon 40:2177-2183.

Oliveira, L. C. A., Rios, R., Fabris, J. D., Sapag, K., Garg, V. K. and Lago, R. M. 2003. Clay-iron oxide magnetic composites for the adsorption of contaminants in water. Applied Clay Science 22:169-177.

Peng, S., Wang, C., Xie, J. and Sun, S. H. 2006. Synthesis and stabilization of monodisperse Fe nanoparticles. Journal of the American Chemical Society 128:10676-10677.

Rios, L. A., Weckes, P. P., Schuster, H. and Hoelderich, W. F. 2005. Resin catalyzed alcoholysis of epoxidized fatty esters: Effect of the alcohol and the resin structures. Applied Catalysis a-General 284:155-161.

Sheldon, R. A. 2000. Atom utilisation, E factors and the catalytic solution. Comptes Rendus De L Academie Des Sciences Serie Ii Fascicule C-Chimie 3:541-551.

Theppaleak, T., Tumcharern, G., Wichai, U. and Rutnakornpituk, M. 2009. Synthesis of water dispersible magnetite nanoparticles in the presence of hydrophilic polymers. Polymer Bulletin 63:79-90.

Trost, B. M. 1991. The atom economy - a search for sythetic efficiency. Science 254:1471-1477.

Chapter 8 - Conclusions and recommendations

Conclusions

The polymers derived from functionalized plant oils have a viscoelastic behavior. The polymers themselves can be utilized as PSAs or lubricants using their viscoelastic nature. The functionalized plant oils are currently used as coatings, paints, inks, plasticizers, plastic crosslinking agents, etc. For example, biopolyol for polyurethane, copolymerized with isocyanate resins, is a huge potential market of oleochemicals. However, there were limited studies that reported in depth chemical characterizations beyond physical properties so as to hinder their further applications due to a lack of understanding of their chemical structural natures. In addition, the product processes were barely considered to be green chemistry regarding environmental impacts.

In this study, the chemical pathways of most broadly known olechemicals were introduced and demonstrated. The plant oil-based PSA derived for mixture of ESO and DSO in presence of phosphoric acid recorded comparable peel strength to the commercial scotch tapes, but the nature of their phosphate ester crosslinkages could not last long in humid conditions, and the process involved solvent. Therefore, solvent free UV curing PSAs were studied using AESO and ESO/DSO. Although previous researchers reported poor potentials of UV cured ESO and AESO for PSA applications, the high shear PSA from AESO and the high performance PSA from ESO/DSO/rosin ester were first accomplished in this study. In addition, biobased content of the products was up to 97%. In a future study, the mechanical properties of the sustainable PSAs will be optimized with various photoinitiators and tackifiers up on each purpose.

Moreover, this study suggested various solutions to overcome current problems of the non-green process of the ring opening reaction for lubricant and biopolyol applications. Stearic acid was utilized as a solvent free ring opening by previous researchers, but their atom economy and E factor were poor, and syntheses with strong acid or in toxic solvent cannot be considered as green chemistry. In this study, the conversion rate and product yields of each process using stearic acid and its salts were evaluated, and magnesium stearate presented overwhelming performance for the ring opening of epoxidized methyl oleate. Based on the chemical investigation, the biogrease (semisolid lubricant) was synthesized and characterized in this study.

The biopolyol market might be currently the biggest market for functionalized plant oils. The biopolyol is now replacing petroleum-based polyol for polyurethane composites which can cover most plastic applications. However, the LCA of syntheses of biopolyol have never been conducted regarding catalysts. Green chemistry desires recyclable heterogeneous catalysts to reduce environmental impacts caused by non-recyclable homogeneous catalysts. However, the heterogeneous catalysts have some disadvantages, such as low catalytic activity, high energy consumption, low conversion rate, low product yields, and so forth. In this study, a novel acid functionalized iron/iron oxide core shell nanoparticle catalyst was developed for a greener biopolyol process, and its catalytic properties for the biopolyol synthesis showed excellent environmental benefits with convenient recyclability, high magnetic response of the iron core structure, and similar catalytic activity compared to a strong homogeneous acid catalyst.

In summary, this study has elucidated chemical biases of oleochemicals based on the principal chemical studies for further applications. The in-depth chemical, rheological, and mechanical characterizations promise potential applications of the plant oil-based polymers to replace current petroleum-based polymers. In addition, several greener chemical syntheses are suggested for the ring-opening of epoxidized oleochemicals for their future polymeric material applications.

Future recommendations

The shelf life of the PSAs is very important for practical applications. The nature of phosphate ester crosslinks is venerable to hydrolysis in moist conditions, which decreased the shelf life of the PSA with phosphate ester crosslink. Thereby, either a specific application of the phosphate ester crosslinked PSA (e.g., biological applications using its degradation in moisture condition) or a copolymerization with moisture tolerant agents (e.g. silicone) would be recommended for future study. Meanwhile, the UV curable PSAs showed long shelf life in our preliminary studies. Further research on UV curable PSAs would be recommended to enhance its adhesion strength by incorporating with various tacky materials. In addition, various commercially available photoiniators and tackifiers are suggested to be applied for commercial applications to reduce UV radiation dose (energy consumption) and increase their mechanical strength. The PSA's properties can be modulated for a specific application by using those additives mentioned above. For the biogrease, common ASTM tests for grease characteristics are

recommended to be conducted for classification of its practical uses, including apparent viscosity, bleeding, migration, syneresis, consistency, penetration, and National Lubricating Grease Institute (NLGI) numbers, contaminants, corrosion- and rust-resistance, dropping point, evaporation, fretting wear and false brinelling, oxidation stability, pumpability and slumpability, shear stability, high- and low-temperature effects, texture, and water resistance. For the acid functionalized NPs catalyst, a scale-up would be a challenge since a complete isolation from air (Oxygen) is required to obtain Fe(0) core in the synthetic process for a strong magnetic field. Therefore, further research to scale up in terms of commercial manufacturing process is recommended. In addition, the strong acidic and magnetic properties of the NP catalyst can be useful for other recyclable acid catalytic applications beyond ring opening of epoxide. Therefore, various acid catalyzed reactions are recommended to be studied using this NP catalyst for future applications.